

Experimental and Ab initio Studies of Intramolecular Ph/Cl Exchange on Wilkinson's Catalyst and Ligand-centered Electrochemistry of Ligand Substituted Metal Carbonyls (M = Cr, Mo, W, Ir)

By

Elvin Igartúa-Nieves

A dissertation submitted in partial fulfillment of the requirements for the degree of

DOCTOR OF PHILOSOPHY

in

Applied Chemistry

UNIVERSITY OF PUERTO RICO

MAYAGÜEZ CAMPUS

2012

Approved by Committee:

Alberto Santana-Vargas, Ph.D.
Member Graduate Studies Committee

Date

Enrique Meléndez-Martínez, Ph.D.
Member Graduate Studies Committee

Date

José A. Rivera-Pagán, Ph.D.
Member Graduate Studies Committee

Date

Mayra E. Cádiz-García, Ph.D.
Member Graduate Studies Committee

Date

José E. Cortés-Figueroa, Ph.D.
President Graduate Studies Committee

Date

María M. Martínez-Iñesta, Ph.D.
Representative Graduate Studies Office

Date

René S. Vieta, Ph.D.
Chairperson of the Department

Date

Abstract

Cyclic voltammetry measurements on $(\eta^2\text{-C}_{60})\text{M}(\text{CO})_5$ complexes (M = Cr, Mo, W) and on $(\text{C}_5\text{H}_{10}\text{N})_3(\text{H})_3\text{C}_{60}$ in dichloromethane showed three C₆₀-centered and reversible reduction/oxidation waves. The $E_{1/2}$ values of these waves are shifted to positive values relative to the corresponding uncoordinated C₆₀ values. A Jahn-Teller type effect due to C₆₀ spherical surface distortion promoted by C₆₀-metal π -backbonding may explain the observed positive shifts.

The complex $\text{Ir}(\text{CO})(\text{PPh}_3)_2(\text{Cl})(\text{C}_{60})$ was spectroscopically detected in C₆₀-saturated liquid solutions. Instead, the species $\text{Ir}(\text{CO})(\text{PPh}_3)_2(\text{Cl})(\text{C}_{60}^{n-})$ (n = 4, 5, 6) were detected electrochemically. Results suggest that electrochemically produced C₆₀⁴⁻ and C₆₀⁵⁻ displace acetonitrile from $\text{Ir}(\text{CO})(\text{PPh}_3)_2(\text{Cl})(\text{CH}_3\text{CN})$ forming $\text{Ir}(\text{CO})(\text{PPh}_3)_2(\text{Cl})(\text{C}_{60}^{4-})$ and $\text{Ir}(\text{CO})(\text{PPh}_3)_2(\text{Cl})(\text{C}_{60}^{5-})$ followed by one-electron electrochemical reductions forming $\text{Ir}(\text{CO})(\text{PPh}_3)_2(\text{Cl})(\text{C}_{60}^{5-})$ and $\text{Ir}(\text{CO})(\text{PPh}_3)_2(\text{Cl})(\text{C}_{60}^{6-})$, respectively.

The Wilkinson's catalyst when dissolved in benzene or C₆D₆ under nitrogen or under high vacuum undergoes a series of unreported reactions at room temperature. The species $(\text{Ph}_3\text{P})_2\text{Rh}(\eta^2\text{-(C}_6\text{H}_4\text{PPh}_2))(\text{Ph})(\text{H})$, Ph-C₆D₅ and $(\text{Ph}_3\text{P})_3\text{Rh}(\text{D})$ were detected in addition to expected formation of the chloro-bridged $(\text{Ph}_3\text{P})_4\text{Rh}_2(\mu\text{-Cl})_2$. The mechanistic description of the reactions based on the behavior of its fluoro-congener, kinetics experiments, and *ab initio* computational studies, involves reversible intramolecular P-Ph/Rh-Cl exchange on the catalyst producing the non-steady-state intermediate *cis*-(Ph₃P)₂Rh(Ph)(Ph₂PCl) via metal-phosphido formation. Intermolecular PPh₃/PPh₂Cl exchange on *cis*-(Ph₃P)₂Rh(Ph)(Ph₂PCl) produces

$(\text{Ph}_3\text{P})_3\text{Rh}(\text{Ph})$, that in turn undergoes cyclometalation, solvent oxidative addition and reductive elimination producing $\text{Ph-C}_6\text{D}_5$.

Resumen

Medidas de voltametría cíclica en los complejos de $(\eta^2\text{-C}_{60})\text{M}(\text{CO})_5$ ($\text{M} = \text{Cr}, \text{Mo}, \text{W}$) y en $(\text{C}_5\text{H}_{10}\text{N})_3(\text{H})_3\text{C}_{60}$ en diclorometano demostraron tres ondas reversibles de oxidación/reducción centradas en C_{60} . Los valores de $E_{1/2}$ de éstas ondas se desplazaron a valores positivos relativo a los valores correspondientes a C_{60} sin coordinar. Un efecto tipo Jahn -Teller debido a la distorsión de la superficie esférica de C_{60} promovida por retrodonación- π entre C_{60} y el metal explican los desplazamientos positivos.

El complejo $\text{Ir}(\text{CO})(\text{PPh}_3)_2(\text{Cl})(\text{C}_{60})$ fue detectado espectroscópicamente en soluciones líquidas saturadas de C_{60} . En lugar, las especies $\text{Ir}(\text{CO})(\text{PPh}_3)_2(\text{Cl})(\text{C}_{60}^{n-})$ ($n = 4, 5, 6$) fueron detectadas electroquímicamente. Los resultados sugieren que las especies producidas electroquímicamente C_{60}^{4-} y C_{60}^{5-} desplazan a acetonitrilo del complejo $\text{Ir}(\text{CO})(\text{PPh}_3)_2(\text{Cl})(\text{CH}_3\text{CN})$ formando $\text{Ir}(\text{CO})(\text{PPh}_3)_2(\text{Cl})(\text{C}_{60}^{4-})$ e $\text{Ir}(\text{CO})(\text{PPh}_3)_2(\text{Cl})(\text{C}_{60}^{5-})$ seguido por reducciones electroquímicas de un electrón formando $\text{Ir}(\text{CO})(\text{PPh}_3)_2(\text{Cl})(\text{C}_{60}^{5-})$ e $\text{Ir}(\text{CO})(\text{PPh}_3)_2(\text{Cl})(\text{C}_{60}^{6-})$ una vez son reducidas, respectivamente.

El catalítico de Wilkinson al disolverse en benceno o C_6D_6 bajo nitrógeno ó bajo vacío lleva a cabo una serie de reacciones a temperatura ambiente no reportadas. Las especies $(\text{Ph}_3\text{P})_2\text{Rh}(\eta^2\text{-(C}_6\text{H}_4\text{PPh}_2))(\text{Ph})(\text{H})$, $\text{Ph-C}_6\text{D}_5$ y $(\text{Ph}_3\text{P})_3\text{Rh}(\text{D})$ fueron detectadas además de la esperada formación de complejo con puentes de cloro $(\text{Ph}_3\text{P})_4\text{Rh}_2(\mu\text{-Cl})_2$. La descripción mecanística de las reacciones basadas en el comportamiento del congénero de flúor, experimentos cinéticos, y cálculos *ab initio*, envuelven intercambio reversible intramolecular de P-Ph/Rh-Cl en el catalizador produciendo el intermediario en estado no-estacionario *cis*- $(\text{Ph}_3\text{P})_2\text{Rh}(\text{Ph})(\text{Ph}_2\text{PCl})$ vía formación de metal-fosfido. El intercambio $\text{PPh}_3/\text{PPh}_2\text{Cl}$ en *cis*-

$(\text{Ph}_3\text{P})_2\text{Rh}(\text{Ph})(\text{Ph}_2\text{PCl})$ produce $(\text{Ph}_3\text{P})_3\text{Rh}(\text{Ph})$, el cual lleva a cabo ortociclometalación, adición oxidativa del disolvente y eliminación reductiva, la cual produce $\text{Ph-C}_6\text{D}_5$.

© 2012 Elvin Igartúa-Nieves

To my wife Débora and my son Evan.

Acknowledgements

I would like to convey my gratitude to the president of my graduate committee, Dr. José E. Cortés-Figueroa for giving me the opportunity of working with inorganic systems and for all his support and lectures through my academic development.

José Rivera-Pagán, Ph.D., Mayra E. Cádiz-García, Ph.D., Enrique Meléndez-Martínez, Ph.D., Gustavo López-Quñones, Ph.D., Andrei Jitianu, Ph.D., Alberto Santana-Vargas, Ph.D. and María M. Martínez-Inesta, Ph.D. are greatly acknowledged for their scientific training, collaboration and helpful comments and suggestions in this work.

NSF Graduate STEM Fellows in K-12 Education Fellowship Program, NSF - Louis Stokes Alliances for Minority Participation (LSAMP) Fellowship Program, NACME & Alfred P. Sloan Foundation Graduate Scholarship Fellowship Program and the University of Puerto Rico Chemistry Department for their support.

Donors of The Petroleum Research Fund, administered by the American Chemical Society, (ACS-PRF # 36623-B3 and ACS- PRF-41267-B3) and the National Science Foundation (Grant CHE-0102167) are acknowledged for the financial support of this work.

I would also like to thank Samirah Mercado, Anthony Cruz, Aracelys Cardona, Sindia Ramos, Tamara Félix-Massa, Wanda Pérez-Mercado, Cacimar Ramos-Álvarez, Ph.D., Ruth Pietri-Meléndez, Ph.D., Denisse Igartúa-Barreto and my parents Edwin Igartúa-Pellot and Nilda E. Nieves-Cabán for their help and support.

Table of Contents

Abstract.....	ii
Resumen.....	iv
Acknowledgements.....	viii
List of Tables.....	xi
List of Figures.....	xii
1. Introduction.....	1
1.1. Scientific Background.....	1
1.1.1. Metal Carbonyls and [60]fullerene.....	1
1.1.2. Reactions of Metal Carbonyls with [60]fullerene.....	2
1.1.3. Interactions of Saturated Hydrocarbons with Organometallic Compounds.....	3
1.2. Objectives.....	8
2. The Electrochemical Profile of $(\eta^2\text{-C}_{60})\text{M}(\text{CO})_5$ (M = Cr, Mo, W) and its subsequent Ligand-Ligand Reactions.....	10
2.1. Introduction.....	10
2.2. Materials and Methodology.....	11
2.2.1. General.....	11
2.2.2. Electrochemical Studies.....	12
2.3. Electrochemical Profile of $(\eta^2\text{-C}_{60})\text{M}(\text{CO})_5$ (M = Cr, Mo, W).....	16
2.3.1. Preparation of $(\eta^2\text{-C}_{60})\text{M}(\text{CO})_5$ (M = Cr, Mo, W).....	16
2.3.2. Results and Discussion.....	16
2.4. Electrochemical detection of the C ₆₀ -Piperidine Adduct.....	20
2.4.1. Preparation of the C ₆₀ -piperidine Adduct.....	20
2.4.2. Electrochemical Studies of C ₆₀ -Piperidine Adduct.....	21
2.4.3. Results and Discussion.....	23
3. Electrochemical Detection of Ir(CO)(PPh ₃) ₂ Cl coordinated to C ₆₀ ⁴⁻ , C ₆₀ ⁵⁻ and C ₆₀ ⁶⁻ Species..	26
3.1. Introduction.....	26
3.2. Materials and Methods.....	27
3.2.1. General.....	27
3.2.2. Preparation of $(\eta^2\text{-C}_{60})\text{Ir}(\text{CO})(\text{PPh}_3)_2\text{Cl}$	28
3.2.3. Electrochemical Studies.....	28
3.3. Results and Discussion.....	29
3.3.1. Infrared Spectroscopy Characterization.....	29
3.3.2. Electrochemical Studies.....	30
4. Experimental and Theoretical Mechanistic Description of C-H and P-C Bond Activation by Wilkinson's Catalyst.....	35
4.1. Introduction.....	35
4.2. Materials and Methods.....	38
4.2.1. General.....	38
4.2.2. Kinetics Experiments.....	38
4.2.3. ¹ H NMR Experiments.....	39
4.2.4. Computational Studies.....	39
4.2.4.1. General.....	39
4.2.4.2. Optimization of Single Point Energy Structures and Transition States Structures.....	40

4.3. Mechanistic Description of Unexpected Room Temperature C-H and P-C Bond Activation by Wilkinson's Catalyst.	41
4.3.1. Results.....	41
4.3.1.1. Kinetics Experiments of Rh(PPh ₃) ₃ Cl	41
4.3.1.1.1. Kinetics Experiments of Rh(PPh ₃) ₃ Cl in Benzene.....	42
4.3.1.1.2. Kinetics Experiments of Rh(PPh ₃) ₃ Cl in Benzene with added PPh ₃	42
4.3.1.1.3. Data Analysis for Kinetics Experiments.....	44
4.3.1.2. ¹ H NMR Spectroscopy Studies on Rh(PPh ₃) ₃ Cl.....	46
4.3.1.3. Interpretation of Kinetics Experiments and ¹ H NMR Studies	47
4.4. A Computational Approach to Study the Mechanism of C-H and P-C Bond Activation by Wilkinson's Catalyst.	56
4.4.1. General.....	56
4.4.2. Results.....	57
4.4.2.1. Experimental and Computational Convergence	57, 59, 71
4.4.3. Discussion.....	75
5. Conclusions.....	77
6. References.....	80

List of Tables

Table 1 Half-wave potentials ($E_{1/2}$) of the $(\eta^2\text{-C}_{60})\text{M}(\text{CO})_5$ complexes ($\text{M} = \text{Cr}, \text{Mo}, \text{W}$) and C_{60} in dichloromethane at room temperature ^a	18
Table 2 $E_{1/2}^n$ values for C_{60} and $\text{C}_{60}(\text{C}_5\text{H}_{10}\text{N})_3(\text{H})_3$ and $\Delta E_{1/2}^n$ values for $\text{C}_{60}(\text{C}_5\text{H}_{10}\text{N})_3(\text{H})_3$	22
Table 3 Rate constant values for reactions of $\text{Rh}(\text{PPh}_3)_3\text{Cl}$ in Benzene.....	42
Table 4 Rate constant values for reactions of $\text{Rh}(\text{PPh}_3)_3\text{Cl}$ and $[\text{PPh}_3]_{\text{added}}$ in benzene.....	43
Table 5 Rate constant values and activation parameters for reactions of 1Cl and added PPh_3 in benzene.	54
Table 6 Rate constant and activation parameter values for reactions of 1Cl in benzene.	54
Table 7 Rh-P Bond Distances (\AA) and Angles (deg) for crystallographically characterized and computed complexes $(\text{PPh}_3)_3\text{Rh}(\text{X})^a$ ($\text{X} = \text{Cl}, \text{F}$).....	60
Table 8 Energy differences between cyclometalated structures.	69

List of Figures

Figure 1 Schematic representation of the vacuum line used to transfer and mix reagents in electrochemical runs.	15
Figure 2 Cyclic voltammetric responses recorded at a glassy carbon working electrode on dichloromethane solution containing, 0.1 M TBPF ₆ of (A) C ₆₀ (saturated solution), and traces of decamethylferrocene (Fc) scan rate 100 mV/s. The E _{1/2} for Fc/Fc ⁺ is 339 mV. The E _{1/2} for C ₆₀ are -998, -1391 and -1860 mV vs. Fc/Fc ⁺ , (B) (η ² -C ₆₀)Cr(CO) ₅ (saturated solution), and traces of decamethylferrocene (Fc) scan rate 100 mV/s. The E _{1/2} for Fc/Fc ⁺ is 385 mV. The E _{1/2} for (η ² -C ₆₀)Cr(CO) ₅ are -996, -1380 and -1839 mV vs. Fc/Fc ⁺ , (C) (η ² -C ₆₀)Mo(CO) ₅ (saturated solution), and traces of decamethylferrocene (Fc) scan rate 100 mV/s. The E _{1/2} for Fc/Fc ⁺ is 218 mV. The E _{1/2} for (η ² -C ₆₀)Mo(CO) ₅ are -977, -1411 and -1862 mV vs. Fc/Fc ⁺ and (D) (η ² -C ₆₀)W(CO) ₅ (saturated solution), and traces of decamethylferrocene (Fc) scan rate 100 mV/s. The E _{1/2} for Fc/Fc ⁺ is 313 mV. The E _{1/2} for (η ² -C ₆₀)W(CO) ₅ are -982, -1374 and -1844 mV vs. Fc/Fc ⁺ . All recorded at T = 20 °C.	17
Figure 3 Cyclic voltammetric responses recorded at a glassy carbon working electrode on dichloromethane solution containing, 0.1 M TBPF ₆ for (A) C ₆₀ (saturated solution), and traces of decamethylferrocene (Fc) scan rate 100 mV/s. The E _{1/2} for Fc/Fc ⁺ is 339 mV. The E _{1/2} for C ₆₀ are -998, -1391 and -1860 mV vs. Fc/Fc ⁺ and (B) C ₆₀ (H) ₃ (NC ₅ H ₁₀) ₃ (saturated solution), and traces of decamethylferrocene (Fc) scan rate 100 mV/s. The E _{1/2} for Fc/Fc ⁺ is 373 mV. The E _{1/2} for C ₆₀ (H) ₃ (NC ₅ H ₁₀) ₃ are -487, -729, and -1188 mV vs. Fc/Fc ⁺ . T = 20 °C	22
Figure 4 Infrared spectra for (A) piperidine, (B) <i>n</i> -amine-fullerene adduct and (C) fullerene in dichloromethane.....	24
Figure 5 Infrared spectrum in benzene of: A. Ir(CO)(PPh ₃) ₂ Cl and B. (η ² -C ₆₀)Ir(CO)(PPh ₃) ₂ Cl in a C ₆₀ -saturated solution.....	30
Figure 6 Cyclic voltammetric responses of (A) C ₆₀ , (B) mixture of C ₆₀ , (*) Ir(CO)(PPh ₃) ₂ Cl(C ₆₀ ⁵⁻) and (**) Ir(CO)(PPh ₃) ₂ Cl(C ₆₀ ⁶⁻) species, (C) C ₆₀ , showing the first four reduction waves, and (D) C ₆₀ , showing the first three reduction waves in a acetonitrile:toluene (1:5) solution containing 0.1M of TBPF ₆ at a 100 mV/s scan rate. T=20°C.....	32
Figure 7 Osteryoung square wave voltammogram of a mixture of C ₆₀ and Ir(CO)(PPh ₃) ₂ Cl showing the waves of the suggested (*) Ir(CO)(PPh ₃) ₂ Cl(C ₆₀ ⁵⁻) and (**) Ir(CO)(PPh ₃) ₂ Cl(C ₆₀ ⁶⁻) species in 1:5 (v/v) acetonitrile:toluene with TBPF ₆ as a supporting electrolyte at 25°C at a 100 mV/s scan rate. T=20°C	33
Figure 8 Proposed mechanistic pathways for the P-Ph/Rh-F exchange on 1F (obtained from reference [74a]).....	37
Figure 9 Plots of absorbance (370 nm) vs. time for reactions of 1Cl with benzene. (a), at 62.1 °C; (b), at 42.1 °C; (c), at 56.1°C; (d), at 32.1 °C in presence added [PPh ₃] _{added} = 2.29 x 10 ⁻⁴ M; (e), at 32.1 °C; (f), at 32.1 °C in presence added [PPh ₃] _{added} = 7.37 x 10 ⁻³ M.	42
Figure 10 ¹ H NMR spectra of (a) 1Cl in C ₆ D ₆ /C ₆ H ₆ *(0.04%), (b) and (c) 1Cl in C ₆ D ₆ /PPh ₃ solution [PPh ₃] _{added} = 0.0314 M.	46
Figure 11 Mechanistic description of reactions of 1Cl in benzene (or in C ₆ D ₆).	49
Figure 12 Plot of <i>k'</i> _{obsd} vs. [PPh ₃] for reactions of 1Cl with benzene containing added [PPh ₃] at 32.1 °C (■) (<i>k'</i> _{obsd} = 0.21(1) [PPh ₃] _{added} , 42.1 °C (●) (<i>k'</i> _{obsd} = 0.44(2) [PPh ₃] _{added}) and 52.1 °C (▲) (<i>k'</i> _{obsd} = 0.44(2) [PPh ₃] _{added}).	51
Figure 13 Plots of ln(<i>k</i> /Temperature) vs. 1/Temperature. <i>k</i> = <i>k</i> _{PPh₂Cl/PPh₃} on 2Cl (▲); <i>k</i> = <i>k</i> _{dim} on 3Cl (■); <i>k</i> = <i>k</i> _{exch} on 1Cl (●); <i>k</i> = <i>k</i> _{exch} on 1F (◆) from reference [74a].	53

Figure 14 Computational profile map based of the reactions of $(\text{PPh}_3)_3\text{RhCl}$ in C_6D_6 . Numbered labels are used to distinguish bonding sites.	58
Figure 15 Optimized structures of $(\text{PPh}_3)_3\text{RhCl}$ in singlet state $^1\text{1Cl}$ and triplet state $^3\text{1Cl}$ which exhibit pseudo planar square geometry and distorted tetrahedral geometry, respectively.	60
Figure 16 Computed reaction profile (kJ/mol) for Path 1 <i>cis</i> in vacuo.....	61
Figure 17 Computed reaction profile (kJ/mol and kcal/mol) for Path 1 <i>cis</i> in vacuo where phosphorus atoms retained their geometry through the activation barrier.	63
Figure 18 Structures of $(\text{PPh}_3)_3\text{RhCl}$ for (A) non-optimized <i>cis</i> Cl-Rh-Ph, (B) optimized <i>cis</i> Cl-Rh-Ph and (C) optimized <i>trans</i> Cl-Rh-Ph.....	64
Figure 19 Computed reaction profile (kJ/mol) for the first activation barrier of Path 1 via <i>cis</i> in (A) vacuo and (B) in benzene ($\epsilon = 2.2706$). Negative value resembles the stabilization of $^1\text{1Cl}$ in the presence of benzene.	65
Figure 20 Computed reaction profile (kJ/mol) for the first activation barrier of Path 1 via <i>trans</i> in (A) vacuo and (B) in benzene ($\epsilon = 2.2706$).	66
Figure 21 Optimized structures of I_{2-1} with five –coordinate phosphorus center with (A) trigonal bipyramidal geometry and (B) chloride atom lies in between the Ph ligands.	67
Figure 22 Computed reaction profile (kJ/mol) for the activation barrier of cyclometalation of 9 in vacuo.	68
Figure 23 Optimized structures for the cyclometalation of 2Cl from (A) PPh_3 <i>trans</i> to Ph-Rh, (B) PPh_3 <i>cis</i> to Ph-Rh and (C) PPh_2Cl <i>cis</i> to Ph-Rh in vacuo. Hydrogens omitted for simplicity. ...	69
Figure 24 Computed profile energy barrier (kJ/mol) for the intramolecular cyclometalation of <i>cis</i> 2Cl to 4Cl-P4	70
Figure 25 Optimized structure of I_{5-1} where H_{105} in Rh comes from C_{106} . All other hydrogen atoms are omitted.....	71
Figure 26 Computed reaction profile (kJ/mol) for the simplified first activation barrier of Path 1 via <i>cis</i> Ph exchange and <i>trans</i> Cl-Rh-Ph intermediate arrangement for (A) vacuo and (B) in benzene ($\epsilon = 2.2706$).	73
Figure 27 Computed reaction profile (kJ/mol) for the simplified first activation barrier of Path 1 via <i>cis</i> Ph exchange and <i>cis</i> Cl-Rh-Ph intermediate arrangement for (A) vacuo and (B) in benzene ($\epsilon = 2.2706$).	73
Figure 28 Computed profile (kJ/mol) for the activation barrier of Path 1 <i>trans</i> with Ph transferring to the axial position for (A) in vacuo and (B) in benzene ($\epsilon = 2.2706$).	74
Figure 29 Computed profile (kJ/mol) for the activation barrier of Path 2 via <i>cis</i> in (A) vacuo and (B) benzene ($\epsilon = 2.2706$).	75
Figure 30 Experimental and computed reaction profile summary for the reactions of $^1\text{1Cl}$, red question marks resemble non-computed transition states. Hydrogen atoms are omitted for simplicity.....	77

1. Introduction

Organometallic chemistry is the chemistry of compounds that hold at least one metal-carbon bond. The interaction between the metal and the carbon has been described by Parshal as “ionic or covalent, localized or delocalized between one or more carbon atoms of organic group or molecule and a transition, lanthanide, actinide, or main group metal atom” [1]. This field has grown in the past decades by integrating materials, engineering, biological, biomedical, and environmental fields, among others. It encompasses a variety of molecules of types that are uncommon in organic chemistry and its reactions. The latter may be similar to those in organic chemistry; however in most cases they differ by to a great extent since these metal-carbon interactions are responsible for different behavior due to slight differences in structure and bound species. This bridge between organic and inorganic chemistry has revealed chemical species of appealing nature that that meet industrial needs such as pharmaceuticals, fragrances, flavors, semiconductors, agrochemicals and most importantly a gamma of useful catalysts [1]. Organometallic catalysts are known for their ability to lower activation barriers and for taking chemical reactions to a less energetic route. Thus, they have become of great importance when it comes to high temperature dependent methods which need to be minimized in chemical processes due to minimum fuel use from an economical and environmental point of view or simply because of the diminishing supply of fossil fuels.

1.1. Scientific Background

1.1.1. Metal Carbonyls and [60]fullerene

Metal carbonyl complexes are one of the most studied type of organometallic complexes. These complexes contain central transition metals and a bound carbon monoxide that acts as a ligand. Even though this ligand is not considered to be a particularly strong a Lewis base it has

the potential to form strong bonds with metals in low oxidation states. In addition, when involved in ligand exchange reactions the chemical information that can be obtained as a consequence of the infinite diversity in structure and reactivity is of great value in many areas of science.

[60]Fullerene is a molecule that has been known to be involved in ligand exchange reactions with metal carbonyls. The discovery of this molecule goes back to 1985 when Kroto *et al.* first reported its discovery [2]. [60]Fullerene or C₆₀, shows several extraordinary properties such as extremely high hydrophobicity, high cohesive force between fullerene molecules, photoactivity, ability to accept and release electrons, and relatively high reactivity that allows structural modifications [3]. Another interesting feature of [60]fullerene is that it can form endohedral adducts by insertion of metals or noble gases in their inner cavity. Fullerenes also react with alkali metals and organic molecules to form new superconducting materials, organic compounds, polymers, plays a role as cancer killing catalysts, in solar cells for energy performance, hydrogen absorption and hydrogen storage [5-7]. [60]Fullerene has a unique reactivity and hydrophobicity which has created an interdisciplinary interest in modifying its polyfunctional structure which contains 30 reactive double bonds located at the junctions of two hexagons via an extended number of addition reactions [8,9].

1.1.2. Reactions of Metal Carbonyls with [60]fullerene

Organometallic derivatives such as $(\eta^2\text{-chelate})_n\text{M}(\text{CO})_{6-2n}$, where M is a metal from the first, second and third transition series of group VIB, Cr, Mo, and W, respectively, react with [60]fullerene. The coordination of [60]fullerene to the metal is via a dihapto mode (η^2), [10-27] having very similar bonding properties as olefin [14] to form $(\eta^2\text{-chelate})_n(\eta^2\text{-C}_{60})\text{M}(\text{CO})_{5-2n}$.

Upon coordination to the metal it has been reported to have metal-C₆₀ bond enthalpies of 60 to 130 kJ/mol [14, 15]. This range depends on the bonded metal and the influence of co-coordinating ligands which can affect the electronic environment of C₆₀ [10-27]. The coordinated [60]fullerene has π -acceptor capacity [14, 15] that can be explained on the basis that [60]fullerene has a strong tendency to accept electrons [10–27]. Interestingly, cyclic voltammetry studies on C₆₀ show six reduction waves at potentials that range from -0.50 to -3.26V (vs. ferrocene/ferrocinium) which confirms the theoretical prediction that its LUMO should be able to accept six electrons to form diamagnetic C₆₀⁶⁻ [28].

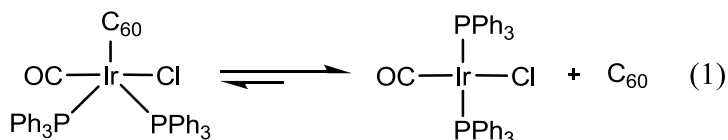
The complexes (η^2 -C₆₀)M(CO)₅ (n = 0) and *fac*- and *mer*-(η^2 -dppe)(η^2 -C₆₀)M(CO)₃ and *fac*-(η^2 -phen)(η^2 -C₆₀)M(CO)₃ (n = 1, dppe = 1,2 bis(diphenylphosphino)-ethane, phen =1,10-phenanthroline) have been prepared and characterized in our research group and other groups [12-27]. The resulting exohedral metal complexes exhibits π -backbonding between [60]fullerene and the metal center. The extent of the π -backbonding will depend on the co-coordinated ligands. For example, [60]fullerene acts as a *cis*-labilizing ligand in *fac*- and *mer*-(η^2 -chelate)-(η^2 -C₆₀)M(CO)₃ (chelate = dppe and phen) [12-13]. In addition, ligands such as piperidine displace dppe from *fac*-(η^2 -dppe)(η^2 -C₆₀)Cr(CO)₃ to produce *fac*-(pip)₂(η^2 -C₆₀)Cr(CO)₃ and *fac*-(η^2 -dppe)(η^1 -piperidine)Cr(CO)₃.

1.1.3. Interactions of Saturated Hydrocarbons with Organometallic Compounds

Reactions where the activation of a C-H bond takes place via a transition-metal have been widely used in synthesis and catalysis [29-38]. These transition metal complexes known as organometallic catalysts have been used for synthesis of organic compounds such as pharmaceutical, natural products and other fine chemicals. The chemical interactions between

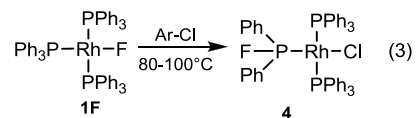
coordinatively-unsaturated organometallic compounds and weakly coordinating molecules such as alkanes have been the object of investigations during the past two decades [29-54]. Understanding the key mechanistic steps towards C-H bond activation by transition metal compounds and the role of solvent molecules has been the motive of such extensive research activity on the mechanisms of homogeneous transition metal-catalyzed processes. Due to the fast reaction under normal reaction conditions of solvation processes it has been necessary to use techniques such as low-temperature glasses, photo-acoustic calorimetry, low temperature IR spectroscopy, or fast and ultra fast time-resolved IR absorption spectroscopy [29-52].

Vaska's complex, $\text{Ir}(\text{CO})(\text{PPh}_3)_2\text{Cl}$, (**1Ir**) is an iridium based transition carbonyl complex that has been reported to react with C_{60} under mild conditions and to play a role in C-H activation [53-55]. The synthesis of $(\eta^2\text{-C}_{60})\text{Ir}(\text{CO})(\text{PPh}_3)_2\text{Cl}$ (**2Ir**) was reported by Balch, Catalano, and Lee [54]. It was characterized on solid phase because in liquid solution the equilibrium described by eq. 1 is favored to the right [55].

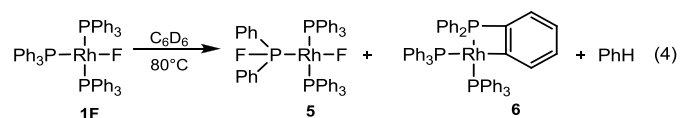


It has been reported that solvent interactions with photochemically-generated transient organometallic species under binary solvent mixtures where one solvent, acting as a token ligand, is displaced from the coordination sphere by the other solvent or by a ligand [47-52, 54-63]. Our group has reported the mechanism of solvent/ C_{60} exchange on $(\eta^2\text{-C}_{60})\text{Ir}(\text{CO})(\text{PPh}_3)_2\text{Cl}$ and solvent/solvent exchange on $\text{Ir}(\text{CO})(\text{PPh}_3)_2(\text{Cl})(\text{solvent})$. Solvent/ C_{60} exchange on $(\eta^2\text{-C}_{60})\text{Ir}(\text{CO})(\text{PPh}_3)_2\text{Cl}$ in binary solvent mixtures (solvent_1 and solvent_2) produces $\text{Ir}(\text{CO})(\text{PPh}_3)_2(\text{Cl})(\text{solvent}_1)$ and $\text{Ir}(\text{CO})(\text{PPh}_3)_2(\text{Cl})(\text{solvent}_2)$ in non-equilibrium mixtures [55]. Once produced, the solvated species undergo a relative fast solvent exchange

with a 30% of dissociation found by ^{31}P NMR [72]. The same degree of dissociation was reported recently in the fluoro analogue $(\text{Ph}_3\text{P})_3\text{RhF}$ (**1F**). In addition, it was reported that to C-Cl bond cleavage when (**1F**) was heated in chlorobenzene at 80-100°C (eq. 3) [72].



The presence of biphenyl as a reaction product is a result of the oxidative addition of the aromatic halide followed by a reductive elimination of the added aromatic ring along with a phenyl group of the phosphine. It has been also reported that when (**1F**) is heated in benzene at 80°C it undergoes thermal decomposition involving Rh-F and P-F bond formation producing *trans*- $(\text{Ph}_3\text{P})_2\text{Rh}(\text{Ph}_2\text{PF})(\text{F})$ (**5**), the cyclometalation product $(\text{Ph}_3\text{P})_2\text{Rh}(\eta^2\text{-}(\text{C}_6\text{H}_4\text{PPh}_2))$ (**6**) and PhH produced from the reductive elimination of **6**. (eq. 4)



Both products were found in equimolar amounts in the mixture of products. The mechanistic description of the formation of these organometallic complexes was described by Macgregor *et al.* [74]. The π -donating or π -accepting properties of ligands such as halides and PPh_3 (PPh_3 = triphenylphosphine) bonded to the square planar d^8 transition metal coordination sphere seem to be the key factors of ligand exchange reactions.

In our effort to mitigate, analyze and report the connection between structure and reactivity of organometallic catalyst we are conducting investigations on reactions of organometallic compounds with different metal center and ligand arrangements. Some organometallic reactions can form stable products which can be analyzed by spectroscopic and electrochemical techniques be used to further elucidate their reaction mechanism. In contrast,

the call for stability in other reactions makes difficult to isolate intermediates and products. Hence, we have recurred to computational approaches in order to understand key mechanistic descriptions of these systems. Herein, we report the experimental and ab initio studies of intramolecular Ph/Cl exchange on Wilkinson's catalyst and ligand-centered electrochemistry of ligand substituted metal carbonyls (M = Cr, Mo, W, Ir).

1.2. Objectives

The study of the relation of chemical reactivity, electronic structure and molecular structure involves a series of parallel and consecutive assessments that converge in one or more plausible interpretations. These interpretations will enable the understanding of key mechanistic steps of organometallic reactions involving solvents and/or ligands. Following the reactions progress by UV/V will enable the determination of reactions rate constant values that in turn will be compared to corresponding values of mechanistically derived rate constants. If experimental and mechanistic rate constant are mathematically indistinguishable, then the proposed reaction mechanism holds. Infrared and ^1H NMR spectroscopy will be used to study the electronic and molecular structure of the species involved in the reaction. The electronic environment will be assessed by cyclic voltammetry (CV) and Osteryoung wave voltammetry (OSWV) studies. Computational methods contained in *Gaussian*TM package based on Density Functional Theory (DFT) will be used to estimate enthalpy of activation barriers of processes that cannot be examined experimentally with the resources available in our laboratory.

Specific Project Aims:

1. To prepare, and perform electrochemical, kinetics and mechanistic studies of ligand exchange reactions on $(\eta^2\text{-C}_{60})\text{M}(\text{CO})_5$ (M = Cr, Mo, W) complexes which allows assessment of the electron donor/acceptor capacity of C_{60} .
2. To prepare and perform electrochemical studies on the complex $\text{Ir}(\text{CO})(\text{PPh}_3)_2\text{Cl}$ coordinated to C_{60} .
3. To explore and describe key mechanistic details of room temperature reactions that Wilkinson's catalyst exhibits when it is dissolved in benzene.

4. To use DFT as a powerful supporting tool of interpretation of enthalpy and entropic activation values obtained experimentally, thus sustaining, or disproving proposed mechanism(s).

2. The Electrochemical Profile of $(\eta^2\text{-C}_{60})\text{M}(\text{CO})_5$ (M = Cr, Mo, W) and Ligand-Ligand Reactions.

2.1. Introduction

It has been known that the formation of [60]fullerene–metal complexes may be favored by the ability of [60]fullerene to participate in π -back bonding [12-14]. The [60]fullerene–metal bond dissociation energies have been estimated in $(\eta^2\text{-C}_{60})\text{M}(\text{PH}_3)_2$ (M = Ni, Pd, Pt) complexes by density functional calculations [77-79]. In addition, the study of the electronic structure of [60]fullerene-metal has been assessed by electrochemical studies of some [60]fullerene-substituted metal carbonyl complexes of group 6 have been reported [13-16, 18-21, 80]. Also, subsequent reactions with organic compounds have lead to organometallic functionalization of [60]fullerene, offering a mean to study its electronic and chemical properties. The large size of [60]fullerene, its high electron affinity, [81-88] and its capacity to participate in π -back bonding with transition metals give [60]fullerene the potential to be used as organometallically-functionalized [60]fullerene catalysts or to modify and improve the capacity of existing organometallic catalysts. Although the molecular structure and electronic properties of [60]fullerene are well understood and documented, the electronic, structural, and chemical properties of organometallically-functionalized [60]fullerene appears to depend on no easily separated factors such as the nature of the metal to which it is coordinated, position within the coordination sphere, and the nature of co-coordinated ligands within the same coordination sphere. Thus, manipulation of [60]fullerene's chemical and electronic properties for technological applications may be achieved via metal coordination. Interesting properties of [60]fullerene observed when it is acting as ligand in transition metal organometallic complexes are: i) that despite its size and number of olefinic units on its curved surface, its preferentially coordinates to only one organometallic fragment per [60]fullerene unit, ii) it can weaken metal-

ligand bonds of co-coordinated ligands, and iii) it can stabilize transition states or intermediates species involved in [60]fullerene/ligand exchange reactions. However, to our knowledge, reports on the plausible relation between their reactivities toward [60]fullerene–ligand exchange reactions and their electrochemical profiles are scarce.

Hence, we report the results on the preparation, electrochemical, kinetics and mechanistic studies of the ligand exchange reactions on $(\eta^2\text{-C}_{60})\text{M}(\text{CO})_5$ ($\text{M} = \text{Cr}, \text{Mo}, \text{W}$) complexes and [60]fullerene-ligand reaction.

2.2. Materials and Methodology

2.2.1. General

The complexes $(\eta^2\text{-C}_{60})\text{M}(\text{CO})_5$ were prepared from [60]fullerene, and the corresponding metal hexacarbonyl complex ($\text{M} = \text{Cr}, \text{Mo}, \text{W}$). The [60]fullerene-piperidine adducts were also prepared from [60]fullerene and piperidine as purchased. All reagents were purchased from Aldrich. Benzene was purchased from Aldrich and was distilled under sodium and fractionally distilled under nitrogen. In order to prevent oxidation of the reagents and complexes, all reactions were carried out under a nitrogen atmosphere. Group theory concepts were applied in order to predict the infrared active CO-stretching bands (ν_{CO}) for CO containing complexes [89]. Infrared spectra were obtained on a Bruker Vector 22 Fourier transform infrared spectrophotometer equipped with a KBr cell with a 0.10 mm light path and UV-visible spectra on a Perkin Elmer Lambda 25 UV/vis spectrophotometer. All reactions were carried out under an inert nitrogen atmosphere. A Julabo F 12-EC model heating and refrigerating circulator and a K/J Fluke digital thermometer equipped with a bead thermocouple were used as temperature control devices. Elemental analyses were carried out in Midwest Microlabs in order to

determine the composition of the synthesized complexes. Thin layer chromatography was performed using silica gel (25 μm , pore size 60 \AA , Aldrich). The components were visualized by treating the thin layer chromatogram with iodine. Column chromatography was performed using a 15 cm long (1 cm diameter) column packed with 62 grade, 60-2000 mesh, 150 \AA silica gel purchased from Aldrich or Fisher Scientific.

2.2.2. Electrochemical Studies

Cyclic voltammetry experiments were performed at ambient temperature and low pressure in a voltametric work station equipped with a high vacuum line and a Bioanalytical systems BAS CV-50W Electrochemical Analyzer as described previously. The high vacuum line was used to transfer and mix reagents. Dichloromethane (Aldrich), used as solvent, was dried over phosphorus pentoxide, fractionally distilled under nitrogen, transferred and stored over dried silica under vacuum. The silica was dried by heating it with a Bunsen burner under high vacuum. Tetrabutylammonium hexafluorophosphate (TBPF_6) (Aldrich), used as supporting electrolyte, was recrystallized from 95% ethanol and dried under vacuum prior to use. Ferrocene (Fc)/ferrocenium (Fc^+) couple was used as internal reference in all measurements.

A three-electrode configuration was used consisting of a glassy carbon working electrode (3 mm in diameter), a platinum wire (Pt-wire) counter electrode, and a non-aqueous silver pseudo-reference electrode. The non-aqueous silver pseudo reference electrode consists of a silver wire inside a 4 mm (O. D.) Pyrex tubing which contains a small amount of a 0.1 M TBPF_6 solution in dichloromethane and separated from the bulk solution by a Vycor glass frit located at the tip of the tube. This electrode configuration prevents peak potentials drift due to small changes in the solutions ionic strength during the electrochemical measurements. The working electrode was

polished before use with 0.25 μm diamond polishing compound (Metadi II) purchased from Buehler and a microcloth (BAS) and sonicated for approximately 10 seconds in deionized water to remove adsorbed polishing materials. The Pt-wire was cleaned by exposing it to a flame for approximately 30 seconds and the silver wire was rinsed with acetone and deionized water to remove impurities.

A custom-made electrochemical cell equipped with two arm adapters, described previously, was used for the electrochemical experiments. The sample of the compound to be studied was placed in one of the cell's arm adapters (enough amounts to obtain a solution of approximately 0.5 mM to 1.0 mM in 3 mL of dichloromethane). A minute amount of the internal reference, ferrocene, can be placed at the beginning of the experiment in the other arm adapter. The supporting electrolyte (ca. 0.12 g of TBPF_6) and a small spinning bar was placed in the cell and connected to the vacuum line. The cell was opened to the vacuum line (10^{-5} to 10^{-6} mmHg) and the supporting electrolyte was heated with a heat gun for approximately five seconds followed by cooling at room temperature. The heating and cooling process was repeated five times to ensure that the supporting electrolyte was completely dry. Approximately 3 mL of dichloromethane were transferred to the cell directly through the vacuum line by cooling the cell with liquid nitrogen. Once the solvent transfer was accomplished, the whole cell ensemble was disconnected from the vacuum line and allowed to reach room temperature. The background voltammogram, dichloromethane and supporting electrolyte was recorded before the sample electrochemical measurement at a scan rate of 100 mV/s between 0 mV and -2000 mV. When determination of the cyclic voltammogram involved multiple scans, the solution was stirred between each scan using the spinning bar placed in the cell. Then, the supporting electrolyte solution was transferred over the sample and a complete scan was carried out from +1000 mV to

-2000 mV. To record the sample voltammogram versus the internal reference, the solution was then transferred over ferrocene and the CV was scanned in the same voltage range. When ferrocene was not added at the beginning of the experiment, the cell was opened under argon and a small amount of the reference was placed in one of the cell's arm. The vacuum was then reestablished slowly.

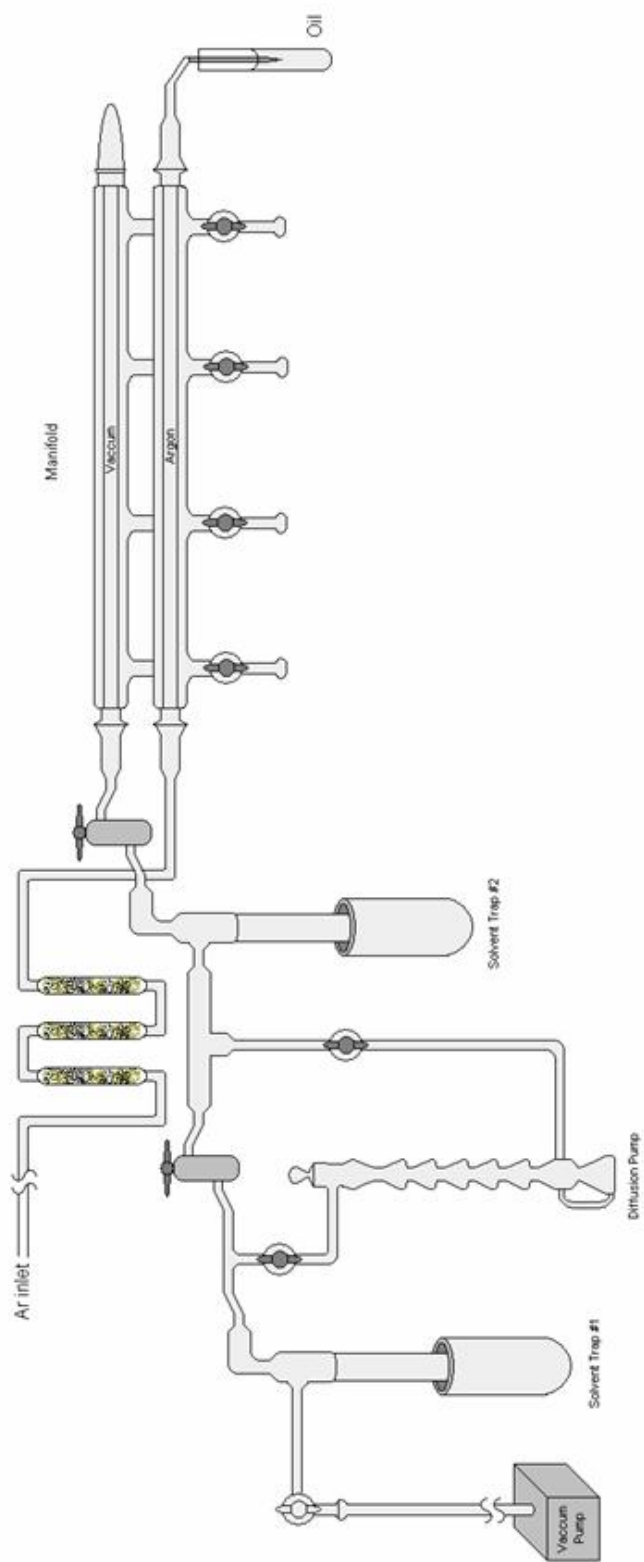


Figure 1 Schematic representation of the vacuum line used to transfer and mix reagents in electrochemical runs.

2.3. Electrochemical Profile of $(\eta^2\text{-C}_{60})\text{M}(\text{CO})_5$ (M = Cr, Mo, W)

2.3.1. Preparation of $(\eta^2\text{-C}_{60})\text{M}(\text{CO})_5$ (M = Cr, Mo, W)

The complexes $(\eta^2\text{-C}_{60})\text{M}(\text{CO})_5$ were prepared photochemically from $\text{M}(\text{CO})_6$ (Aldrich) and [60]fullerene (Aldrich) using a medium pressure mercury lamp following a published procedure [14,15]. Each complex was identified by its infrared spectrum in the carbonyl stretching region (ν_{co}). The ν_{co} of the complexes dissolved in *n*-hexane showed the expected ν_{co} bands for a C_{4v} local symmetry: ν_{co} for $(\eta^2\text{-C}_{60})\text{W}(\text{CO})_5$; 2085 cm^{-1} , 1996 cm^{-1} , and 1972 cm^{-1} ; ν_{co} for $(\eta^2\text{-C}_{60})\text{Mo}(\text{CO})_5$; 2089 cm^{-1} , 1984 cm^{-1} , and 1970 cm^{-1} ; ν_{co} for $(\eta^2\text{-C}_{60})\text{Cr}(\text{CO})_5$; 2079 cm^{-1} , 1987 cm^{-1} , and 1969 cm^{-1} .

2.3.2. Results and Discussion

The half peak potentials of $(\eta^2\text{-C}_{60})\text{M}(\text{CO})_5$ (M = Cr, Mo, W) and C_{60} are given in Table 1 and their corresponding cyclic voltammograms are shown in Figure 2.

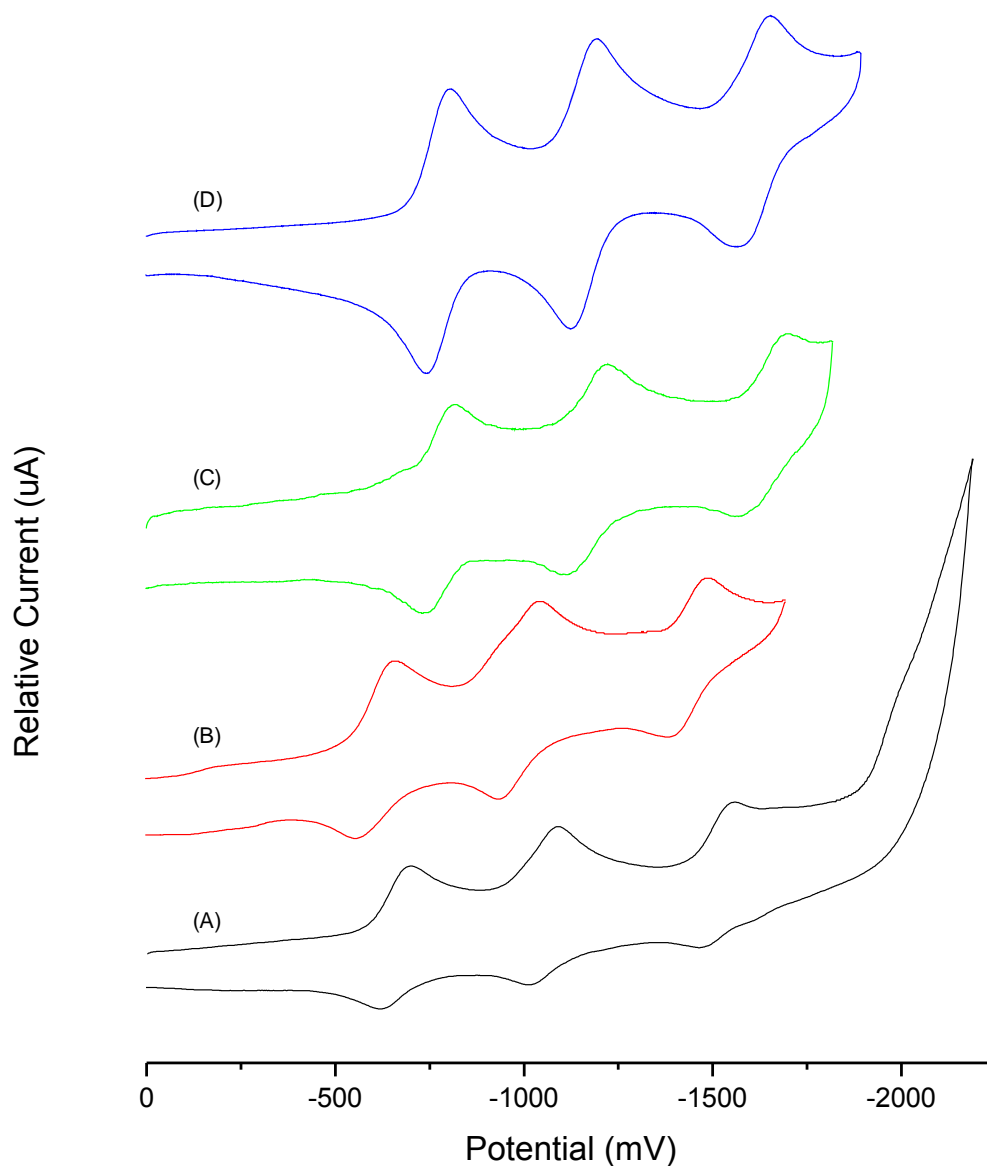


Figure 2 Cyclic voltammetric responses recorded at a glassy carbon working electrode on dichloromethane solution containing, 0.1 M TBPF₆ of (A) C₆₀ (saturated solution), and traces of decamethylferrocene (Fc) scan rate 100 mV/s. The $E_{1/2}$ for Fc/Fc⁺ is 339 mV. The $E_{1/2}$ for C₆₀ are -998, -1391 and -1860 mV vs. Fc/Fc⁺, (B) (η^2 -C₆₀)Cr(CO)₅ (saturated solution), and traces of decamethylferrocene (Fc) scan rate 100 mV/s. The $E_{1/2}$ for Fc/Fc⁺ is 385 mV. The $E_{1/2}$ for (η^2 -C₆₀)Cr(CO)₅ are -996, -1380 and -1839 mV vs. Fc/Fc⁺, (C) (η^2 -C₆₀)Mo(CO)₅ (saturated solution), and traces of decamethylferrocene (Fc) scan rate 100 mV/s. The $E_{1/2}$ for Fc/Fc⁺ is 218 mV. The $E_{1/2}$ for (η^2 -C₆₀)Mo(CO)₅ are -977, -1411 and -1862 mV vs. Fc/Fc⁺ and (D) (η^2 -C₆₀)W(CO)₅ (saturated solution), and traces of decamethylferrocene (Fc) scan rate 100 mV/s. The $E_{1/2}$ for Fc/Fc⁺ is 313 mV. The $E_{1/2}$ for (η^2 -C₆₀)W(CO)₅ are -982, -1374 and -1844 mV vs. Fc/Fc⁺. All recorded at T = 20 °C.

Table 1 Half-wave potentials ($E_{1/2}$) of the $(\eta^2\text{-C}_{60})\text{M}(\text{CO})_5$ complexes ($\text{M} = \text{Cr}, \text{Mo}, \text{W}$) and C_{60} in dichloromethane at room temperature^a.

Complex	$E_{1/2, \text{red}}^1$ (mV) ^a	$E_{1/2, \text{red}}^2$ (mV) ^a	$E_{1/2, \text{red}}^3$ (mV) ^a
C_{60}	-998	-1391	-1860
$(\eta^2\text{-C}_{60})\text{Cr}(\text{CO})_5$	-996	-1380	-1839
$(\eta^2\text{-C}_{60})\text{Mo}(\text{CO})_5$	-977	-1411	-1862
$(\eta^2\text{-C}_{60})\text{W}(\text{CO})_5$	-982	-1374	-1844

^a All half wave potential are in mV vs. Fc/Fc^+ at 100 mV/s scan rate. The solvent/supporting electrolyte mixture is 0.1M $\text{TBPF}_6/\text{CH}_2\text{Cl}_2$.

The cyclic voltammogram of the complexes $(\eta^2\text{-C}_{60})\text{M}(\text{CO})_5$ in dichloromethane, exhibit three reversible one-electron reduction waves corresponding to the formation of $(\eta^2\text{-C}_{60})\text{M}(\text{CO})_5^-$, $(\eta^2\text{-C}_{60})\text{M}(\text{CO})_5^{2-}$ and $(\eta^2\text{-C}_{60})\text{M}(\text{CO})_5^{3-}$, respectively. The observed reductions are reversible suggesting that they are [60]fullerene-centered [28]. Except for the second and third reduction waves of $(\eta^2\text{-C}_{60})\text{Mo}(\text{CO})_5$, they are all shifted to positive potentials relative to the corresponding potentials of the uncoordinated [60]fullerene. This observation is at variance with the observed negative shift potential (cathodic shift) for other [60]fullerene–M ($\text{M} = \text{Mo}, \text{W}$) complexes with non-CO co-coordinated ligands [18-21]. For example, observation of cathodic shifts of approximately 0.2 V for $\text{M}(\eta^2\text{-C}_{60})(\text{CO})_2(\text{phen})(\text{dbm})$ [18,19], $\text{M}(\eta^2\text{-C}_{60})(\text{CO})_3(\text{dppe})$ [20], $\text{M}(\eta^2\text{-C}_{60})(\text{CO})_3(\text{dppb})$ [20], and $\text{M}(\eta^2\text{-C}_{60})(\text{CO})_3(\text{dppf})$ [21] complexes ($\text{phen} = 1, 10$ -phenanthroline, $\text{dbm} =$ dibutyl maleate, $\text{dppe} =$ bis-(1,2-diphenylphosphino)ethane, $\text{dppb} =$ bis-(1,2-diphenylphosphino)benzene, $\text{dppf} = 1, 1'$ -(diphenylphosphino)ferrocene) suggests that the extent of the shift is independent of the number and nature of co-coordinated ligands. Positive shifts are reported for the iron complexes $[(\eta^2\text{-C}_{60})(\mu\text{-S}_2)\text{Fe}_2(\text{CO})_6]$, $[(\eta^2\text{-C}_{60})(\mu\text{-S}_2)\text{Fe}_2(\text{CO})_6]_2$, $[(\eta^2\text{-C}_{60})(\mu\text{-S}_2)\text{Fe}_2(\text{CO})_6]_3$ [27]. It has been suggested that the inductive effect exerted by the metal on [60]fullerene and the disruption of C=C double bond conjugation caused by [60]fullerene π -back electron acceptance are opposed effects that cancel each other to some

extent. This means that the metal in the complex $(\eta^2\text{-C}_{60})\text{M}(\text{CO})_5$ has the capacity of having a spherical distortion of the C_{60} but to a similar extent π -back electron acceptance which disfavors the reduction of the complex and is reflected in the negative shifts. Also the more π -back electron acceptance from the M-C_{60} moiety the lesser π -back electron acceptance from the carbonyl *trans* to the C_{60} which enhances the bond character of the $\text{C}\equiv\text{O}$ group thus making it more rigid. The inductive effect can either disfavor or favor the reduction of [60]fullerene, whereas disruption of $\text{C}=\text{C}$ conjugation by [60]fullerene π -back electron acceptance disfavors reduction. In the present study the first one-electron reduction in each $(\eta^2\text{-C}_{60})\text{M}(\text{CO})_5$ complex is shifted to positive values with respect to uncoordinated [60]fullerene. In the case of $(\eta^2\text{-C}_{60})\text{Mo}(\text{CO})_5$, a cathodic shift is observed in the second reduction wave ($\Delta E_{1/2}^2 = -20$ mV), while the cathodic shift of the third reduction band is small ($\Delta E_{1/2}^3 = -2$ mV). The shifts on the reductions of $(\eta^2\text{-C}_{60})\text{M}(\text{CO})_5$ complexes are positive despite the fact that [60]fullerene is a good π -acceptor. This positive potential shift may be attributable to metal coordination. Donation of electron density into the triply-degenerate [60]fullerene LUMOs should lower the energy of at least one of the triply-degenerate LUMOs so that reduction of the [60]fullerene moiety in [60]fullerene– M complexes occurs at a lower energy relative to uncoordinated [60]fullerene [90]. No direct correlation was found between the $\Delta E_{1/2}^1$ values with the M-L ($\text{L} = \text{C}_{60}$, benzene) bond enthalpies nor with the carbonyl stretching wavenumber of the carbonyl *trans* to C_{60} in $(\eta^2\text{-C}_{60})\text{M}(\text{CO})_5$ complexes.

2.4. Electrochemical detection of the C₆₀-Piperidine Adduct

2.4.1. Preparation of the C₆₀-piperidine Adduct

The adduct (C₅H₁₀N)₃(H)₃C₆₀ was prepared at room temperature from [60]fullerene and piperidine. In a 100 mL round bottom flask equipped with a magnetic stirring bar, a condenser, and a nitrogen inlet 0.03072g (0.043 mmol) of [60]fullerene and 0.03630g (0.43 mmol) of piperidine were dissolved in 25 mL of nitrogen-purged and dried benzene (Aldrich). Nitrogen was bubbled through the resulting solution during approximately 10 minutes to displace oxygen from the reaction mixture. The reaction mixture was then stirred during 24 hours at room temperature under a slow and continuous flow of nitrogen. Benzene was then vacuum-distilled from the reaction mixture. The resulting brownish solid was then dissolved in approximately 10 mL of carbon disulfide (CS₂). Thin layer chromatography analysis showed two components. The two components were separated by column chromatography. The first component was eluted using carbon disulfide and identified as [60]fullerene from its distinctive purple color and by comparing its R_f value with the corresponding value of an actual sample. The other component, later identified as (C₅H₁₀N)₃(H)₃C₆₀, was eluted using dichloromethane. Dichloromethane was then nitrogen-purged to obtain 0.01223 g (0.013 mmol, *ca.* 29 % yield) of a bright reddish-yellow solid.

2.4.2. Electrochemical Studies of C₆₀-Piperidine Adduct

The adduct dissolved in dichloromethane exhibits one irreversible reduction wave at a potential value of -487 mV and two reversible one-electron reduction waves at half peak potential values ($E_{1/2}$) of -729 mV and -1188 mV (Figure 3). All the reported $E_{1/2}$ values are relative to the $E_{1/2}$ value of ferrocene. The $E_{1/2}$ values for the adduct and for uncoordinated [60]fullerene (Figure 3) are presented in Table 2. The reduction waves of the adduct are shifted to positive potentials relative to the corresponding potentials of the uncoordinated [60]fullerene, suggesting that the adduct has a higher electron affinity than uncoordinated [60]fullerene.

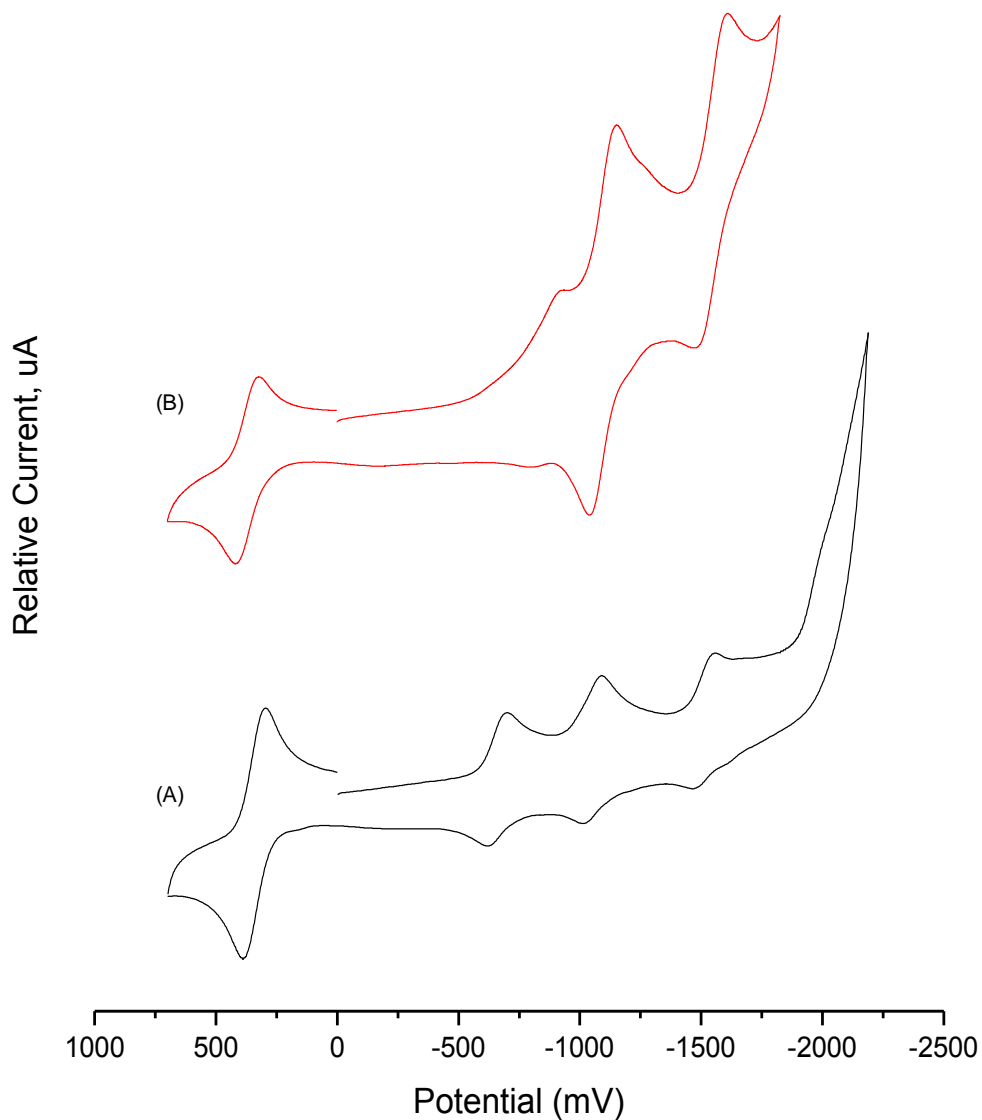


Figure 3 Cyclic voltammetric responses recorded at a glassy carbon working electrode on dichloromethane solution containing, 0.1 M TBPf6 for (A) C_{60} (saturated solution), and traces of decamethylferrocene (Fc) scan rate 100 mV/s. The $E_{1/2}$ for Fc/Fc⁺ is 339 mV. The $E_{1/2}$ for C_{60} are -998, -1391 and -1860 mV vs. Fc/Fc⁺ and (B) $C_{60}(H)_3(NC_5H_{10})_3$ (saturated solution), and traces of decamethylferrocene (Fc) scan rate 100 mV/s. The $E_{1/2}$ for Fc/Fc⁺ is 373 mV. The $E_{1/2}$ for $C_{60}(H)_3(NC_5H_{10})_3$ are -487, -729, and -1188 mV vs. Fc/Fc⁺. T = 20 °C

Table 2 $E_{1/2}^n$ values for C_{60} and $C_{60}(C_5H_{10}N)_3(H)_3$ and $\Delta E_{1/2}^n$ values for $C_{60}(C_5H_{10}N)_3(H)_3$.

Potential	C_{60}	$C_{60}(H)_3(NC_5H_{10})_3$	$\Delta E_{1/2}$
$E_{1/2, red}^1$ (mV)	-998	-487	+511
$E_{1/2, red}^2$ (mV)	-1391	-729	+242
$E_{1/2, red}^3$ (mV)	-1860	-1188	+672

2.4.3. Results and Discussion

Solutions containing [60]fullerene possess an intense violet color, which after reaction with piperidine becomes reddish-orange in color. A reddish-orange solid is obtained after separation of unreacted [60]fullerene from the reaction mixture by column chromatography followed by evaporation of the solvent.

The reaction product was characterized by elemental analysis, infrared spectroscopy, and cyclic voltammetry. Elemental analysis by combustion, performed by Midwest Microlab, LLC, showed formation of ash as a residue in two of the three samples submitted for analysis. The report of the third sample analysis is consistent with an adduct containing three piperidine molecule per molecule of C₆₀. The composition calculated for C₈₀H₃₃N₃ is %C, 90.54; %H, 4.18; %N, 5.28. The reported composition was %C, 90.24; %H, 4.38; %N, 5.35.

The infrared spectra of piperidine, [60]fullerene-piperidine adduct, and [60]fullerene are presented in Figure 4.

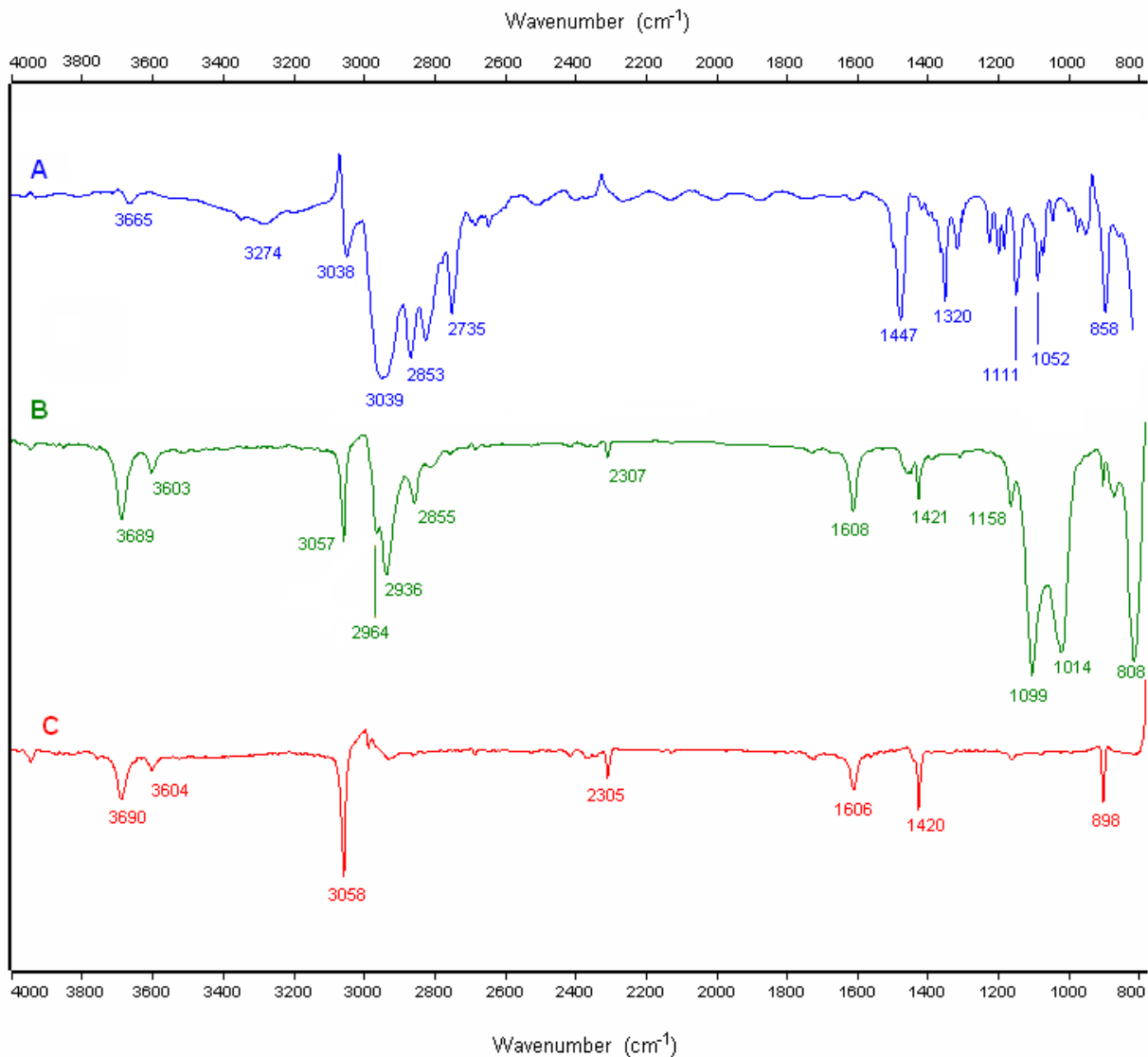


Figure 4 Infrared spectra for (A) piperidine, (B) *n*-amine-fullerene adduct and (C) fullerene in dichloromethane.

A close examination of these spectra show that: i) the band in the N-H stretching region located at 3600 cm^{-1} in the piperidine spectrum (A) is absent in the corresponding spectrum of the adduct (B), ii) the bands in the C-H stretching region from 2964 cm^{-1} to 2935 cm^{-1} in spectrum A and B suggest formation of C-H bonds (for example the band at 2964 cm^{-1} in B is assigned to allylic $\text{C}_{60}\text{-H}$ bonds), iii) the bands in the N-C stretching region from 1099 cm^{-1} to 1014 cm^{-1} in B are assigned to two types of N-C bonds.

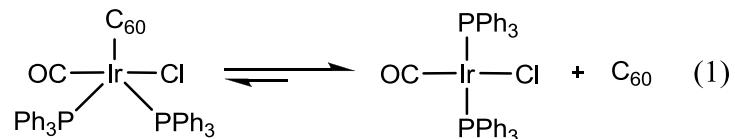
The reduction shifts, $\Delta E_{1/2}$ ($\Delta E_{1/2} = E_{1/2,\text{functionalizedC60}} - E_{1/2,\text{C60}}$), are given in Table 2. Electrochemistry of [60]fullerene-metal complexes is instructive about how functionalization of [60]fullerene affects its reduction waves. Although positive $\Delta E_{1/2}$ are reported for [60]fullerene-metal complexes, the general trend is that upon metal coordination, $\Delta E_{1/2}$ values are negative. It seems that an interplay of not easily separated structural and electronic effects determine whether $\Delta E_{1/2}$ values are positive or negative. For example, interruption of C=C bond conjugation caused by functionalization disfavor reduction of the [60]fullerene moiety, thus causing negative $\Delta E_{1/2}$ values. In [60]fullerene-metal complexes the interruption of C=C bond conjugation is caused by dihapto-C₆₀-metal coordination. Inductive effects such as σ -electron donation and σ -electron withdrawal should favor and disfavor reduction, respectively. Stabilization of one or two of the triply-degenerate [60]fullerene LUMOs caused by [60]fullerene π -back electron acceptance donated from an organometallic group attached to its curved surface, should favor reduction.

3. Electrochemical Detection of Ir(CO)(PPh₃)₂Cl coordinated to C₆₀⁴⁻, C₆₀⁵⁻ and C₆₀⁶⁻ Species.

3.1. Introduction

The preferred dihapto (η^2) mode of C₆₀-transition metal coordination resembling an olefin-metal bond [10-27] is a consequence of [60]fullerene's capacity to participate in π -back bonding [12-24] with transition metals and to its radially-oriented p molecular orbitals [91-93], preventing higher hapticities [94-96]. [60]fullerene's high electron affinity [81-88] also facilitates its organometallic functionalization. [60]fullerene has the potential to modify and improve the efficiency of existing organometallic catalysts by altering their chemical reactivity. For example, C₆₀ can labilize bonds of co-coordinated ligands [14], and it has the potential to stabilize electron rich transition states or intermediates species involved in the catalysts ligand exchange reactions [15].

Coordinatively-unsaturated organometallic catalysts such as the Vaska's complex (**1Ir**) and Wilkinson's catalyst (**1Cl**) are candidates for chemical modification by C₆₀. The preparation of the C₆₀-coordinated Vaska's complex ((η^2 -C₆₀)Ir(CO)(PPh₃)₂(Cl) (**2Ir**) is reported in the chemical literature [54]. The chemical characterization of (η^2 -C₆₀)Ir(CO)(PPh₃)₂(Cl) was based on crystallographic data, elemental analysis, and solid phase IR spectroscopy. However, no characterization of the complex in solution has been reported. It seems that in solution the equilibrium described by eq. 1 favors the dissociated and solvated species



[60]fullerene reacts like an electro-deficient olefin [14]. For example, the coordination of C₆₀ to Ir and the C-Ir bond lengths (2.19(2) Å) in **2Ir** resemble the coordination and bond lengths

(2.15(1) Å) in $\text{Ir}(\text{CO})(\text{PPh}_3)_2(\text{Cl})(\text{TCNE})$ (TCNE = tetracyanoethylene) [54]. However, unlike **2Ir**, the complex $\text{Ir}(\text{CO})(\text{PPh}_3)_2(\text{Cl})(\text{TCNE})$ is stable in solution. Thus, one is tempted to ascribe labilization of the C_{60} -Ir dihapto bond in $(\eta^2\text{-C}_{60})\text{Ir}(\text{CO})(\text{PPh}_3)_2(\text{Cl})$ to steric repulsions from the two co-coordinated triphenylphosphine ligands. Interestingly, it seems that steric repulsion between C_{60} and the two triphenylphosphine ligands is mitigated by the folding back of the two phosphine ligands. In the crystal structure of $(\eta^2\text{-C}_{60})\text{Ir}(\text{CO})(\text{PPh}_3)_2(\text{Cl})$ the two phosphine ligands are folded back and positioned nearly *cis* with respect to each other, different from their original *trans* positions in $\text{Ir}(\text{CO})\text{Cl}(\text{PPh}_3)_2$. On the other hand, the carbonyl and chloride ligands retain their original relative *trans* positions [54].

Herein, it is being reported infrared spectroscopy evidence of the C_{60} -coordinated Vaska's catalyst formed in C_{60} -saturated liquid solution and the electrochemical detection of $\text{Ir}(\text{CO})(\text{PPh}_3)_2(\text{Cl})(\text{C}_{60}^{4-})$ and $\text{Ir}(\text{CO})(\text{PPh}_3)_2(\text{Cl})(\text{C}_{60}^{5-})$ species formed in the solvent displacement reactions on $\text{Ir}(\text{CO})(\text{PPh}_3)_2(\text{Cl})(\text{CH}_3\text{CN})$ by C_{60}^{4-} and C_{60}^{5-} anions, respectively.

3.2. Materials and Methods

3.2.1. General

The complex $(\eta^2\text{-C}_{60})\text{Ir}(\text{CO})(\text{PPh}_3)_2(\text{Cl})$ was prepared from [60]fullerene, and $\text{Ir}(\text{CO})(\text{PPh}_3)_2(\text{Cl})$. The [60]fullerene-piperidine adducts were also prepared from [60]fullerene and piperidine as purchased. All reagents were purchased from Aldrich. Benzene was purchased from Aldrich and was distilled under sodium and fractionally distilled under nitrogen. In order to prevent oxidation of the reagents and complexes, all reactions were carried out under a nitrogen atmosphere. Group theory concepts were applied in order to predict the infrared active CO-stretching bands (ν_{CO}) for CO containing complexes [89]. Infrared spectra was obtained on a

Bruker Vector 22 Fourier transform infrared spectrophotometer equipped with a KBr cell with a 0.10 mm light path.

3.2.2. Preparation of $(\eta^2\text{-C}_{60})\text{Ir}(\text{CO})(\text{PPh}_3)_2\text{Cl}$

The complex $(\eta^2\text{-C}_{60})\text{Ir}(\text{CO})(\text{PPh}_3)_2\text{Cl}$ was prepared from $\text{Ir}(\text{CO})(\text{PPh}_3)_2\text{Cl}$ and C_{60} following a method reported by Balch, Catalano, and Lee [54]. In a 15 mL round bottom flask equipped with a magnetic stirrer and a nitrogen inlet, 20.28 mg (25.99 μmol) of $\text{Ir}(\text{CO})(\text{PPh}_3)_2\text{Cl}$ and 18.60 mg (25.83 μmol) of C_{60} were dissolved in 10 mL of benzene. This mixture was purged with nitrogen and paced under a slow flow of nitrogen for approximately 1.5 hours. After a few minutes, the color of the mixture became dark green. The solvent was evaporated from the mixture by slowly bubbling nitrogen thru the mixture producing an olive-green solid. The complex $(\eta^2\text{-C}_{60})\text{Ir}(\text{CO})(\text{PPh}_3)_2\text{Cl}$ showed the reported characteristic ν_{CO} at 2012 cm^{-1} [54].

3.2.3. Electrochemical Studies

Electrochemical measurements were performed at ambient temperature and low pressure using a BAS CV-50W voltammetric work station. A high vacuum line was used to transfer and mix reagents. A dry 1:5 acetonitrile:toluene mixture that was prepared, transferred and stored over dried silica under vacuum was used as solvent. The silica was dried by heating with a Bunsen burner under high vacuum. The supporting electrolyte, tetrabutylammonium hexafluorophosphate (TBPF_6) (Aldrich), was recrystallized from an ethanol/ H_2O (95: 5) solution and dried under vacuum prior to use. Ferrocene (Fc)/ferrocenium (Fc^+) couple was used as internal reference in all measurements. A three-electrode configuration consisting of a glassy carbon working electrode (3 mm in diameter), a platinum wire (Pt-wire) counter electrode, and a non-aqueous silver pseudo reference electrode was used to perform the electrochemical

experiments. The non-aqueous silver pseudo-reference electrode consists of a silver wire inside a 4mm (O.D.) PyrexTM tubing which contains a small amount of a 0.1 M TBPF₆ solution in the 1:5 acetonitrile:toluene mixture and separated from the bulk solution by a Vycor glass frit located at the tip of the tube. This electrode configuration prevents peak potential drift due to small changes in the solution ionic strength during the electrochemical measurements. The working electrode was polished before use with a 0.25 μm diamond polishing compound (Metadi II) purchased from Buehler and a microcloth (BAS) and sonicated for a few seconds in deionized water to remove adsorbed polishing materials. The Pt-wire was cleaned by exposing it to a flame for approximately 30 s and the silver wire was rinsed with acetone (purity ≥99.9%) and deionized water to remove impurities.

3.3. Results and Discussion

3.3.1. Infrared Spectroscopy Characterization

The IR spectra in the CO stretching region (ν_{CO}) of Ir(CO)(PPh₃)₂(Cl), and Ir(CO)(PPh₃)₂(Cl)(C₆₀) are presented in Figure 5. Each ν_{CO} band was unequivocally assigned by comparing the spectrum of each species to actual samples or literature value [54]. The ν_{CO} band at 2012 cm⁻¹ of Ir(CO)(PPh₃)₂(Cl)(C₆₀) is observed only when Ir(CO)(PPh₃)₂(Cl)(C₆₀) is dissolved in C₆₀-saturated solutions of solvents where C₆₀ has a relatively high solubility such as benzene and toluene [97]. This band is absent when Ir(CO)(PPh₃)₂(Cl)(C₆₀) is dissolved in pure benzene, toluene, or dichloromethane, indicating that the equilibrium described in eq. 1 favors the dissociated species Ir(CO)(PPh₃)₂(Cl) and C₆₀. Thus, experiments for electrochemical characterization of Ir(CO)(PPh₃)₂(Cl)(C₆₀) must be conducted under flooding conditions where [C₆₀] >> [Ir(CO)(PPh₃)₂(Cl)(C₆₀)] to drive the equilibrium toward Ir(CO)(PPh₃)₂(Cl)(C₆₀).

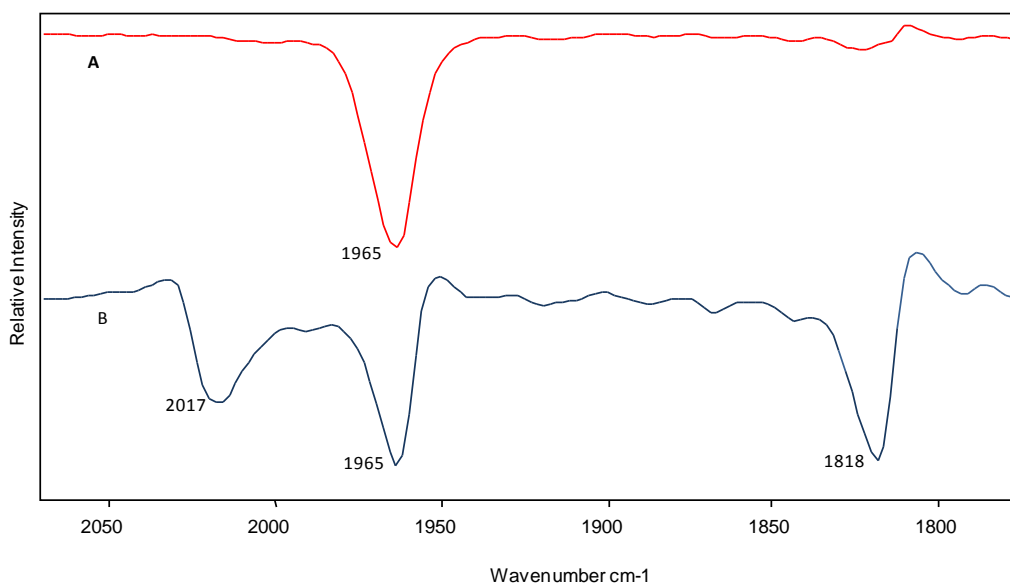
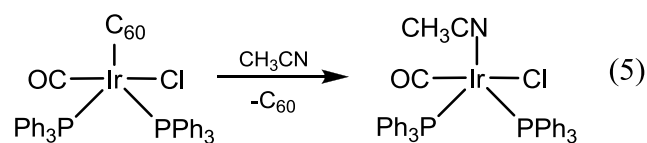


Figure 5 Infrared spectrum in benzene of: A. $\text{Ir}(\text{CO})(\text{PPh}_3)_2\text{Cl}$ and B. $(\eta^2\text{-C}_{60})\text{Ir}(\text{CO})(\text{PPh}_3)_2\text{Cl}$ in a C_{60} -saturated solution.

3.3.2. Electrochemical Studies

Attempts to conduct CV and OSWV experiments on $\text{Ir}(\text{CO})(\text{PPh}_3)_2(\text{Cl})(\text{C}_{60})$ on most solvents were unsuccessful either because C_{60} or the supporting electrolyte, TBPF_6 , were insoluble in the solvents and mixtures of solvents used. For example, in 1, 2-dichloroethane TBPF_6 is soluble enough to attain concentrations in the vicinity of 0.1 M necessary for the electrochemical experiments, but C_{60} is only soluble at traces concentrations. Likewise, in toluene [60]fullerene's solubility is relatively high (2.8 mg/mL) but TBPF_6 's is only sparingly soluble. It was promising that the solubility of C_{60} and TBPF_6 in a 1:5 (v/v) acetonitrile:toluene mixture were high enough and suitable for electrochemical experiments as reported [28d, 54-55, 97]. However, acetonitrile acted as a ligand capable of coordinating Ir according to eq. 5 at the experimental conditions of the electrochemical experiments.



The cyclic voltammogram of C_{60} in a 1:5 acetonitrile:toluene mixture at 25 °C is presented in Figure 6 (6A). Five reduction waves at potentials $E_{1/2}^n$ values relative to Fc/Fc^+ (-986, -1397, -1913, -2429, and -2921 mV) are close to values reported for experiments under similar conditions but at lower temperature (-10°C) [28d-e]. Figure 6 (6B) also displays a series of cyclic voltammograms of the same mixture (C_{60} in a 1:5 acetonitrile:toluene) after addition of 15.9 mg of $Ir(CO)(PPh_3)_2(Cl)$. Examination of the voltammogram 6B shows two new irreversible reductions waves, not present in the voltammogram of free C_{60} , at $E_{1/2}$ values of -2617 and -3084 mV. Analysis of voltammogram 6D obtained by performing a scanning up to the potential corresponding to the third one-electron reduction of C_{60} demonstrates that the first three reductions waves are fully reversible. Likewise, the corresponding experiment up to the fourth reduction wave of C_{60} (voltammogram labeled as 6C) demonstrates that fourth wave is quasi reversible. This information indicates that successive electrochemical formation of $Ir(CO)(PPh_3)_2(Cl)(C_{60}^{-5})$ and $Ir(CO)(PPh_3)_2(Cl)(C_{60}^{-6})$ takes place after electrochemical formation of C_{60}^{4-} . Osteryoung square wave voltammogrammetry was used to maximize Figure 6B seven reduction/oxidation waves' intensities.

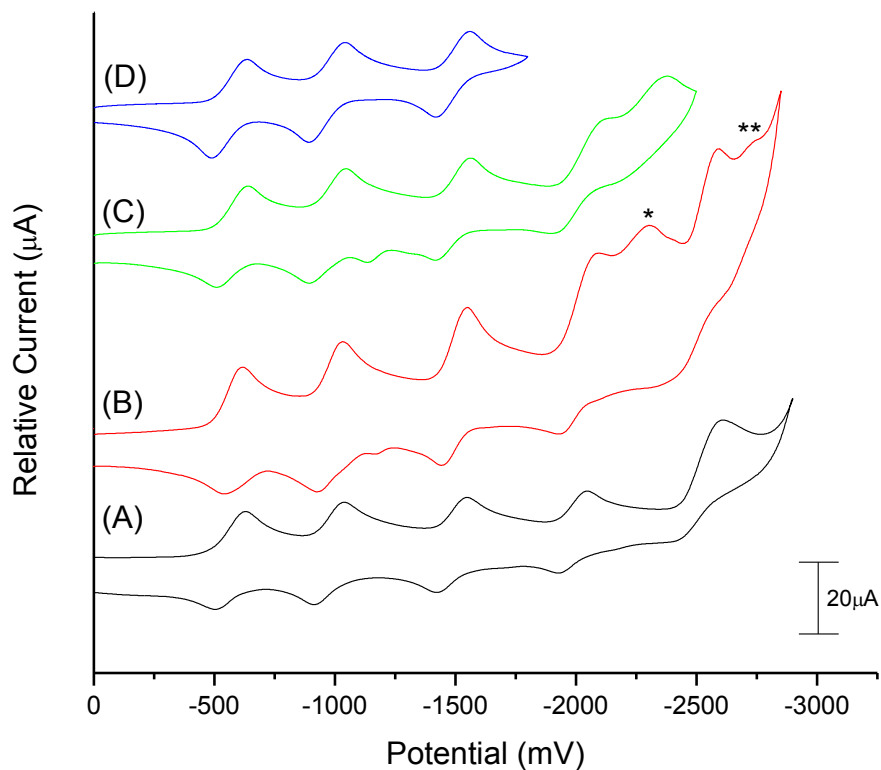


Figure 6 Cyclic voltammometric responses of (A) C_{60} , (B) mixture of C_{60} , (*) $Ir(CO)(PPh_3)_2Cl(C_{60}^{5-})$ and (**) $Ir(CO)(PPh_3)_2Cl(C_{60}^{6-})$ species, (C) C_{60} , showing the first four reduction waves, and (D) C_{60} , showing the first three reduction waves in a acetonitrile:toluene (1:5) solution containing 0.1M of $TBPF_6$ at a 100 mV/s scan rate. $T=20^\circ C$

Figure 7 depicts the corresponding OSWV electrochemical responses of the mixture used to obtain voltammogram 6B in Figure 6, showing the waves ascribed to successive one-electron reduction of $Ir(CO)(PPh_3)_2Cl(C_{60}^{4-})$ and $Ir(CO)(PPh_3)_2Cl(C_{60}^{5-})$ species. The small OSWV wave after the third reduction/oxidation cycle (*ca.* -1750 mV) may indicate one-electron reduction/oxidation on traces of $Ir(CO)(PPh_3)_2Cl(C_{60}^{3-})$. This low-intensity signal is only detected in OSWV because combination of the reduction and oxidation waves increases the signal intensity of $Ir(CO)(PPh_3)_2Cl(C_{60}^{3-})$ present in trace concentration.

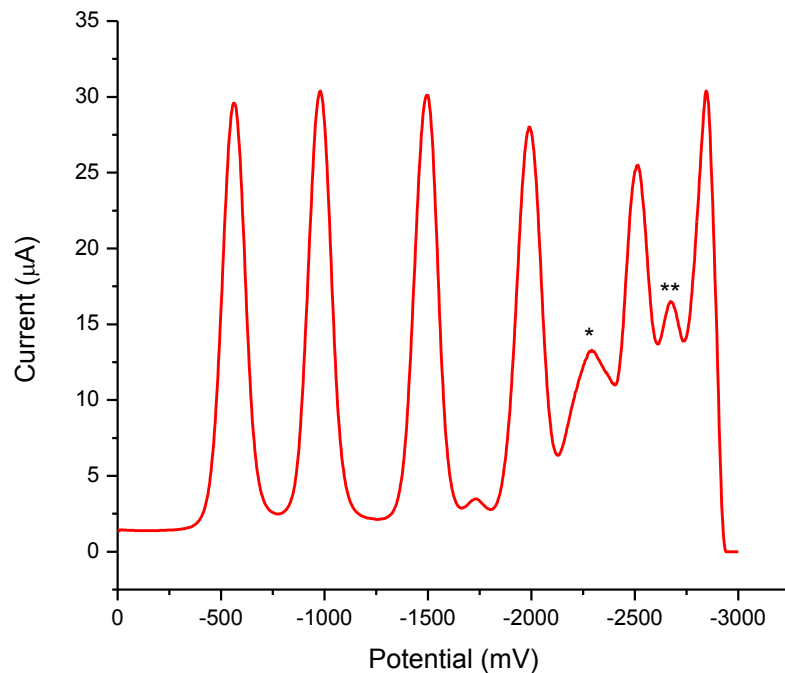
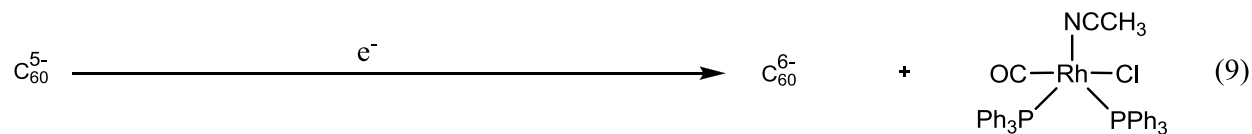
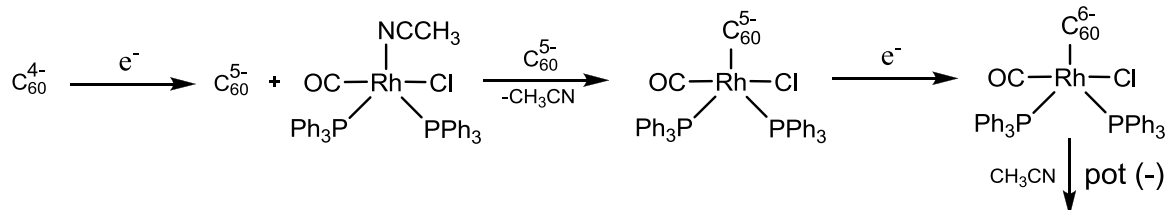
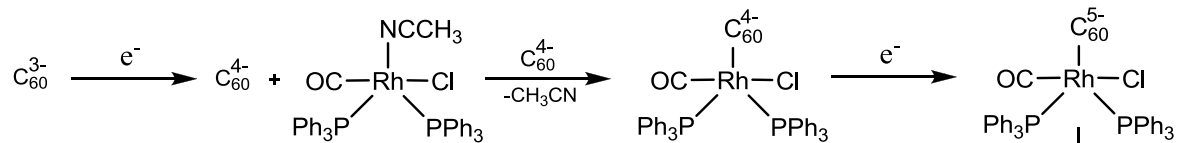
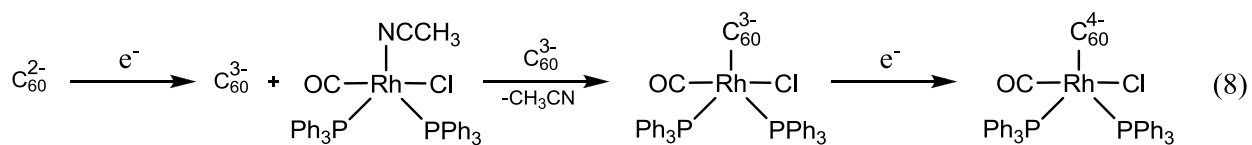
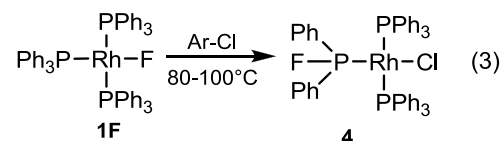


Figure 7 Osteryoung square wave voltammogram of a mixture of C_{60} and $Ir(CO)(PPh_3)_2Cl$ showing the waves of the suggested (*) $Ir(CO)(PPh_3)_2Cl(C_{60}^{5-})$ and (**) $Ir(CO)(PPh_3)_2Cl(C_{60}^{6-})$ species in 1:5 (v/v) acetonitrile:toluene with $TBPF_6$ as a supporting electrolyte at $25^\circ C$ at a 100 mV/s scan rate. $T=20^\circ C$

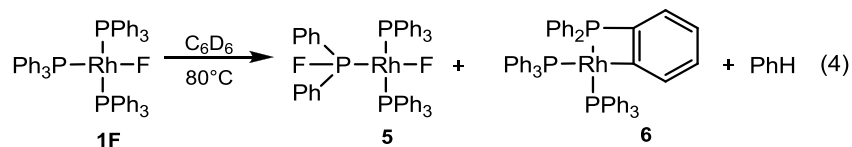
Although spectroscopic evidence such as solid state ^{13}C NMR and ESR spectroscopy is necessary for unequivocal assignments of the reductions waves at $E_{1/2} = -2617$ and -3084 mV , *in situ* experiments suggest that these new reduction waves correspond to consecutive one-electro reductions of the complexes $Ir(CO)(PPh_3)_2(Cl)(C_{60}^{4+})$ and $Ir(CO)(PPh_3)_2(Cl)(C_{60}^{5-})$ forming $Ir(CO)(PPh_3)_2(Cl)(C_{60}^{5-})$ and $Ir(CO)(PPh_3)_2(Cl)(C_{60}^{6-})$ upon reduction, respectively. It is being proposed that C_{60}^{3-} , C_{60}^{4-} and C_{60}^{5-} displaces acetonitrile from $Ir(CO)(PPh_3)_2(Cl)(CH_3CN)$ followed by one-electron electrochemical reductions according to eq. 6 thru 9.



countless stoichiometric and catalytic reactions which involve **1Cl** [69]. It was reported that unlike **1Cl** that was thought to produce $(\text{Ph}_3\text{P})_4\text{Rh}_2(\mu\text{-Cl})_2$ (**3Cl**) and traces of $(\text{Ph}_3\text{P})_2(\text{Ph})\text{Rh}(\text{Cl})_2$ as the sole products when dissolved and heated in aromatic solvents, **1F** exhibits a series of unexpected reactions [74-76]. Reactions of **1F** with Ar-Cl (Ar = Ph, p-tolyl) produce *trans*- $(\text{Ph}_3\text{P})_2\text{Rh}(\text{Ph}_2\text{PF})(\text{Cl})$ (**4**) and Ar-Ph (eq 3).



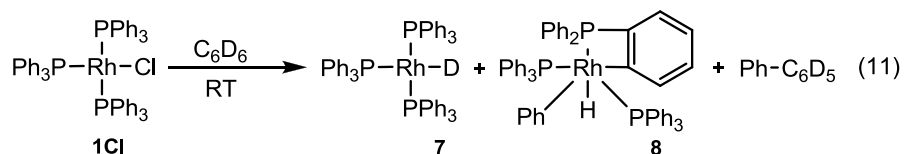
In C_6D_6 **1F** produces *trans*- $(\text{Ph}_3\text{P})_2\text{Rh}(\text{Ph}_2\text{PF})(\text{F})$ (**5**) and the long known cyclometalation product of insertion of rhodium into the hydrogen-carbon bond which occurs at the *ortho*-position $(\text{Ph}_3\text{P})_2\text{Rh}(\eta^2\text{-}(\text{C}_6\text{H}_4\text{PPh}_2))$ (**6**) (eq. 4) [74-76]. Cyclometalation reactions resulting on a d^8 complex of square planar structure have also reported for $(\text{Ph}_3\text{P})_3\text{M}(\text{Me})$ (M = Ru, Pd, Me = methyl). [68, 71, 99]



It was proposed that reactions in eq. 3 and eq. 4 proceed via rate determining reversible intramolecular P-Ph/Rh-F exchange [74, 75].

We are reporting that **1Cl** exhibits a similar activity under milder conditions than reported for **1F**. In addition to formation of the chloro-bridged dimer (**3Cl**), **1Cl** undergoes a series of reactions when it is dissolved in benzene (or in C_6D_6) at room temperature under nitrogen or under high vacuum. However, unlike **1F** that produces *trans*- $(\text{Ph}_3\text{P})_2\text{Rh}(\text{Ph}_2\text{PF})(\text{F})$ (**5**) and

$(\text{Ph}_3\text{P})_2\text{Rh}(\eta^2\text{-}(\text{C}_6\text{H}_4\text{PPh}_2))$ (**6**) when it is dissolved in C_6D_6 , **1Cl** produces $(\text{Ph}_3\text{P})_3\text{Rh}(\text{D})$ (**7**), $(\text{Ph}_3\text{P})_2\text{Rh}(\eta^2\text{-}(\text{C}_6\text{H}_4\text{PPh}_2))(\text{Ph})(\text{H})$ (**8**) and $\text{Ph-C}_6\text{D}_5$ when it is dissolved in C_6D_6 (eq 11).



Reported computational studies of the fluoro analogue of Wilkinson's Catalyst, $\text{Rh}(\text{PPh}_3)_3\text{F}$ have suggested that it undergoes intramolecular Ph/F exchange via metal-phosphido or metallophosphorane through an activated complex or a phosphonium salt described as Pathway 1 and 2, respectively [74, 75].

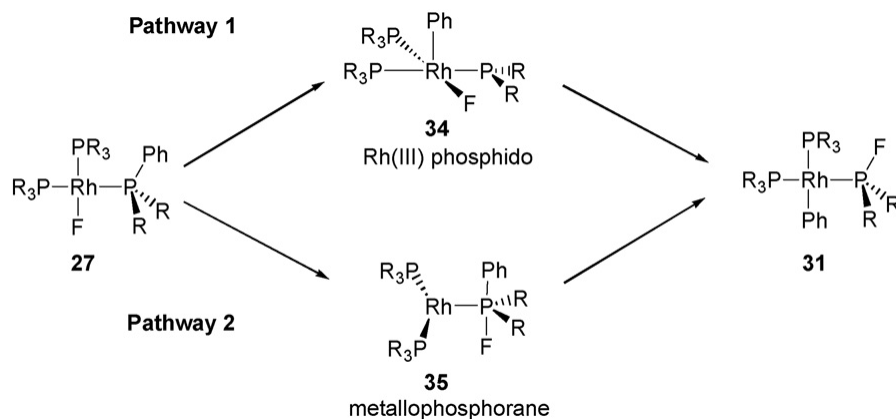


Figure 8 Proposed mechanistic pathways for the P-Ph/Rh-F exchange on **1F** (obtained from reference [74a])

These statements are in agreement with similar reported systems and with computational approaches [74-76]. The latter have been performed by modeling the transition states involved in the reaction. These species have been simplified by replacing phenyl rings attached to the phosphorous centers with hydrogen atoms [74, 100-105]. This simplified model has been reported in many theoretical organometallic chemistry studies involving Wilkinson's catalyst or similar catalyst. This substitution has become appealing to many researchers since it reduces

computational cost and time. However, here it is being reported the results from our laboratory using simplified and non-simplified models to study the reactions of Wilkinson's catalyst.

4.2. Materials and Methods

4.2.1. General

All chemicals were purchased from Aldrich and TCI America. Benzene was distilled under sodium and fractionally distilled under nitrogen prior to each analysis. In order to prevent oxidation of the reagents and complexes, all reactions were carried out under vacuo or nitrogen atmosphere. To be certain of the purity of the starting material and the ligands, ^1H NMR was used.

4.2.2. Kinetics Experiments

UV/Vis spectra were obtained using a Beckman Coulter DU 640 UV/vis spectrophotometer and a Perkin Elmer UV-visible Lambda 25 spectrophotometer. The temperature was set to be constant ($< \pm 0.1^\circ\text{C}$) using a Julabo F-12 heating and refrigerating circulator and a K/J Fluke digital thermometer equipped with a bead thermocouple was used for temperature control.

In order to select the radiation wavelength where the reaction progress was to be monitored, a UV/Vis scan was performed to a solution of the complex and the reacting ligand. The chosen wavelength to monitor the reactions progress was the wavelength where a significant change in absorbance was observed between reactants (reaction time = 0) and products (reaction time for completion). A solution of $\sim 1.30\text{mg}$ (*ca.* $1.40 \times 10^{-3}\text{mmol}$) of **1CI** in benzene was prepared and placed in a UV/Vis jacketed and temperature-controlled cell with a light path of 10 mm. Experiments were performed in absence and in presence of added PPh_3 ($1.68 - 165 \times 10^4$ M). The reaction of benzene and **1CI** was carried out under nitrogen and followed by UV/Vis at

370nm at temperatures ranging from 32-62°C. The reactions were monitored at constant temperature for 2000 to 7200s for fast and slow reactions, respectively (until no change in net absorbance).

4.2.3. ¹H NMR Experiments

To obtain the spectrum in Figure 2a, a sample of **1Cl** (1.08 mg) was dissolved in C₆D₆ (0.500 mL). The spectrum in Figure 2b was obtained from a solution containing **1Cl** (1.08 mg) and PPh₃ (4.14 mg) dissolved in C₆D₆ (0.500 mL). Spectra were referenced with C₆D₆ (99.96% D atom)/C₆H₆(0.04% H atom). ¹H NMR 1D sequence spectra were recorded on a 500 MHz Bruker Advance NMR 500 Spectrometer operated at 500 MHz using a 30 degree flip angle (pulse program zg30). Experiments were conducted under controlled temperature at 25°C and processed using a computer equipped with Linux software.

4.2.4. Computational Studies

4.2.4.1. General

Computational models for our studies are based on *ab initio* techniques within the density functional approximation (DFT) [106, 107]. The Becke three parameter hybrid functional termed B3LYP was used along with the LanL2DZ Gaussian basis set. Various stationary points for full geometry optimization were performed to all systems under study. The systems were prepared in various initial geometries in order to assure the determination of the lowest energy structure. Vibrational frequencies were determined to the optimized structure to ensure that it was either minima (positive eigenvalues) or a transition state (1 imaginary eigenvalue). All calculations were performed using Gaussian 03 and 09 [106, 107] installed on an SGI 2000 computer. Benzene-solvated single point optimizations and transition states were performed

using the SCRF parameter which takes into account the dielectric constant of benzene ($\epsilon=2.2706$) by using the keyword: `scrf=(solvent=benzene)`. This keyword requests that a calculation be performed in the presence of benzene by placing the solute in a cavity within the solvent reaction field [108].

4.2.4.2. Optimization of Single Point Energy Structures and Transition States Structures

Computational models used are based on *ab initio* techniques within the Density Functional Theory approximation (DFT). The large Rh molecules systems were optimized and characterized within Gaussian 03 and Gaussian 09 [106, 107] using the Becke three parameter hybrid functional termed B3LYP basis set along with LanL2DZ pseudopotential. Various stationary points for full geometry optimization were performed to all systems under study in order to assure the lowest energy structure.

For calculation purposes, the general reaction was used for all transition state calculations.



Where R is the reactant TS is the transition state and P is the product. The reactant and product can be also considered as intermediates of subsequent reactions. Before a transition state calculation was performed the reactant and product were fully optimized to a minimum. The optimized reactant and product were then used to find a transition state using the *Synchronous Transit-Guided Quasi-Newton* (STQN) Method. This method was developed by H. B. Schlegel and coworkers and consists of a linear synchronous transit or quadratic synchronous transit approach to draw near to the quadratic region around the transition state. Once this is accomplished a quasi-Newton or eigenvector-following algorithm is used to complete the optimization. In order to complete a minimization, it performs optimizations by default using

redundant internal coordinates. This method will converge efficiently to the actual transition structure using an empirical estimate of the Hessian and suitable starting structures. The three molecule specification is given by the QST3 option on the optimization (Opt) keyword. This specification is given in a single command file as reactant, product and transition state input [109].

4.3. Mechanistic Description of Unexpected Room Temperature C-H and P-C Bond Activation by Wilkinson's Catalyst.

4.3.1. Results

4.3.1.1. Kinetics Experiments of Rh(PPh₃)₃Cl

Plots of absorbance vs. time were biexponential decays. Data of the kinetics experiments were analyzed using *OriginLab*TM, a non-linear least-squares computer program. Consecutive pseudo-first order constant values were determined in triplicate from the biexponential functions that best described the absorbance *versus* time plots. The biexponential decays of two consecutive absorbance decay were classified as:

- Fast segment of the plot - a relatively rapid absorbance decay
- Slow segment of the plot - a relatively slow absorbance decay

Absorbance *versus* time plots for temperatures 32.1, 42.1, 56.1 and 62.1°C is shown in Figure 9.

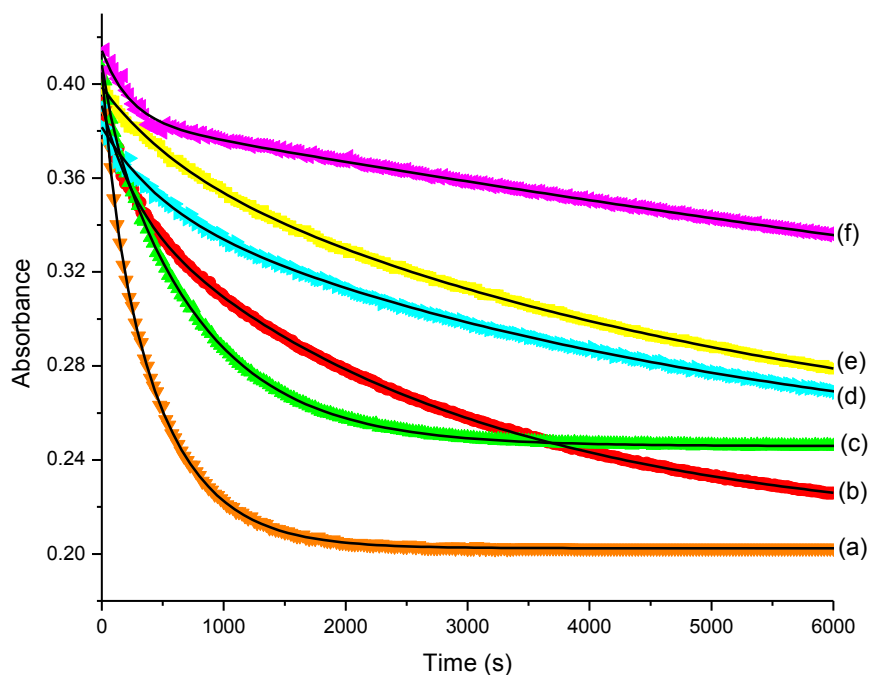


Figure 9 Plots of absorbance (370 nm) vs. time for reactions of **1Cl** with benzene. (a), at 62.1 °C; (b), at 42.1 °C; (c), at 56.1°C; (d), at 32.1 °C in presence added $[\text{PPh}_3]_{\text{added}} = 2.29 \times 10^{-4} \text{ M}$; (e), at 32.1 °C; (f), at 32.1 °C in presence added $[\text{PPh}_3]_{\text{added}} = 7.37 \times 10^{-3} \text{ M}$.

4.3.1.1.1. Kinetics Experiments of $\text{Rh}(\text{PPh}_3)_3\text{Cl}$ in Benzene

The rate constants k_1 and k_2 obtained from the data analysis were separated as k_{obsd} and k'_{obsd} for the fast and slow segment, respectively.

Table 3 Rate constant values for reactions of $\text{Rh}(\text{PPh}_3)_3\text{Cl}$ in Benzene.

Temp/K	$k_{\text{fast}} (\text{s}^{-1}) \times 10^4$	$k_{\text{slow}} (\text{s}^{-1}) \times 10^4$
305.25	15.6(9)	2.0(5)
315.25	42(1)	4.45(5)
329.25	114(8)	13.1(1)
335.25	120(8)	23.2(2)

4.3.1.1.2. Kinetics Experiments of $\text{Rh}(\text{PPh}_3)_3\text{Cl}$ in Benzene under flooding conditions where $[\text{PPh}_3]_{\text{added}}$ was constant

The rate constants k_1 and k_2 obtained from the data analysis were separated as k_{fast} and k_{slow} for the fast and slow segment, respectively.

Table 4 Rate constant values for reactions of $\text{Rh}(\text{PPh}_3)_3\text{Cl}$ and $[\text{PPh}_3]_{\text{added}}$ in benzene.

Temp/K	$[\text{PPh}_3]_{\text{added}} \times 10^4, \text{ M}$	$k_{\text{fast}} (\text{s}^{-1}) \times 10^4$	$k_{\text{slow}} (\text{s}^{-1}) \times 10^4$
305.25	1.68	29.1(8)	1.99(3)
	2.29	21.05(1)	1.97(6)
	3.81	19.42(5)	1.41(4)
	6.79	-	2.1(3)
	113	-	21(1)
	165	29(5)	37(2)
315.25	1.75	6.16(2)	4.13(2)
	16.2	2.2(1)	9.5(5)
	29.1	2.94(6)	14.0(7)
	126.8	2.0(6)	63(4)
	163.6	9.0(3)	72(8)
325.25	4.31	-	7.41(2)
	5.64	5(2)	5.50(2)
	14.2	7.320(3)	47(1)
	16.8	4.6(1)	19.1(6)
	45.2	2.0(4)	110.70(4)

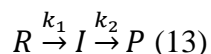
4.3.1.1.3. Data Analysis for Kinetics Experiments

The mathematical equation which better described the behavior of the experimental data points for reactions which consisted on two exponential decay segments is given by eq. 12

$$y = y_0 + A_1 e^{-x/t_1} + A_2 e^{-x/t_2} \quad (12)$$

where y is the dependent variable, y_0 is the y offset, A_1 and t_1 are the amplitude and the decay constant for the first segment, respectively, A_2 and t_2 are the amplitude and the decay constant for the second segment, respectively, and x is the independent variable. The computer program, *OriginTM*, performs the necessary parameters initialization. It also sets y_0 to an appropriate fixed number which is close to the asymptotic value of the y variable for large x values. The creation of the mathematical fit is produced by an iterative procedure. The mainframe fitter computes the Variance-Covariance matrix at each iteration using the previous iteration value. This matrix depends on the fitting function, the number of parameters and the data set assignments.

The analysis made by the computer program is adaptable to chemical kinetics equations for reactions consisting of a sequence of two pseudo-first order reactions which intermediate I builds and later falls eq. 13



were R is the reactant, which is the monitored species, I is the intermediate, in non steady state, P is the product(s), k_1 and k_2 are the pseudo-first-order rate constants that govern the path from R to I and I to P, respectively [110]. These conditions can be adapted to our kinetic conditions when absorbance (A) is the monitored physical property. Thus eq. 12 becomes eq. 14

$$A_t = \alpha e^{-k_1 t} + \beta e^{-k_2 t} + A_\infty \quad (14)$$

where A_t and A_∞ are absorbance at time t and at time infinity, respectively, and the coefficients α and β (eqs. 15 and 16) are constants whose values depend on k_1 , k_2 , and on the extinction coefficients (ε) of the chemical species involved (R, I and P) in the consecutive reactions [110]

$$\alpha = \frac{(\varepsilon_I - \varepsilon_R)k_1 + (\varepsilon_R - \varepsilon_P)k_2}{k_2 - k_1} \quad (15)$$

$$\beta = \frac{(\varepsilon_P - \varepsilon_I)k_1}{k_2 - k_1} [R]_0 \quad (16)$$

Thus, the observed biexponential decay of absorbance with time is mathematically described by eq. 14 and is equivalent to eq. 12 obtained from the computer program. Caution should be exercised on the correct assignment rate constants in a consecutive process which will be explained on Section 4.3.1.3.

4.3.1.2. ^1H NMR Spectroscopy Studies on $\text{Rh}(\text{PPh}_3)_3\text{Cl}$

The reactions' progress was monitored with ^1H NMR which permitted the correlation of the segments of the biexponential plots to specific chemical processes involved in the reactions of $\text{Rh}(\text{PPh}_3)_3\text{Cl}$ in benzene with added and non-added PPh_3 shown in Figure 10.

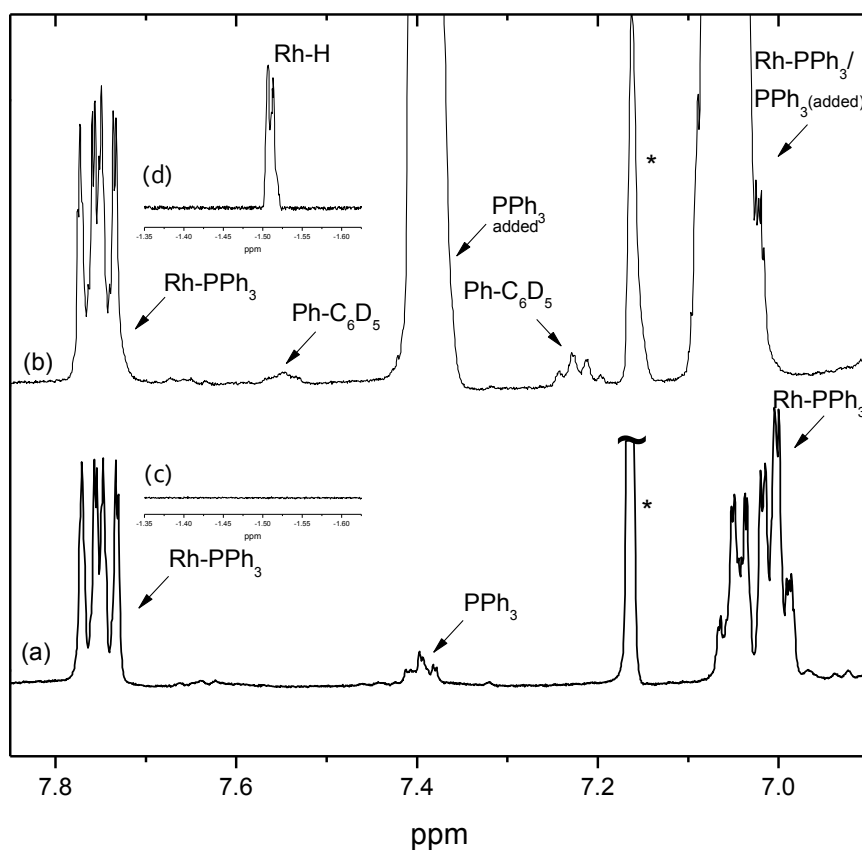


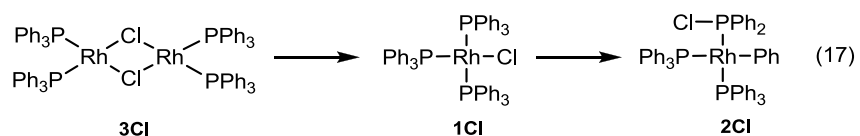
Figure 10 ^1H NMR spectra of (a) and (c) **1Cl** in $\text{C}_6\text{D}_6/\text{C}_6\text{H}_6^*(0.04\%)$, (b) and (d) **1Cl** in $\text{C}_6\text{D}_6/\text{PPh}_3$ solution $[\text{PPh}_3]_{\text{added}} = 0.0314 \text{ M}$.

Spectrum (a) was taken approximately 5 minutes after the mixture of **1Cl** dissolved in benzene- d_6 was placed in the NMR sample tube. The signals around 7.00 ppm and 7.75 ppm in spectrum (a) are attributed to the phosphorous-bonded phenyl (Ph) groups bonded to rhodium. The signal centered at 7.4 ppm in spectrum (a) is attributed to free PPh_3 which would be expected to form from **3Cl** forming **1Cl** and free PPh_3 .

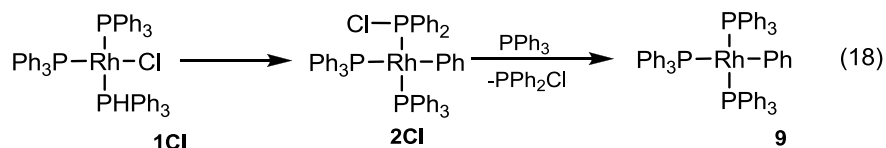
Spectrum (b) shows the ^1H NMR chemical shifts for added PPh_3 signals. The presence of two new signals at low field at 7.23 and 7.55 ppm, not observed in spectrum (a), are attributed to the formation of $\text{C}_6\text{D}_5\text{-Ph}$. These signals may differ from those of $\text{C}_6\text{H}_5\text{-Ph}$ since only one side of the molecule would exhibit resonance, thus making a different splitting pattern in the signal. At high field, spectrum (d) which is concomitant to spectrum (b), shows a signal at -1.5 ppm (doublet of doublets, not observed in spectrum (c)), consistent with the formation of a Rh-H hydride.

4.3.1.3. Interpretation of Kinetics Experiments and ^1H NMR Studies

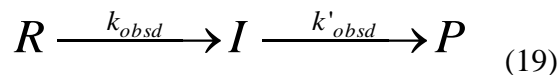
Assignment of pseudo-first order rate constant values, obtained from the biexponential plots of absorbance *versus* time of solutions of **1Cl** in benzene shown in Figure 9, to specific chemical processes depend on the experimental conditions (*vide infra*). In reactions of **1Cl** with benzene, the fast and slow segments of the plots were correlated to consecutive reconversions of **1Cl** from **3Cl** and to intramolecular P-Ph/Rh-Cl exchange [74] on **1Cl** producing **2Cl**, respectively (eq. 17).



Alternatively, under flooding conditions where $[\text{PPh}_3]_{\text{added}} \gg [\text{1Cl}]_0$, the fast and slow segments of the plots were correlated to intramolecular P-Ph/Rh-Cl exchange on **1Cl** and to intermolecular $\text{PPh}_3/\text{PPh}_2\text{Cl}$ exchange on **2Cl**. It is being proposed that the hydrido and Ph_2 species are respectively produced by a parallel intramolecular oxidative addition (cyclometalation) and intermolecular oxidative addition of benzene to $(\text{Ph}_3\text{P})_3\text{Rh}(\text{Ph})$ (**9**), that in turn is produced by intermolecular $\text{PPh}_3/\text{PPh}_2\text{Cl}$ exchange on **2Cl** (eq. 18).



The set of consecutive reactions in equations 17 and 18 can be expressed as a general set of consecutive first order reactions (eq. 13) where the pseudo-first-order rate constants k_1 and k_2 can be expressed as k_{obsd} and k'_{obsd} , respectively (eq. 19) [55, 110]. Equation 20 is the corresponding integrated and evaluated form of the rate law when absorbance is used to monitor the reaction progress also adapted from eq. 14. In equation 20, A_t and A_∞ are absorbance at time t and at time infinity, respectively, and the coefficients α and β are constants whose values depend on k_{obsd} , k'_{obsd} , and on the extinction coefficients of the chemical species involved in the consecutive reactions (eq. 15 and 16) [110].



$$A_t = \alpha e^{-k_{\text{obsd}}t} + \beta e^{-k'_{\text{obsd}}t} + A_\infty \quad (20)$$

Since the observed biexponential decay of absorbance with time is mathematically equivalent to eq. 20, correlation and assignment of k_{obsd} and k'_{obsd} to specific chemical reactions from k_{fast} and k_{slow} obtained from the biexponential plots depends on the experimental conditions.

Results from experiments where the reactions of **1Cl** with C_6D_6 were monitored by ^1H NMR spectroscopy evidenced formation of uncoordinated PPh_3 (Figure 10). Observation of free PPh_3 is consistent with formation of **3Cl**. Interestingly, formation of $\text{C}_6\text{D}_5\text{-Ph}$ and a Rh-H hydride was observed only under flooding conditions where $[\text{PPh}_3]_{\text{added}} \gg [\mathbf{1Cl}]$. The interpretation of these observables is that oxidative addition of C_6D_6 to **2Cl** followed by

reductive elimination accounts for the formation of C_6D_5-Ph . In turn, the hydrido species is formed from **9**. The basis for this interpretation rests on the observation that 1H NMR spectra of solutions containing **1Cl** and added PPh_3 in C_6D_6 displays signals corresponding to C_6D_5-Ph and a Rh-H hydride. The absence of these 1H NMR signals obtained four hours after **1Cl** was dissolved in C_6D_6 without added PPh_3 suggests that C_6D_5-Ph and the hydrido species are formed exclusively from **9** during the time scale of this study. Oxidative addition of C_6D_6 to **9** followed by reductive elimination forming $(Ph_3P)_3Rh(D)$ (**7**) accounts for formation of C_6D_5-Ph but not for the formation of Rh-H hydride (eq. 18). However, intramolecular oxidative addition on **9** accounts for the observation of a Rh-H hydride (eq. 18). It is expected that **9**, like its methyl congener $(Ph_3P)_3Rh(Me)$, will undergo facile cyclometalation [68]. These observations and interpretation are summarized on the mechanistic description in Figure 11.

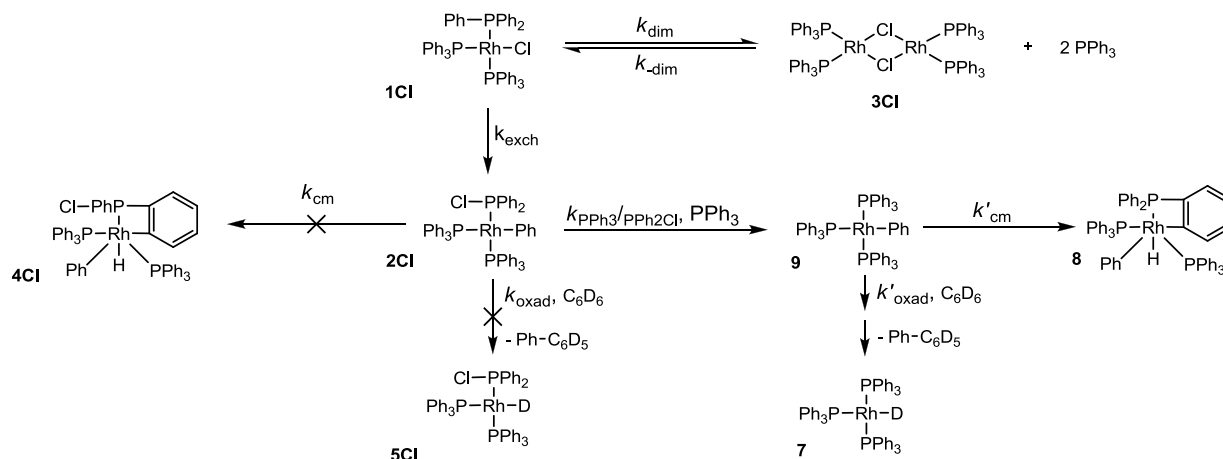


Figure 11 Mechanistic description of reactions of **1Cl** in benzene (or in C_6D_6).

This mechanism's rate law and the rate law from eq. 19 would be mathematically equivalent when **2Cl** (or **1Cl**, depending on experimental conditions) is a non-steady state intermediate. However, one must exercise caution on assigning k_{obsd} and k'_{obsd} to specific mechanistic steps. For example, instead of the previous correlation where k_{obsd} and k'_{obsd} were associate to the set of

consecutive reactions in eq. 17, for reactions under flooding conditions ($[\text{PPh}_3]_{\text{added}} \gg [\mathbf{1Cl}]$), k_{obsd} and k'_{obsd} are related to reactions in Scheme 1 by eq. 21 and 22, respectively [110] and conversely are mathematically related eq. 24 and 25 under the flooding conditions specified above. It was observed that under flooding conditions where $[\text{PPh}_3]_{\text{added}} \gg [\mathbf{1Cl}]$, k_{obsd} and k'_{obsd} are independent and dependent, respectively of $[\text{PPh}_3]_{\text{added}}$. This observation permits associate k_{obsd} to $(k_{\text{exch}} + k_{\text{dim}})$. Because $[\text{PPh}_3]_{\text{added}}$ is expected to inhibit $\mathbf{3Cl}$ formation, $k_{\text{obsd}} \approx k_{\text{exch}}$. Likewise, the observation that k'_{obsd} values are dependent on $[\text{PPh}_3]_{\text{added}}$, permits a preliminary assignment of k'_{obsd} to parallel intermolecular $\text{PPh}_3/\text{Ph}_2\text{Cl}$ exchange on $\mathbf{2Cl}$ and oxidative addition of benzene and cyclometalation on $\mathbf{2Cl}$ (eq 22).

$$k_{\text{obsd}} = k_{\text{exch}} \quad (21)$$

$$k'_{\text{obsd}} = k_{\text{PPh}_3/\text{PPh}_2\text{Cl}}[\text{PPh}_3] + k_{\text{oxid}}[\text{C}_6\text{H}_6] + k_{\text{cm}} = k_{\text{PPh}_3/\text{PPh}_2\text{Cl}}[\text{PPh}_3] \quad (22)$$

$$k'_{\text{obsd}} = k_{\text{PPh}_3/\text{PPh}_2\text{Cl}}[\text{PPh}_3] \quad (23)$$

Equations 21-23 are in accordance for the biexponential decays observed in the absorbance *versus* time plots for non-added PPh_3 (eq. 24) and for added PPh_3 (eq. 25)

$$A_t = \alpha e^{-(k_{\text{obs}} = k_{\text{dim}})t} + \beta e^{-(k_{\text{obs}}' = k_{\text{exch}})t} + A_{\infty} \quad (24)$$

$$A_t = \alpha e^{-(k_{\text{obs}} = k_{\text{exch}})t} + \beta e^{-(k_{\text{obs}}' = k_{\text{PPh}_3/\text{PPh}_2\text{Cl}}[\text{PPh}_3] + k_{\text{oxid}}[\text{C}_6\text{H}_6] + k_{\text{cymet}})t} + A_{\infty} \quad (25)$$

Equation 22 predicts linear plots of k'_{obsd} vs. $[\text{PPh}_3]_{\text{added}}$ (Figure 12) which slope and intercept are related to $k_{\text{PPh}_3/\text{PPh}_2\text{Cl}}$ and $(k_{\text{oxid}}[\text{C}_6\text{H}_6] + k_{\text{cm}})$ values, respectively.

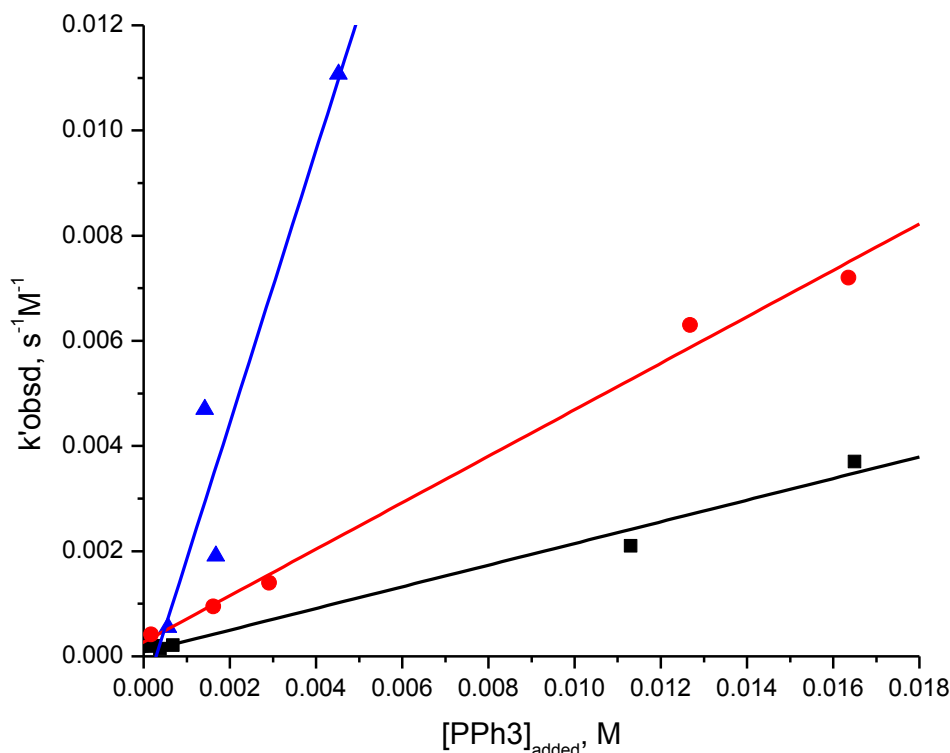


Figure 12 Plot of k'_{obsd} vs. $[\text{PPh}_3]$ for reactions of **1Cl** with benzene containing added $[\text{PPh}_3]$ at 32.1 °C (■) ($k'_{\text{obsd}} = 0.21(1) [\text{PPh}_3]_{\text{added}}$, 42.1 °C (●) ($k'_{\text{obsd}} = 0.44(2) [\text{PPh}_3]_{\text{added}}$) and 52.1 °C (▲) ($k'_{\text{obsd}} = 0.44(2) [\text{PPh}_3]_{\text{added}}$).

The observation that intercept values of these plots are zero within experimental error suggests that oxidative addition of benzene to **2Cl** and cyclometalation on **2Cl** are not competitive processes. This kinetics result is in line with the observation that Rh-H and C₆H₅-C₆D₆ species are formed only under flooding conditions where $[\text{PPh}_3]_{\text{added}} \gg [\text{ICl}]$. As a consequence, eq. 22 reduces to eq. 23.

In order to estimate the activation parameters, Eyring plots were constructed. The Eyring equation based on transition state theory (TST) is

$$k = \frac{k_{\text{B}}T}{h} \exp\left(\frac{\Delta S^\ddagger}{R}\right) \exp\left(-\frac{\Delta H^\ddagger}{RT}\right) \quad (24)$$

where, k_B is the Boltzman's constant (1.38065×10^{-23} J/K), h is the Planck's constant (6.62607×10^{-34} Js), R is the gas constant (8.3145 J/K mol), ΔS^\ddagger is the standard entropy of activation and ΔH^\ddagger is the standard enthalpy of activation.

Equation 24 can be rearranged by dividing both sides by temperature and taking the logarithms on both sides of the equation becoming

$$\ln\left(\frac{k}{T}\right) = \ln\left(\frac{k_B}{h}\right) + \frac{\Delta S^\ddagger}{R} - \frac{\Delta H^\ddagger}{RT} \quad (25)$$

In a small temperature range a plot of $\ln(k/T)$ vs. $1/T$ should be linear. Thus the values of enthalpy of activation and entropy of activation can be estimated from the slope and intercept of the plot, respectively ($\Delta S^\ddagger = R$ (intercept $- \ln(k_B/h)$); $\Delta H^\ddagger = -R$ (slope)).

Values of $k_{\text{PPh}_3/\text{PPh}_2\text{Cl}}$ at 32.1 °C, and 42.1 °C and 52.1 °C obtained from k'_{obsd} vs. $[\text{PPh}_3]_{\text{added}}$ plots in Figure 12 were used to estimate the activation parameters for $\text{PPh}_3/\text{PPh}_2\text{Cl}$ exchange on **2Cl** ($\Delta H^\ddagger = 102(27)$ kJ/mol, $\Delta S^\ddagger = +73(24)$ J/K mol) (Table 5). These activation parameters are in line with values reported for intermolecular $\text{PPh}_3/\text{PPh}_3$ exchange on **1Cl** ($\Delta H^\ddagger = 66.9(8)$ kJ/mol, $\Delta S^\ddagger = +53.7(8)$ J/K mol) [74b].

In kinetics runs where $[\text{PPh}_3]_{\text{added}} = 0$, k_{obsd} was correlated to k_{dim} that governs reconversion of **1Cl** from **3Cl**, whereas k'_{obsd} was associated to k_{exch} . Rate constant values obtained using these correlations for reactions at various temperatures and corresponding estimated activation parameters are being reported for i) formation of **1Cl** from **3Cl** (k_{dim}), ii) intramolecular Ph/Cl exchange on **1Cl** (k_{exch}), and iii) intermolecular $\text{PPh}_3/\text{PPh}_2\text{Cl}$ exchange on **2Cl** ($k_{\text{PPh}_3/\text{PPh}_2\text{Cl}}$). Activation parameters ($\Delta H^\ddagger_{\text{exch}} = 66(2)$ kJ/mol, $\Delta S^\ddagger_{\text{exch}} = -100(8)$ J/K mol) for

intramolecular P-Ph/Rh-Cl exchange were obtained from the Eyring equation by plotting $\ln(k_{\text{obsd}}=k_{\text{exch}})/T$ vs. $1/T$ shown in Figure 13 from actual experimental data from this work and for the reported fluor analogue Ph/F exchange [74a]. The values of the obtained activation parameters along with the assigned pseudo-first-order rate constants for added PPh_3 and non-added PPh_3 experimental designs are presented in Table 5 and Table 6, respectively.

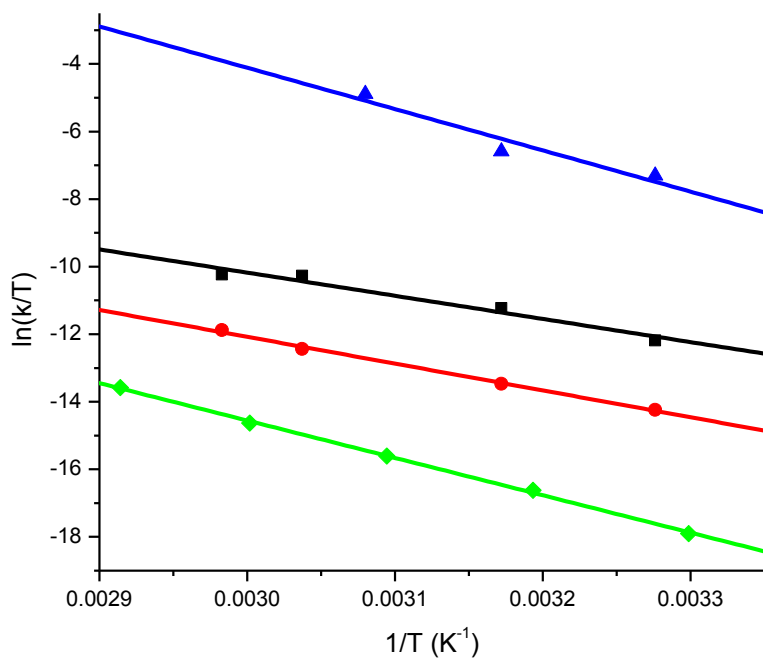


Figure 13 Plots of $\ln(k/\text{Temperature})$ vs. $1/\text{Temperature}$. $k = k_{\text{PPh}_2\text{Cl}/\text{PPh}_3}$ on **2Cl** (▲); $k = k_{\text{dim}}$ on **3Cl** (■); $k = k_{\text{exch}}$ on **1Cl** (●); $k = k_{\text{exch}}$ on **1F** (◆) from reference [74a].

Table 5 Rate constant values and activation parameters for reactions of **1Cl** and added PPh₃ in benzene.

Temp/K	[PPh ₃] _{added} X10 ⁴ , M	k _{obsd} (s ⁻¹) = (k _{exch} on 1Cl) X 10 ⁴	k' _{obsd} (s ⁻¹) x 10 ⁴ (= k _{PPh₃/PPh₂Cl} [PPh ₃] + k _{cm} + k _{oxad} [benzene]) on 2Cl	k _{PPh₃/PPh₂Cl} (s ⁻¹)X 10 ^{4*}	ΔH [‡] _{PPh₃/PPh₂Cl} (kJ mol ⁻¹)	ΔS [‡] _{PPh₃/PPh₂Cl} (J K ⁻¹ mol ⁻¹)
305.25	1.68	29.1(8)	1.99(3)	2060(123)	102(27)	73(24)
	2.29	21.05(1)	1.97(6)			
	3.81	19.42(5)	1.41(4)			
	6.79	25(4)**	2.1(3)			
	113	25(4)**	21(1)			
	165	29(5)	37(2)			
315.25	1.75	6.16(2)	4.13(2)	4419(218)		
	16.2	2.2(1)	9.5(5)			
	29.1	2.94(6)	14.0(7)			
	126.8	2.0(6)	63(4)			
	163.6	9.0(3)	72(8)			
325.25	4.31	5(2)**	7.41(2)	25914(5844)		
	5.64	5(2)**	5.50(2)			
	14.2	7.320(3)	47(1)			
	16.8	4.6(1)	19.1(6)			
	45.2	2.0(4)	110.70(4)			

*values estimated from slope values of k'_{obsd} vs [PPh₃]_{added}. **values estimated from average values of biexponential decays. The digits in parentheses are the uncertainty of the last digit.

Table 6 Rate constant and activation parameter values for reactions of **1Cl** in benzene.

Temp/K	k _{obsd} (s ⁻¹)=(k _{-dim} on 3Cl)X10 ⁻⁴	ΔH [‡] _{obsd=(-dim)} (kJ mol ⁻¹)	ΔS [‡] _{obsd=(-dim)} (J K ⁻¹ mol ⁻¹)	k' _{obsd} (s ⁻¹)=(k _{exch} on 1Cl)X10 ⁻⁴	ΔH [‡] _{obsd=(exch)} (kJ mol ⁻¹)	ΔS [‡] _{obsd=(exch)} (J K ⁻¹ mol ⁻¹)
305.25	15.6(9)	57(8)	-111(30)	2.0(5)	66(2)	100(8)
315.25	42(1)			4.45(5)		
329.25	114(8)			13.1(1)		
335.25	120(8)			23.2(2)		

It has been reported that the series of plausible P-Ph/Rh-F exchange pathways involve formation of a metallophosphorane intermediate [74]. The five-coordinated phosphorus promotes the P-Ph activation, X/Ph exchange and formation of *cis*-RhPh(PPh₃)₂(PXPh₂) [76]. The highly negative experimental entropy of activation ($\Delta S^\ddagger_{\text{exch}} = -100(8)$ J/K mol) in our study indicates substantial loss of degrees of freedom in the transition state structure leading to formation of **2Cl**. The corresponding enthalpy of activation for the formation of **2Cl** ($\Delta H^\ddagger_{\text{exch}} = 65(2)$ kJ/mol) is considerably smaller than experimental ($\Delta H^\ddagger_{\text{exch}} = 92(2)$ kJ/mol, $\Delta S^\ddagger_{\text{exch}} = -42(1)$ J/K mol) [74] and computed ($\Delta H^\ddagger_{\text{exch}} = 92.3$ kJ/mol) [72] values reported for formation of **2F** from **1F**. this set of activations parameter for the formation of **2Cl** and **2F** from **1Cl** and **1F**, respectively, suggests the existence of a compensation effect between $\Delta H^\ddagger_{\text{exch}}$ and $\Delta S^\ddagger_{\text{exch}}$, so that relatively large $\Delta H^\ddagger_{\text{exch}}$ are accompanied by relative large $\Delta S^\ddagger_{\text{exch}}$ [111].

4.4. A Computational Approach to Study the Mechanism of P-Cl/Ph-Ph exchange on Wilkinson's Catalyst.

4.4.1. General

Understanding the relationship between structural properties and chemical and physical behaviour in solution of the above complexes is important not only because it is necessary information to design catalysts for specific applications, but to identify and to mitigate chemical processes that may reduce their catalytic activity. Thus, it is important to design theoretical studies that are in accordance with what has been formerly reported in the literature and our experimental findings. For example, it is known that after **1F** undergoes P-Ph/Rh-F exchange a series of reactions occur that change the chemical environment around the rhodium atom [74-76]. During the reaction many of the species in solution that are formed are short-lived which makes it difficult to characterize them at room temperature with spectroscopic techniques such as IR and ^1H NMR. Thus, computational methods may be used as a reliable tool to study plausible chemical processes that cannot be explored experimentally with the technology available in research group. Computational studies with full geometry optimizations have been done for the intramolecular exchange of PPh_3 in **1Cl** and P-Ph/Rh-F intramolecular exchange in vacuo and THF for the simplified version of **1F**, $(\text{PH}_3)_2(\text{PPhH}_2)\text{RhF}$, but to our knowledge transition state species of non-simplified systems have been reported yet. [74].

4.4.2. Results

4.4.2.1. Experimental and Computational Convergence

The computational design is based on experimental results from our laboratory and from elsewhere [74-76]. Experimental results from our group suggest the existence of P-Ph/Rh-Cl intramolecular exchange on **1Cl** forming **2Cl**. Once **2Cl** is formed it undergoes intermolecular PPh₃/PPh₂Cl exchange producing **9** (Figure 11). It is proposed that species **7** and **8** are formed from (**9**). Formation of **4Cl** and **5Cl** from **2Cl** is ruled out based on kinetics experiments as discussed previously. Figure 14 depicts possible mechanistic pathways for **2Cl** formation.

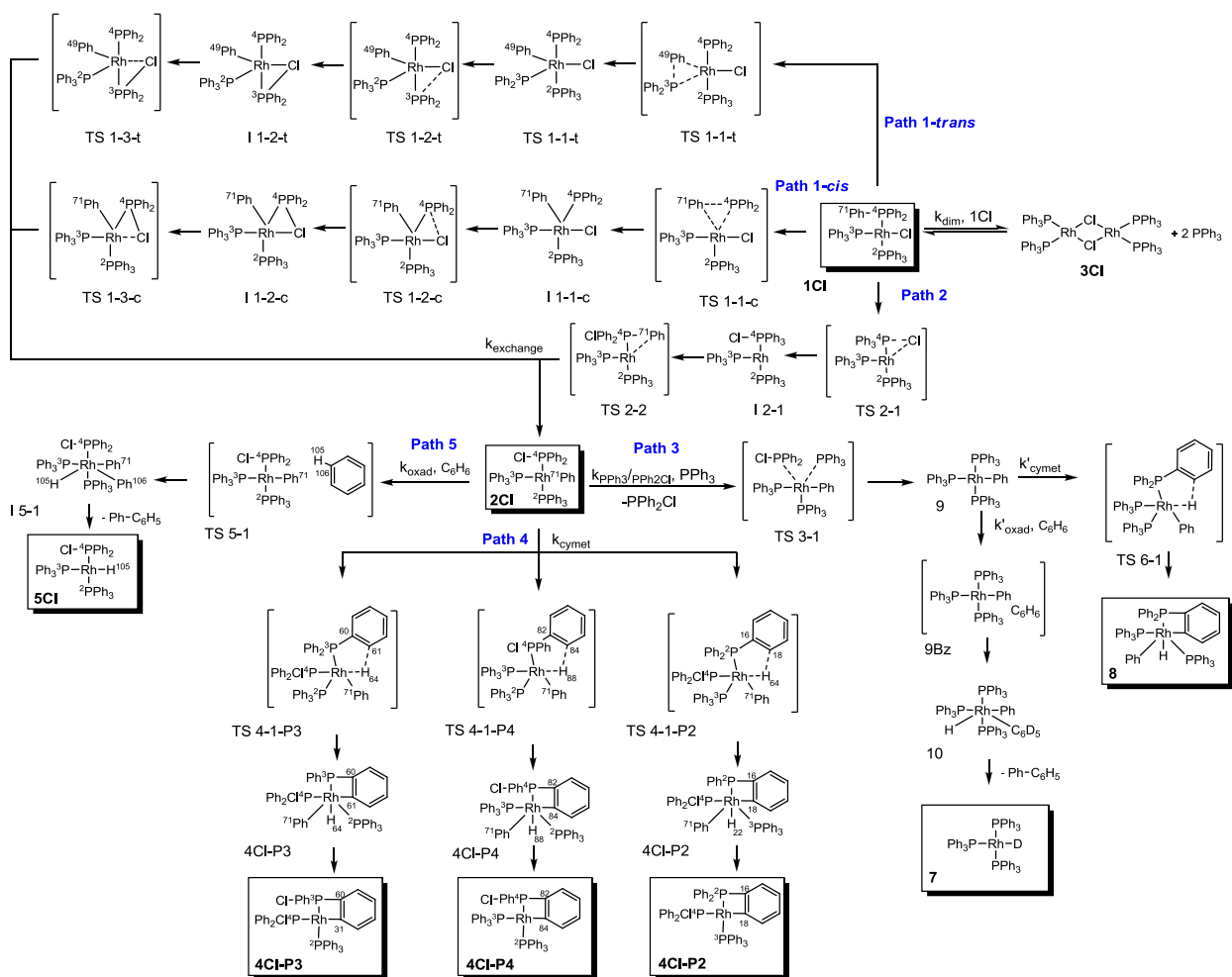


Figure 14 Computational profile map based on the reactions of $(\text{PPh}_3)_3\text{RhCl}$ in C_6D_6 . Numbered labels are used to distinguish bonding sites.

Formation of **2Cl** may employ two general mechanistic paths that vary in the relative order of Ph and Cl transfer to and from Rh and P, respectively. Path 1 describes the Ph transfer from P to Rh as an oxidative cleavage step to form a Rh-phosphide intermediate. The Ph transfer may occur from a phosphine ligand located *cis* or *trans* to Cl. On the other hand, Path 2 involves initial transfer of Cl from Rh to P to form a metallophosphorane intermediate. Once any one of these intermediates is formed Ph transfers to Rh to form **2Cl**. Path 2 is only considered for the *cis* Ph exchange since i) our results showed no location of transition states for this path and ii) is not contemplated for **1F**.

Path 3 describes the intermolecular $\text{PPh}_3/\text{PPh}_2\text{Cl}$ ligand exchange reaction. The phosphoranide ligand in **2Cl** is displaced by PPh_3 to form **9** which in turn produces species **7** and/or the hydrido specie **8** via oxidative addition of $\text{C}_6\text{H}_6/\text{C}_6\text{D}_6$ or irreversible cyclometalation, respectively.

Path 4 describes cyclometalation on **2Cl** involving one of the Ph groups in the phosphoranide ligand or PPh_3 ligands that are *cis* and *trans* to Rh-coordinated Ph. A reductive elimination of Ph-H can lead to formation of d^8 products **4Cl-P2**, **4Cl-P3** and **4Cl-P4**, depending on which P-Ph bonds *ortho* to the Rh metal is involved. Path 5 describes the possible oxidative addition of $\text{C}_6\text{H}_6/\text{C}_6\text{D}_6$ to **2Cl**. This process forms a d^6 intermediate which can later undergo reductive elimination of Ph- $\text{C}_6\text{H}_5/\text{C}_6\text{D}_5$ to form **5Cl**.

4.4.2.2. Computed Profiles for non-simplified Structures

The lowest optimized structure of **1Cl** is found as a singlet when compared to that of a triplet state ($\Delta E = 20.7 \text{ kJ/mol} / 4.95 \text{ kcal/mol}$). The triplet state is not only higher in energy but also exhibits distorted tetrahedral geometry (Figure 15). An increase in energy of 15.4 kcal/mol and similar geometry was reported for BP86 functional for the triplet state and has been attributed to σ -antibonding orbitals in the higher spin state [74b]. The pseudo square planar geometry of the singlet state of **1Cl** is in accordance to the geometry determined crystallographically. To this species was assigned a relative energy of 0.0 kJ/mol. Crystallographic data for the orange form of $(\text{PPh}_3)_3\text{RhCl}$ and computed geometries for **1Cl** are in good agreement (Table 7) Computed profiles for Cl/Ph exchange on **1Cl** via Path 1 are shown in Figure 16.

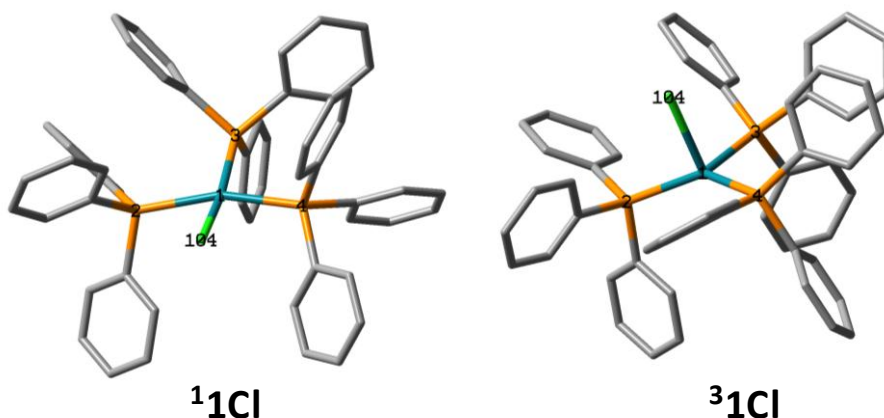
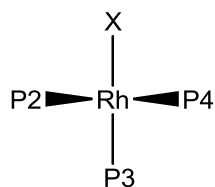


Figure 15 Optimized structures of $(\text{PPh}_3)_3\text{RhCl}$ in singlet state $^1\mathbf{1Cl}$ and triplet state $^3\mathbf{1Cl}$ which exhibit pseudo planar square geometry and distorted tetrahedral geometry, respectively.

Table 7 Rh-P Bond Distances (\AA) and Angles (deg) for crystallographically characterized and computed complexes $(\text{PPh}_3)_3\text{Rh}(X)^a$ ($X = \text{Cl}, \text{F}$)



X	Rh-X	Rh-P3	Rh-P2	Rh-P4	X-Rh-P3	P2-Rh-P4	X-Rh-P4	P4-Rh-P3	P3-Rh-P2	P2-Rh-X
Cl (R) ^b	2.38	2.214	2.335	2.322	156.2	152.9	86.1	100.4	97.8	85.3
Cl (O) ^b	2.40	2.225	2.338	2.304	166.7	159.1	85.3	97.7	96.5	84.5
Cl (N-S) ^c	2.48	2.38	2.48	2.43	165.3	162.5	82.5	98.2	97	84.9
Cl (S) ^d	2.45	2.34	2.38	2.36	179.6	169.2	85.6	94.8	96.1	83.5
Cl (R) ^e	2.42	2.27	2.37	2.35	154.6	150.4	-	-	-	-
Cl (O) ^f	2.42	2.27	2.38	2.35	158.1	154.7	-	-	-	-
F ^b	2.07	2.193	2.325	2.325	166.9	159.7	85.5	96.2	95.8	86.5

^a The arrangement P2-Rh-P4 are projecting toward the reader with the Rh atom in the plane that contains the page. ^b Red form (R) and orange form (O) crystallographically obtained distances [113-115]. ^c Calculated results obtained in our group for the non-simplified (N-S) structure and ^d the simplified structure. ^e Red form (R) and ^f orange form (O) calculated distances obtained from [112-115].

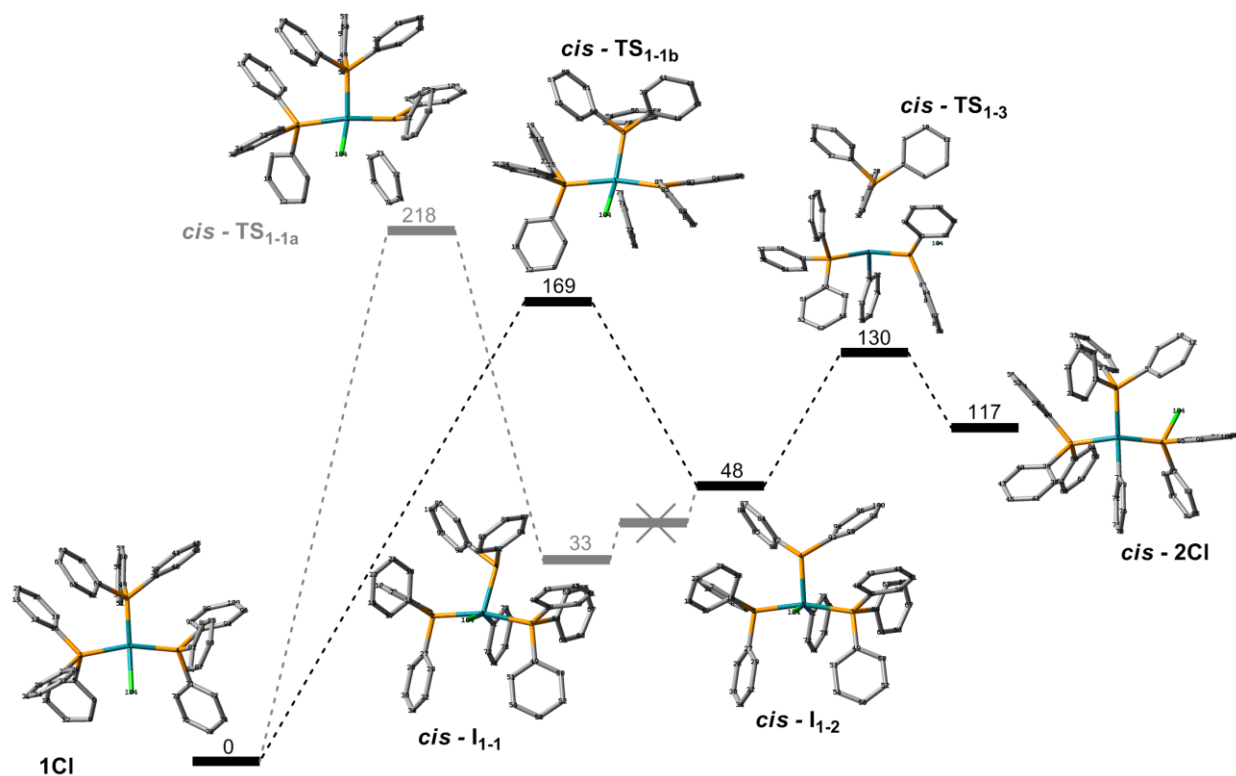


Figure 16 Computed reaction profile (kJ/mol) for Path 1 *cis* in vacuo.

The computed transition state of the first activation barrier of the P-Ph/Rh-Cl intramolecular exchange on **1Cl** had two plausible pathways (Figure 16). One is via **TS_{1-1a}** with relative energy of 218 kJ/mol forming intermediate species **I₁₋₁** which exhibits an energy difference of 34 kJ/mol relative to **1Cl**. Once **I₁₋₁** is formed it was believed to overcome a geometrical rearrangement to form the intermediate species **I₁₋₂**. Attempts to obtain an activation barrier from **I₁₋₁** and **I₁₋₂** were unsuccessful. This prompted to discard **I₁₋₁** as a possible intermediate and to consider **I₁₋₂** for the first activation barrier which obtained a lower energetic transition state of 169 kJ/mol. This new barrier from **1Cl** to **I₁₋₂** exhibited a PPh₃/PPh₂ flip from *trans* Cl-P3 and *cis* Cl-P4 to *cis* Cl-P3 and *trans* Cl-P4, notwithstanding the pathway i.e. **1Cl** to **I₁₋₁** or **1Cl** to **I₁₋₂**. To test whether this flip indeed results in the formation of a more stable

intermediate, series transition states were calculated where no flip occurred from **1Cl** to **I₁₋₂**. This means that the PPh₂ group remains *cis* to Cl from **1Cl** to the formation of the intermediate. This called for optimization of new intermediates *cis* - **I'_{1-1a/b}** (Figure 17). These intermediates (*cis* - **I'_{1-1a/b}**) contain a PPh₃ in the axial position of a square planar pyramid geometry, this means that the remaining PPh₃ is in the equatorial plane. Thus, the PPh₂ (P4) has *cis* and *trans* PPh₃ groups, and *cis* Cl and Ph groups. For these intermediates the transition states were not located on saddle point. Instead the resulting transition states were lower in relative energy than *cis* - **I'_{1-1a/b}**, becoming akin to its initial state (**1Cl**) (Figure 17). Therefore, these intermediates were not considered.

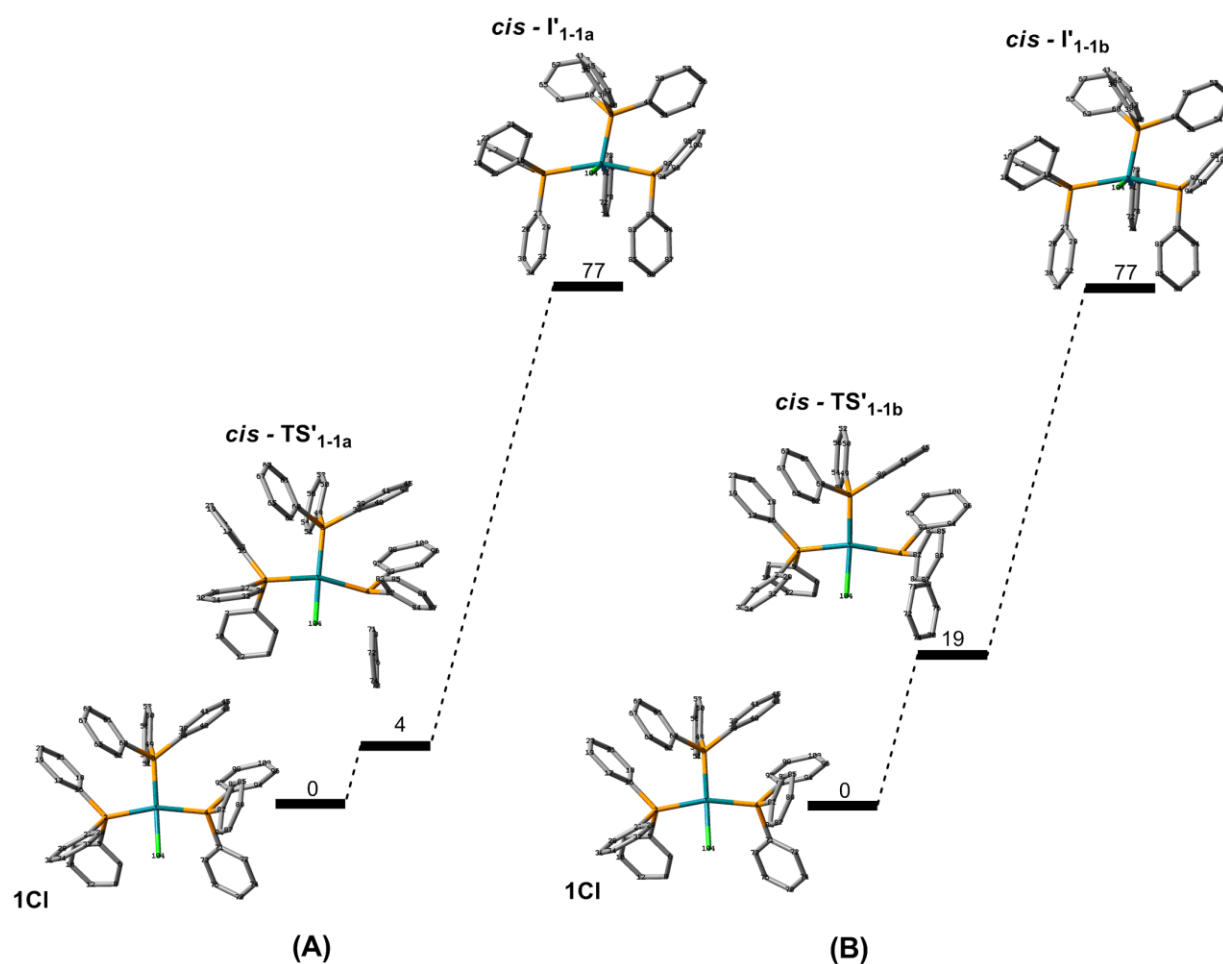


Figure 17 Computed reaction profile (kJ/mol and kcal/mol) for Path 1 *cis* in vacuo where phosphorus atoms retained their geometry through the activation barrier. Hydrogen atoms omitted for simplicity.

A similar flip on intermediate was observed for the first energetic barrier for the P-Ph/Rh-F exchange in $(\text{PH}_3)_2(\text{PH}_2\text{Ph})\text{RhF}$, where the phosphido, PH_2^- , is located in an axial position and F is located *cis* to Ph in the square pyramidal complex. Similarly in our work PPh_2 is located in an axial position in the square pyramidal complex but Cl is located *trans* to Ph. In our studies the *cis* arrangement was crowded around the equatorial plane due to *cis* PPh_3 groups and the overall $\text{PPh}_3\text{-PPh}_3\text{-Cl-Ph}$ equatorial arrangement. As a consequence the phosphorus atom *cis* to PPh_3 and Cl was forced to have a distance of 4.54 Å from the Rh (Figure 18B) in order to find its

minimal energy, but still higher in energy when compared with **I**₁₋₂ in Figure 18 ($\Delta E = 12$ kJ/mol) therefore it was not considered on energy grounds.

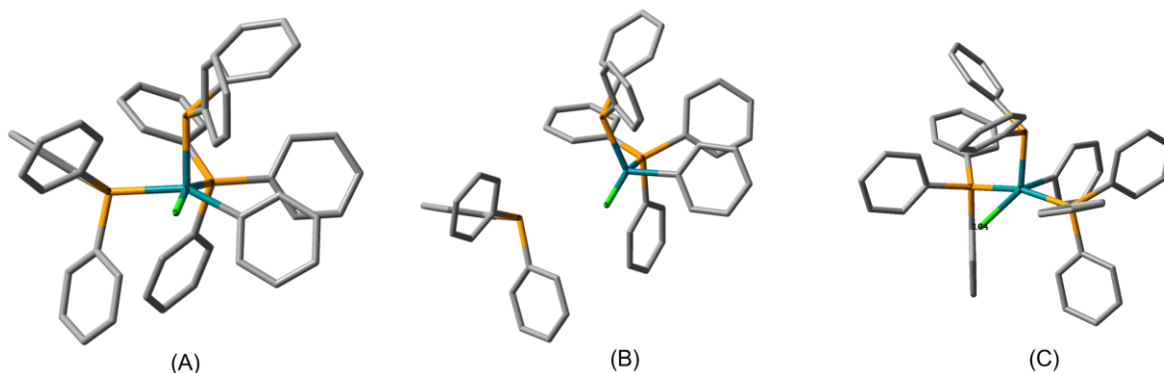


Figure 18 Structures of $(\text{PPh}_3)_3\text{RhCl}$ for (A) non-optimized *cis* Cl-Rh-Ph, (B) optimized *cis* Cl-Rh-Ph and (C) optimized *trans* Cl-Rh-Ph. Hydrogen atoms omitted for simplicity.

To probe the effect on solvent polarity, recomputed energies of the stationary points and transition states were placed in a continuum with a dielectric constant equivalent to that of benzene ($\epsilon = 2.2706$). The energies for Path 1 via *cis* for vacuo, benzene are shown in Figure 19. The presence of benzene does not affect the transition state or its geometry.

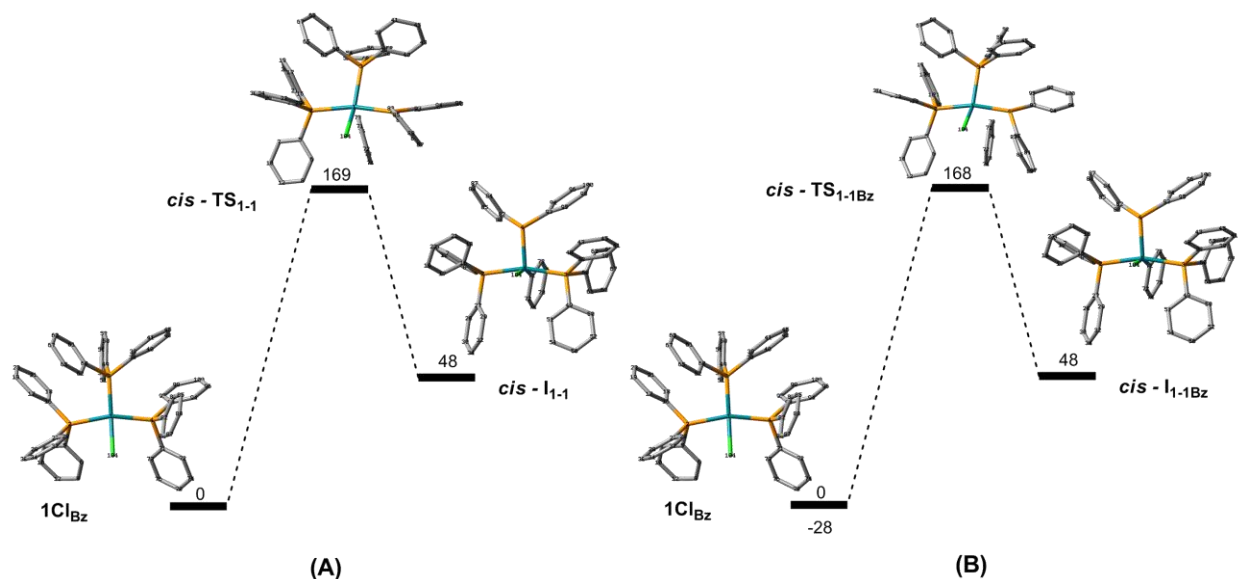


Figure 19 Computed reaction profile (kJ/mol) for the first activation barrier of Path 1 via *cis* in (A) vacuo and (B) in benzene ($\epsilon = 2.2706$). Negative value resembles the stabilization of **1Cl** in the presence of benzene. Hydrogen atoms omitted for simplicity.

Path 1 also contemplates the P-Ph/Rh-Cl intramolecular exchange via *trans* mechanism. This pathway discards the switching possibility of the PPh_3 in the transition state since the leaving Ph will automatically leave the vacant Ph_2 in the axial position. The resulting transition state for the first activation barrier is 143 kJ/mol (34kcal/mol) which is lower by 26 kJ/mol when compared to the *cis* arrangement (Figure 20A). Figure 20 also shows the same reaction profile solvated with benzene.

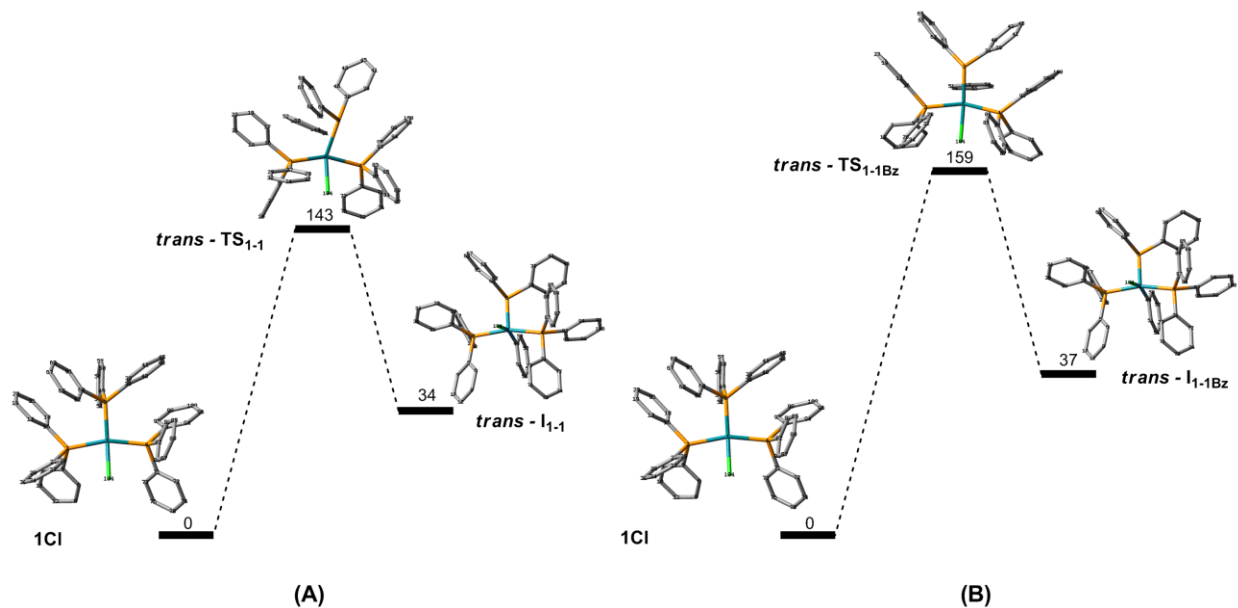


Figure 20 Computed reaction profile (kJ/mol) for the first activation barrier of Path 1 via *trans* in (A) vacuo and (B) in benzene ($\epsilon = 2.2706$). Hydrogen atoms omitted for simplicity.

Comparison of the reaction profiles for Figure 20 A and B shows that the barrier increases with use of the benzene dielectric constant by 16 kJ/mol. An increase using dimethyl sulfoxide (DMSO) dielectric constant ($\epsilon = 46.7$) has been reported for the Ph/Cl intramolecular exchange on *cis* and *trans* $(\text{PH}_3)_2(\text{PH}_2\text{Ph})\text{RhF}$ [74]. This increase with respect to vacuo might be interpreted as a geometrically disfavored charge separation in the transition state. On the contrary, the similar values observed for Path 1 via *cis* might imply that the presence of benzene does not favor or disfavor charge separation on the transition state.

The intermediate species for the metallophosphrane contemplated in Path 2, \mathbf{I}_{2-1} was successfully optimized (Figure 21 A). It embraces a trigonal bipyramidal five-coordinate phosphorus centered geometry with exchanging Ph and Cl in the axial positions with Ph-P-Cl angle of 164° and two Ph and a Rh in the equatorial positions. This axial Ph in $\text{P}(\text{Ph})\text{H}_2\text{Cl}$ is in the vicinity of the vacant Rh where it might encounter a stabilization due to a Ph-Rh interaction.

This *pseudo* square planar intermediate species is more stable when compared to the intermediate where the elongated P-Cl bond lies between the three Ph ligands (Figure 21 B).

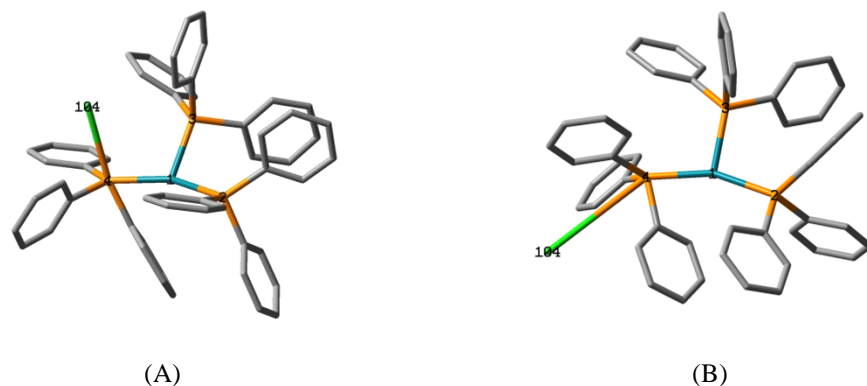


Figure 21 Optimized structures of I_{2-1} with five-coordinate phosphorus center with (A) trigonal bipyramidal geometry and (B) chloride atom lies in between the Ph ligands. Hydrogen atoms omitted for simplicity.

Attempts to locate a metallophosphorane intermediate described by Path 2 have been unsuccessful independently of which intermediate was used to find the transition structure since the Cl atom would transfer back to the position of **1Cl**.

The first step in Path 3 (Figure 14) described by a ligand intermolecular exchange (PPh_3/PPh_2Cl) from **2Cl** to **9** through TS_{3-1} required extensive computational time that did not guarantee results and its CPU usage compromised calculation of other pathways and it was experimentally determined to be 102(27)kJ/mol. On the other hand, the transition state of the subsequent step **9** to **8** was localized with an activation barrier of 107 kJ/mol in vacuo (Figure 22).

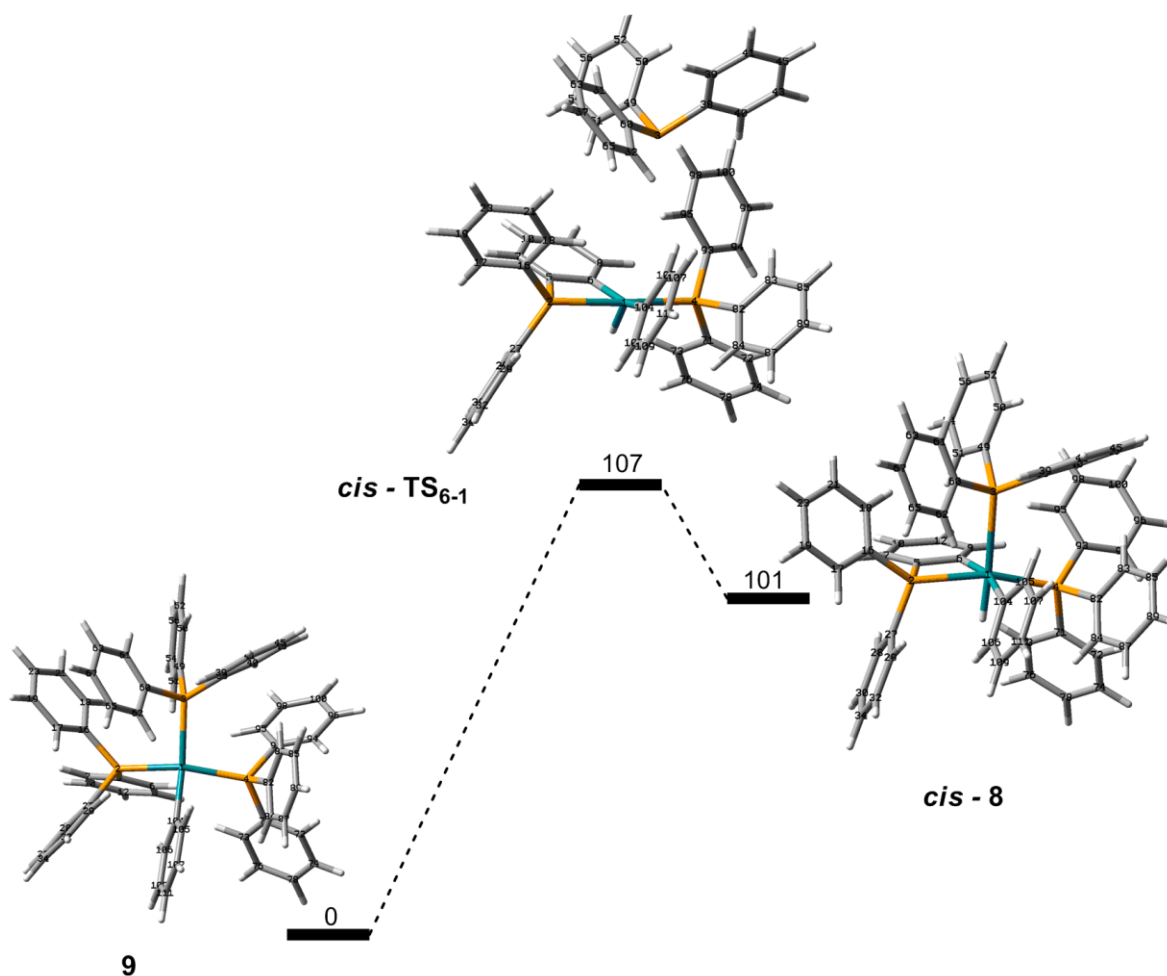


Figure 22 Computed reaction profile (kJ/mol) for the activation barrier of cyclometalation of **9** in vacuo.

Another intramolecular oxidative addition is described in Path 4 with three PPh_3 groups that can undergo cyclometalation in **2Cl**. We have optimized all three of them and computed the transition barrier for the most stable one. The fully optimized structures are shown in Figure 23. The energy difference between these three cyclometalated structures is shown in Table 8.

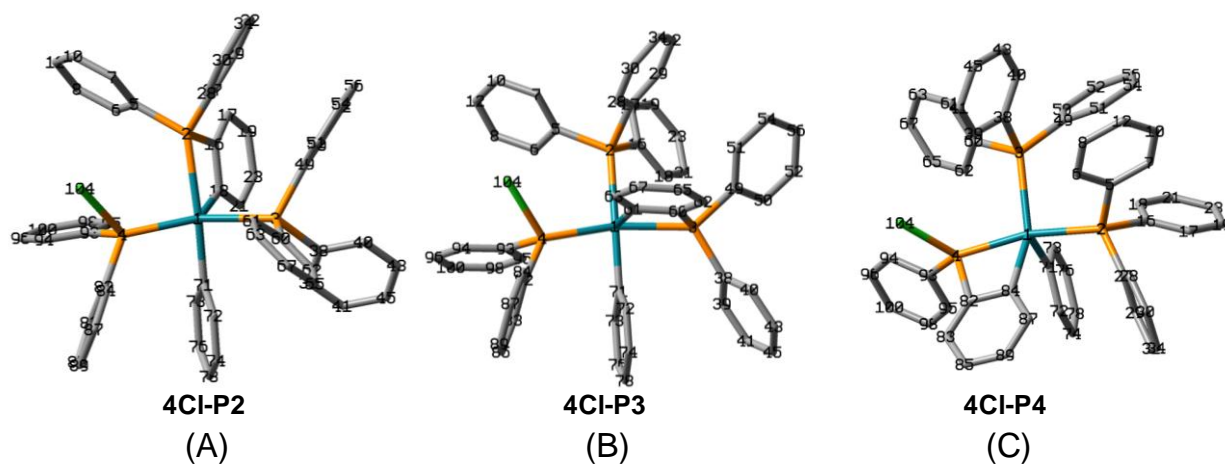


Figure 23 Optimized structures for the cyclometalation of **2Cl** from (A) PPh_3 *trans* to Ph-Rh, (B) PPh_3 *cis* to Ph-Rh and (C) PPh_2Cl *cis* to Ph-Rh in vacuo. Hydrogen atoms omitted for simplicity.

Table 8 Energy differences between cyclometalated structures.

Structures		ΔE (kJ/mol)
4Cl-P3	4Cl-P2	4.8
4Cl-P2	4Cl-P4	17.9
4Cl-P3	4Cl-P4	21.6

Even though complex **4Cl-P4** is the most energetic of all the three structures it was the only structure that led to the location of a transition state with an energy barrier of 162 kJ/mol (Figure 24).

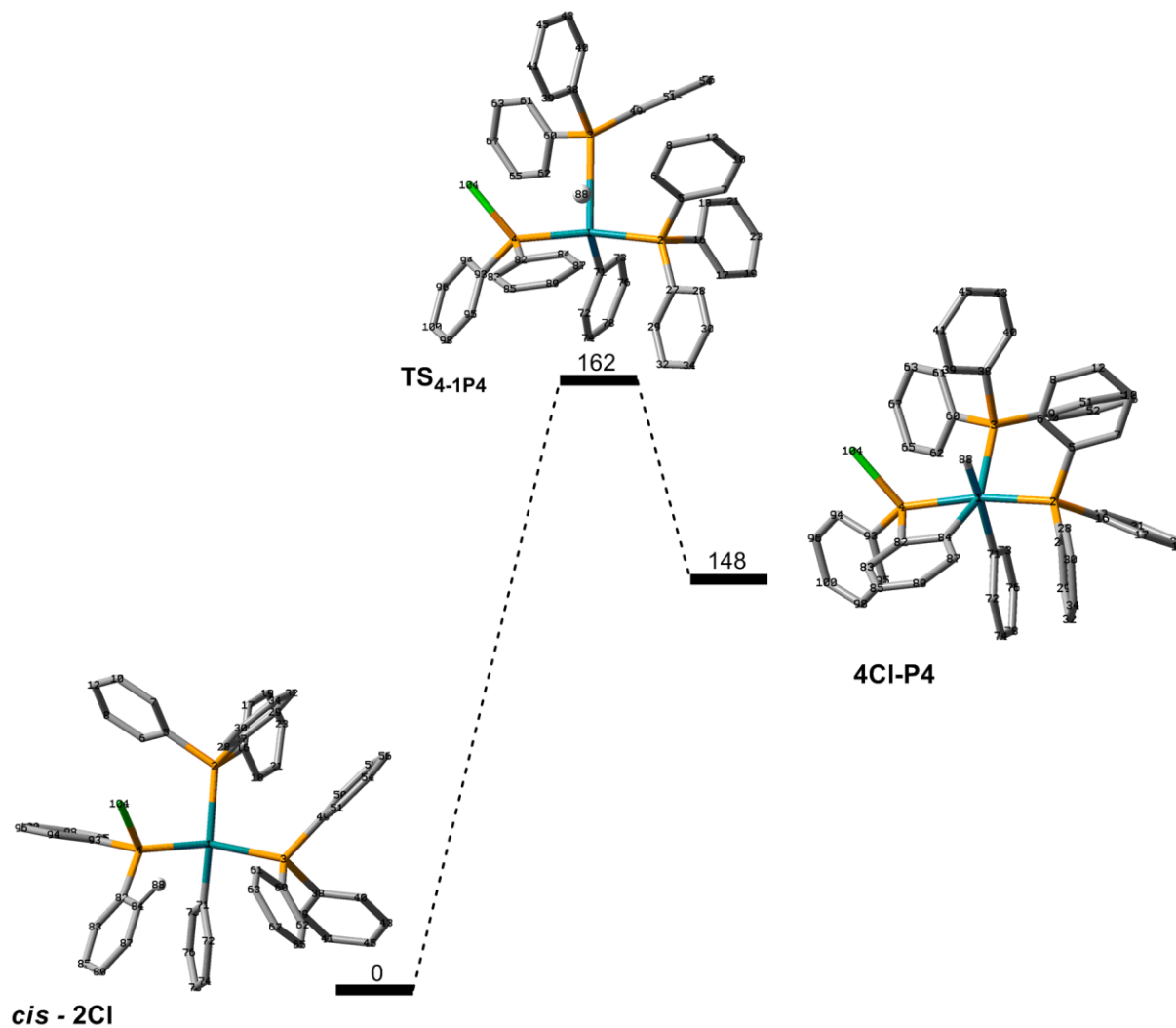


Figure 24 Computed profile energy barrier (kJ/mol) for the intramolecular cyclometalation of *cis* **2Cl** to **4Cl-P4**. Hydrogen atoms omitted for simplicity except for H₈₈)

The Rh-H₈₈ distance goes from 3.87Å in *cis* - **2Cl** to 1.62Å in **TS_{4-1P4}**. The cyclometalated *ortho* Rh-C₈₄ bond length increases from the transition state to the intermediate specie **4Cl-P4** from 2.02 to 2.09Å. Elongation the Rh-P3 bond is observed in the transition state (3.65Å) and decreases after the barrier to 2.69Å.

The structure **I₅₋₁** was optimized for Path 5, where **2Cl** undergoes oxidative addition of benzene to form a Rh-H bond and a new Rh-Ph bond (Figure 25).

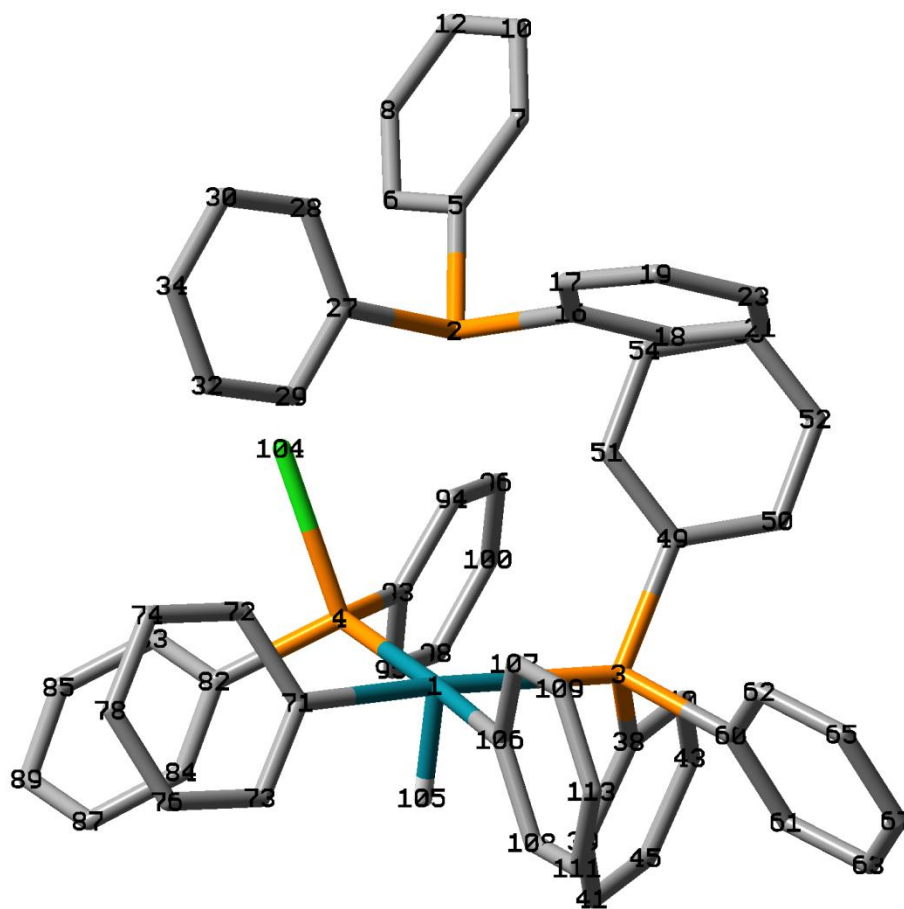


Figure 25 Optimized structure of I_{5-1} where H_{105} in Rh comes from C_{106} . All other hydrogen atoms are omitted.

The optimized structure exhibits an extremely elongated Rh-P2 distance of 5.15\AA . This elongation presented difficulty to locate a transition state. Thus, no transition structures were successfully obtained for Path 5.

4.4.2.3. Computed Profiles for Simplified Structures

The simplified model of **1Cl**, denoted as **1Cl_s**, was optimized as a singlet and assigned a relative energy of 0.0 kJ/mol. The computed profiles consisted on the first activation barriers for *cis* and *trans* Path 1 and *cis* Path 2.

The computed profiles for *cis* Path 1 were computed from two different pathways. The first pathway is through an intermediate specie with similar Rh, P and exchanged Ph arrangement as the optimized structure of Figure 18C, with *trans* Cl-Rh-Ph (Figure 26). A close transition barrier of 66 kJ/mol and 68 kJ/mol was obtained in vacuo and benzene, respectively, but diminished to 47 kJ/mol in the presence of DMSO. This close transition barrier was also observed for the similar geometrical arrangement on the *cis* Path 1 of the non-simplified model. The second pathway is through intermediate specie with Ph and PH₃ *cis* to Cl and a PH₃ *trans* to Cl. This arrangement similar to that of Figure 18B which was not considered in the non-simplified model can be considered here since is less crowded around the Rh due to the less steric effects of hydrogen atoms permitting the *cis* Cl-Rh-Ph arrangement (Figure 27). As a result, a transition state localized with a relative energy of 107 kJ/mol and 63 kJ/mol in vacuo and in benzene, respectively. This 44kJ/mol difference resulting from benzene solvation effects for the *cis* Cl-Rh-Ph are in contrast with those found *trans* Cl-Rh-Ph with an relative energy difference of $\Delta E = 2$ kJ/mol.

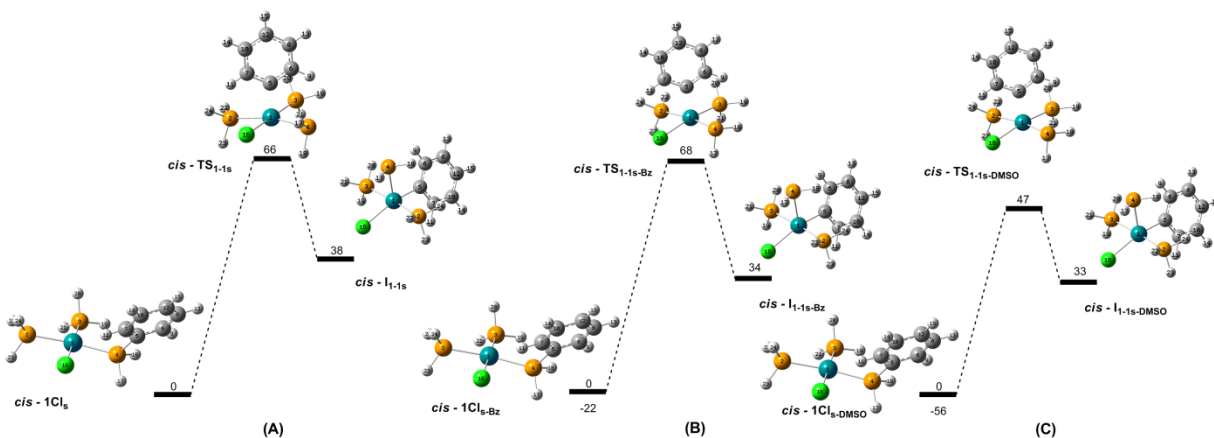


Figure 26 Computed reaction profile (kJ/mol) for the simplified first activation barrier of Path 1 via *cis* Ph exchange and *trans* Cl-Rh-Ph intermediate arrangement for (A) vacuo and (B) in benzene ($\epsilon = 2.2706$).

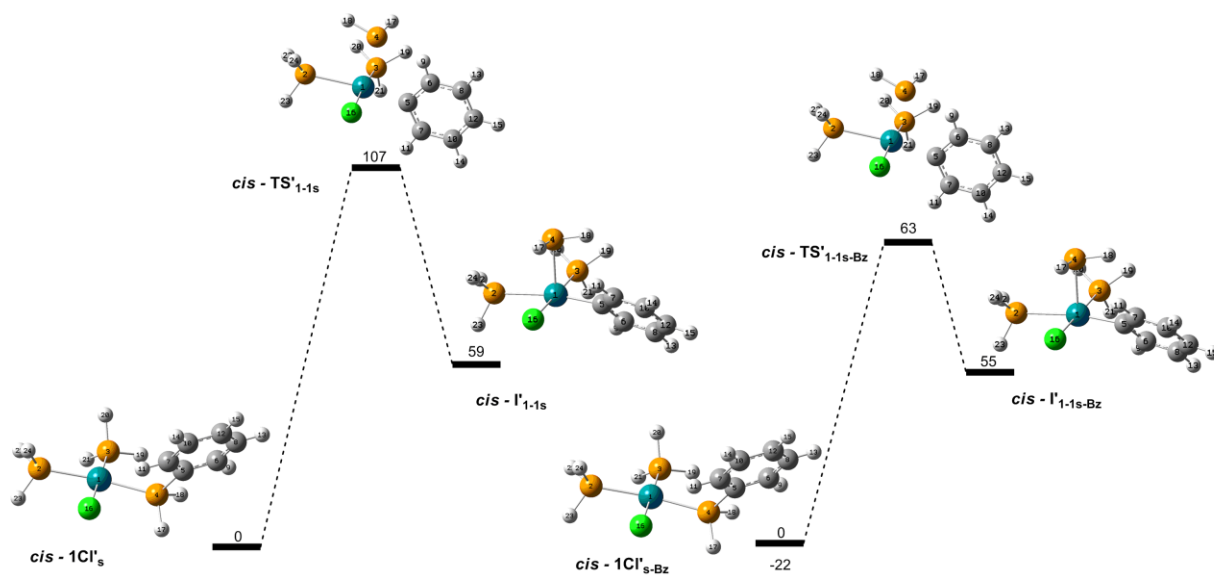


Figure 27 Computed reaction profile (kJ/mol) for the simplified first activation barrier of Path 1 via *cis* Ph exchange and *cis* Cl-Rh-Ph intermediate arrangement for (A) vacuo and (B) in benzene ($\epsilon = 2.2706$).

The transfer of a Ph group *trans* to Cl showed a transition barrier of 131 kJ/mol and 134 kJ/mol in vacuo and benzene, respectively, with a difference of $\Delta E = 3$ kJ/mol. These localized energy barriers are also in contrast in terms of energy difference of 16 kJ/mol for the same pathway in the non-simplified model (Figure 28).

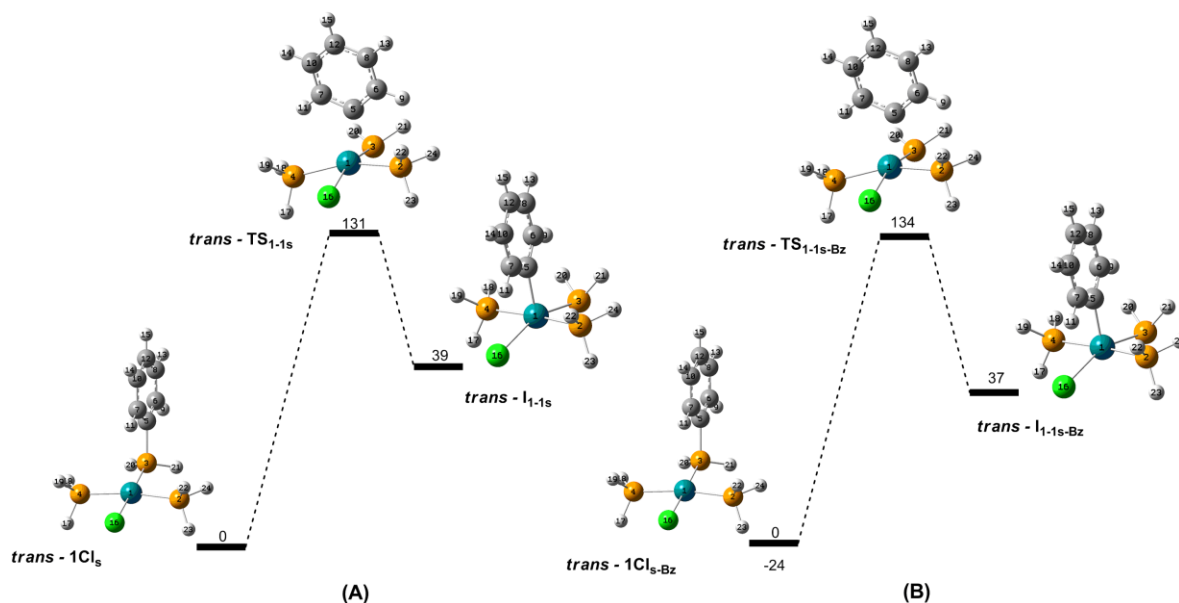


Figure 28 Computed profile (kJ/mol) for the activation barrier of Path 1 *trans* with Ph transferring to the axial position for (A) in vacuo and (B) in benzene ($\epsilon = 2.2706$).

Figure 28 shows the phenyl transfer where the Ph is in the axial position and the PH₂ is *trans* with respect to Cl (*trans* - I_{s/s-Bz}). Similar transition barriers (*ca.* to 130 kJ/mol) were located for transition calculations which also started with *trans* - 1Cl_{s/s-Bz} but with intermediates with PH₂ in the axial position and the Ph is *trans* with respect to Cl. Thus axial Ph and PH₂ with *cis* Cl tend to have similar transition barriers in terms of relative energy.

The location of a transition state for Path 2, which takes under consideration the metallophosphorane intermediate, was made possible using the simplified model (Figure 29). Optimization of *cis* I_{2-1s} resulted on a similar array of the five-coordinated trigonal bipyramidal phosphorous atom of Figure 21A. Instead of a 164° Ph-P-Cl angle observed for the non-simplified model, the simplified model holds a 174° angle. The axial Ph in P(Ph)(H₂)Cl is in a *pseudo trans* position to the *cis* PH₃ (P3) of the exchanging phosphorous group permitting a *pseudo* square planar geometry (Figure 29). The computed transition barrier was found to be 170 kJ/mol and 147 kJ/mol in vacuo and benzene ($\Delta E = 23$ kJ/mol).

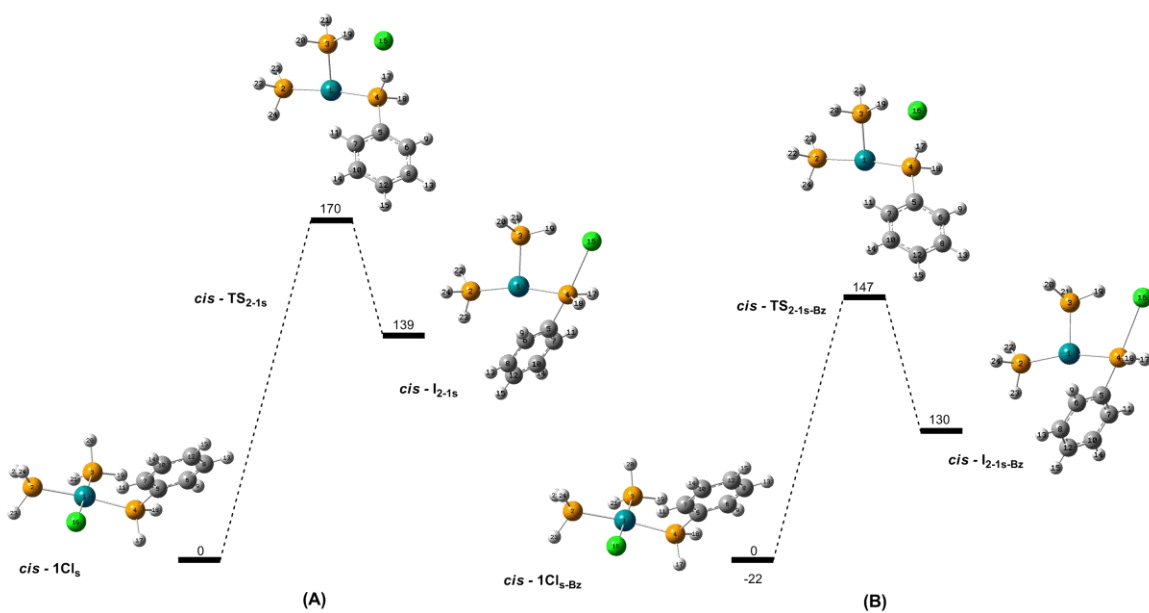


Figure 29 Computed profile (kJ/mol) for the activation barrier of Path 2 via *cis* in (A) vacuo and (B) benzene ($\epsilon = 2.2706$).

4.4.3. Discussion

Reaction profiles for non-simplified and simplified optimized structures have been determined for the reactions of **1Cl**. It was observed that for the *cis* Path 1 the transition state where the Ph group exits *cis* to Cl and transfers *trans* to Cl for both types of models agree in terms of geometry and response to benzene salvation but their energetic barriers differ by *ca.* 100 kJ/mol. These observations were not obtained for the *trans* Path 1 which indicates that the most promising pathway is through *cis* Path 1, via metal-phosphido. These observations make metallophosphorane, described by Path 2, less possible since i) a transition state was not located on the non-simplified model and ii) the transition barrier is higher in energy when compared to that of the metal-phosphido (66/68 kJ/mol vs 170/147 kJ/mol in vacuo/benzene).

It was experimentally observed that the first energetic barrier of Path 3 is 102(27) kJ/mol which was not obtained theoretically for computational cost reasons. This observation is in well agreement to the proposed mechanism since the kinetically ruled out Path 4 and Path 5 exhibit a high energetic barrier of 162 kJ/mol and a non-geometrically favourable intermediate, respectively. A reaction profile for experimental and computed profiles is shown in Figure 30.

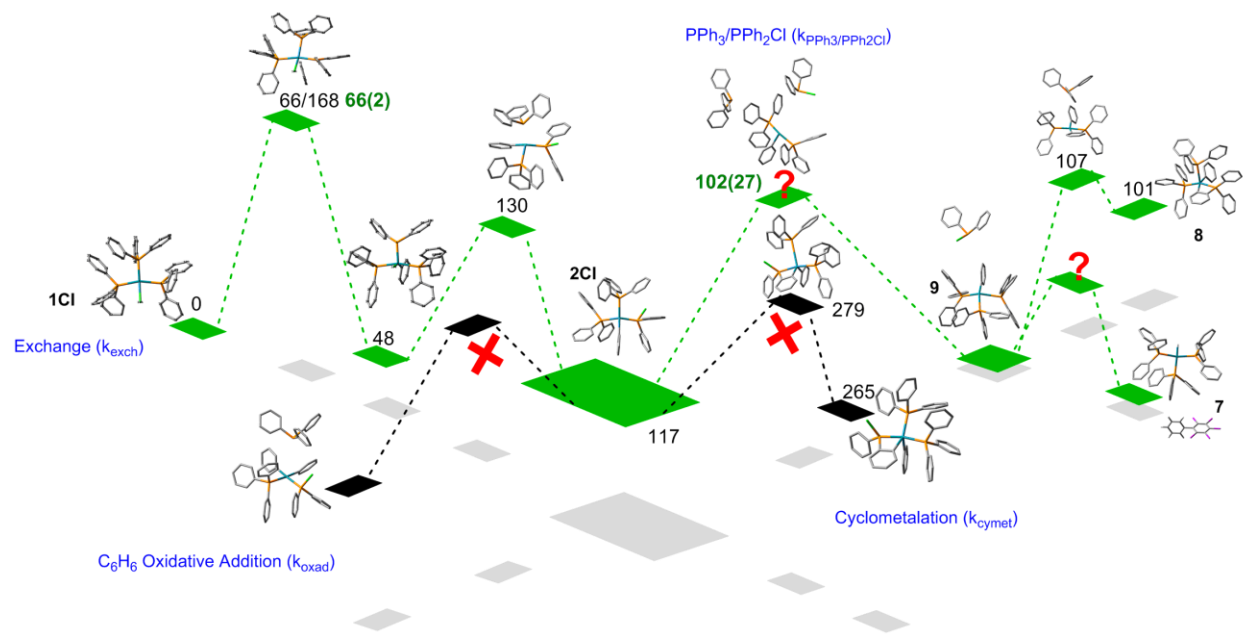


Figure 30 Experimental and computed reaction profile summary for the reactions of **1Cl**. Activation barrier values in green are experimental while values in black are computed. Red question marks and red crosses resemble non-computed transition states and kinetically ruled out pathways, respectively. Hydrogen atoms are omitted for simplicity.

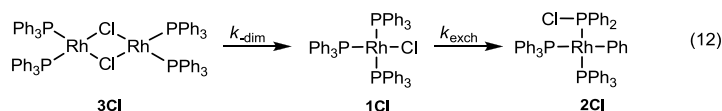
5. Conclusions

The reduction and oxidation potentials of the metal-fullerene complexes studied in this work seems to depend on i) the extent of π -back donation between C_{60} and the metal, ii) degree of distortion of the spherical surface of C_{60} upon coordination. The extent of π -back donation favors negative potential shifts relative to uncoordinated C_{60} whereas larger distortion on the spherical C_{60} surface favors positive potential shifts. This positive potential shift may be attributable to a distortion of the spherical surface of [60]fullerene due to metal coordination. This structural distortion may induce a Jahn-Teller type distortion so that the three degenerate LUMOs in the uncoordinated [60]fullerene become orbitals of different energies in the metal-coordinated [60]fullerene. This Jahn-Teller distortion should lower the energy of at least one of the [60]fullerene LUMOs so that reduction of the [60]fullerene moiety in [60]fullerene-M complexes occurs at a lower energy relative to uncoordinated [60]fullerene.

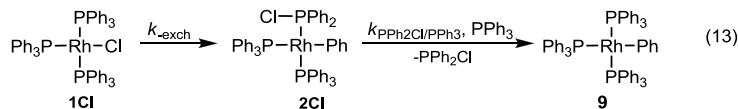
The reduction waves of the $C_{60}(C_5H_5N)_3(H)_3$ are shifted to positive potentials relative to the corresponding potentials of the uncoordinated [60]fullerene. Complexes of the type $(\eta^2-C_{60})M(CO)_5$ ($M = Cr, Mo, W$) also show evidence of this behavior, suggesting that they exhibit higher electron affinity than uncoordinated [60]fullerene. The electronic effect of adding piperidine to the curved surface of [60]fullerene seems to outweighs the structural effect of disruption of C=C bond conjugation. This suggests that [60]fullerides (R= aryl groups) [3] are excellent candidates to form weakly-coordinated lithium salts and [60]fullerene-based metallocenes or buckymetalloceces ($(C_{60})_2M$, for example buckyferrocene for $M = Fe^{2+}$) [112].

We have also presented the evidence of the formation of $\text{Ir}(\text{CO})(\text{PPh}_3)_2(\text{Cl})(\text{C}_{60}^{n-})$ ($n = 0, 4, 5, 6$). The species $\text{Ir}(\text{CO})(\text{PPh}_3)_2(\text{Cl})(\text{C}_{60})$ was unequivocally confirmed by infrared spectroscopy, but spectroscopy confirmation of the species $\text{Ir}(\text{CO})(\text{PPh}_3)_2(\text{Cl})(\text{C}_{60}^{4-})$, $\text{Ir}(\text{CO})(\text{PPh}_3)_2(\text{Cl})(\text{C}_{60}^{5-})$, and $\text{Ir}(\text{CO})(\text{PPh}_3)_2(\text{Cl})(\text{C}_{60}^{6-})$ is necessary. Since these species are quite stable under high vacuum conditions at room temperature, it seems that they can be generated electrolytically at ultrahigh vacuum conditions to study their spectroscopic properties. The species C_{60}^{4-} and C_{60}^{5-} can also be produced by electro synthesis. Once these species are generated their reactions with $\text{Ir}(\text{CO})(\text{PPh}_3)_2(\text{Cl})(\text{CH}_3\text{CN})$ may be monitored by using a suitable method such as Uv-visible spectroscopy to confirm that the complexes $\text{Ir}(\text{CO})(\text{PPh}_3)_2(\text{Cl})(\text{C}_{60}^{4-})$ and $\text{Ir}(\text{CO})(\text{PPh}_3)_2(\text{Cl})(\text{C}_{60}^{5-})$ are electrochemical precursors of $\text{Ir}(\text{CO})(\text{PPh}_3)_2(\text{Cl})(\text{C}_{60}^{5-})$ and $\text{Ir}(\text{CO})(\text{PPh}_3)_2(\text{Cl})(\text{C}_{60}^{6-})$, respectively.

Mechanistic studies of $(\text{PPh}_3)_3\text{RhCl}$ in benzene have risen a set of consecutive reactions ascribable to the two consecutive exponential decays of absorbance (370 nm) with time depending on the experimental conditions. The correlation of corresponding k_{obsd} and k'_{obsd} parameters of each exponential in the equation (eq. 20) depends on experimental conditions: i) when $[\text{PPh}_3]_{\text{added}} = 0$ the consecutive reactions are



($k_{\text{obsd}} = k_{\text{dim}}$ and $k'_{\text{obsd}} = k_{\text{exch}}$); ii) whereas under flooding where $[\text{PPh}_3]_{\text{added}} \gg [\mathbf{1Cl}]_0$, the consecutive reactions are



$$(k_{\text{obsd}} = k_{\text{exch}} \text{ and } k'_{\text{obsd}} = k_{\text{PPh}_3 / \text{PPh}_2\text{Cl}} [\text{PPh}_3]).$$

Computed profiles for the Ph/Cl exchange suggest formation of a metal-phosphido with a similar behavior for the non-simplified and simplified models. Moreover, more theoretical studies need to be done to elucidate these preliminary observations which differ in small structural and electronic differences that have also been observed in $(\text{Ph}_3\text{P})_2(\text{L})\text{Rh}(\text{X})$ ($\text{X} = \text{CF}_3$, CH_3 , H , Ph , F , Cl , I ; $\text{L} = \text{PPh}_3$, PPh_2Cl , PPh_2F) species [113].

We have presented a variety of organometallic complexes which exhibit different reactivity patterns due to their differences in co-coordinating ligands around the metal ($\text{M} = \text{Cr}$, Mo , W , Rh , Ir) coordination spheres. Understanding the relationship between structural properties and chemical and physical behaviour in solution of all the studied complexes is important not only because it is necessary information to design catalysts for specific applications, but to identify and to mitigate chemical processes that may reduce their catalytic activity. For example, Wilkinson's catalyst undergoes a series of reactions in solvent medium that changes its structure, thus creating different reaction pathways due to the resulting reactivity that is structurally driven. One should examine carefully the impact that these patterns have on a system and how these patterns affect organic, inorganic and biological reactions.

6. References

- [1] Parshall, G. W. *Organometallics* **1987**, *6*, 687-692
- [2] (a) Kroto, H. W.; Heath, J. R.; O'Brien, S. C.; Curl, R. F.; Smalley, R. E. *Nature* (London) **1985**, *318*, 162-163; (b) Krätschmer, W.; Lamb, L. D.; Fostiropoulos, K.; Huffman, D. R. *Nature* **1990**, *347*-354; (c) Bürgi, H. B.; Blanc, E.; Schwarzenbach, D.; Liu, S.; Lu, Y.; Kappes, M. M.; Ibers, J. *Angew. Chem., Int. Ed. Engl.* **1992**, *31*, 640; (d) Satpathy, S. *Chem. Phys. Lett.* **1986**, *130*, 545; (e) Hawkins, J. M.; Meyer, A.; Lewis, T. A.; Loren, S.; Hollander, F. J., *Science* **1991**, *252*, 313.
- [3] (a) Nakamura, E.; Isobe, H., *Acc. Chem. Res.*, **2004**, *36*, 807; (b) Nakanishi, I.; Fukuzumi, S.; Konishi, T.; Ohkubo, K.; Fujitsuka, M.; Ito, O.; Miyata, N. *J. Phys. Chem. B*, **2002**, *106*, 2372.
- [4] Cooper, A. C.; Folting, K.; Huffman, J. C.; Caulton, K. G. *Organometallics* **1997**, *16*, 505-507
- [5] Bolink, H. J.; La Rosa, A.; Filippone, S.; Martín, N. *J. Phys. Chem. Lett.*, **2010**, *1* (17), 2566–2571.
- [6] Cates, N. C.; Gysel, R.; Beiley, Z.; Miller, C. E.; Toney, M. F.; Heeney, M.; McCulloch, I.; McGehee, M. D. *Nano Lett.*, **2009**, *9* (12), 4153–4157.
- [7] (a) Saha, D.; Deng, S. *Langmuir*, **2011**, *27* (11), 6780–6786; (b) Pupyshva, O. V.; Farajian, A. A.; Yakobson, B. I. *Nano Lett.*, **2008**, *8* (3), 767–774.
- [8] (a) Taylor, R.; Walton, D. R. M. *Nature* **1993**, *363*, 685; (b) Hirsch, A. *The Chemistry of the Fullerenes*; Thieme: Stuttgart, New York, **1994**; (c) Diederich, F.; Thilgen, C. *Science* **1996**, *271*, 317.
- [9] Guldi, D. M.; Asmus, K. D. *J. Phys. Chem.*, **1997**, *101*, 1472.
- [10] Nunzi, F.; Sgamellotti, A.; Re, N.; Floriani, C. *Organometallics*, **2000**, *19*, 1628.
- [11] Guldi, D. M.; Prato, M. *Acc. Chem. Res.* **2000**, *33*, 695–703

- [12] Rivera-Rivera, L.A.; Crespo-Roman, G., Acevedo-Acevedo, D.; Ocasio-Delgado, Y.; Cortés-Figueroa, J. E. *Inorg. Chim. Acta.* **2004**, 357, 881–887.
- [13] Ocasio-Delgado, Y.; De Jesus-Segarra, J., Cortés-Figueroa, J. E. *J. Organomet. Chem.* **2005**, 690, 3366–3372.
- [14] Rivera-Rivera, L. A.; Colon-Padilla, F.; Del Toro-Novalés, A.; Cortés-Figueroa, J. E. *J. Coord. Chem.* **2001**, 54, 143-151.
- [15] Rivera-Rivera, L. A.; Colon-Padilla, F.D.; Ocasio-Delgado, Y.; Martinez-Rivera, J.; Mercado-Feliciano, S.; Ramos, C. M.; Cortés-Figueroa, J. E. *Inorg. React. Mech.* **2002**, 4, 49-56
- [16] Song, L. C.; Liu, P. C.; Liu, J. T.; Su, F. H.; Wang, G. F.; Hu, Q. M.; Zanello, P.; Laschi, F.; Fontani, M. *Eur. J. Inorg. Chem.* **2003**, 3201– 3210.
- [17] Babcock, A. J.; Li, J.; Lee, K.; Shapley, J. R. *Organometallics*, **2002**, 21, 3940–3946.
- [18] Zanello, P.; Laschi, F.; Cinquantini, A.; Fontani, M.; Tang, K.; Jin, X.; Li, L. *Eur. J. Inorg. Chem.* **2002**, 1345–1350.
- [19] Zanello, P.; Laschi, F.; Fontani, M.; Mealli, C.; Ienco, A.; Tang, K.; Jin, X.; Li, L. *J. Chem. Soc., Dalton Trans.* **1999**, 965–970.
- [20] Zanello, P.; Laschi, F.; Fontani, M.; Song, L. C.; Zhu, Y. H. *J. Organomet. Chem.* 593–594, **2000**, 7–11.
- [21] Song, L. C.; Liu, J. T.; Hu, Q. M.; Wang, G. F.; Zanello, P.; Fontani, M. *Organometallics* **2000**, 19, 5342-5351.
- [22] Igartúa–Nieves, E.; Ocasio-Delgado, Y.; Cortes-Figueroa, J. E. *J. Coord. Chem.* Vol. 60, No. 4, **2007**, 449–456

- [23] Balch, A. L.; Hao, L.; Olmstead, M. M. *Angew. Chem., Int. Ed. Engl.* **1996**, 35, 188-190.
- [24] Fagan, P. J.; Calabrese, J. C.; Malone, B. *Science*, **1991**, 252,1160.
- [25] Chernega, A. N.; Green, M. L. H.; Haggitt, J.; Stephens, A. A. H. *J. Chem. Soc., Dalton Trans.* **1998**, 755-768
- [26] Park, J. T.; Song, H.; Cho, J. J.; Chung, M. K.; Lee, J. H.; Suh, I. H. *Organometallics*. **1998**, 17, 227-236.
- [27] Westmeyer, M. D.; Rauchfuss, T. B.; Verma, A. K. *Inorg. Chem.* **1996**, 35, 7140–7147.
- [28] (a) Echegoyen, L.; Xie, Q.; Haddon, R. C.; Brus, L. E.; Raghavachari, K. *Chem. Phys. Lett.* **1986**, 125, 459. (2) (b) Haymet, A. D. *Chem. Phys. Lett.* **1985**,122,421. (c) Disch, R. L.; Schulman, J. N. *Chem. Phys. Lett.* **1986**, 125,465. (d) Scuseria, G. E. *Chem. Phys. Lett.* **1991**, 176, 423
- [29] Vaska, L.; Peone, J., Jr. *J. Chem. Soc., Chem. Commun.* **1971**, 418.
- [30] Vaska, L.; Peone, J., Jr. *Inorg. Synth.* **1974**, 15, 64.
- [31] Jones, C. M.; Doherty, N. M. *Polyhedron* **1995**, 14, 81.
- [32] Cooper, A. C.; Caulton, K. G. *Inorg. Chim. Acta* **1996**, 251, 41.
- [33] Cooper, A. C.; Huffman, J. C.; Caulton, K. G. *Inorg. Chim. Acta* **1998**, 270, 261.
- [34] Dorta, R.; Egli, P.; Zuercher, F.; Togni, A. *J. Am. Chem. Soc.* **1997**, 119, 10857.
- [35] Krueger, J.; Carreira, E. M. *J. Am. Chem. Soc.* **1998**, 120, 837.
- [36] Barthazy, P.; Togni, A.; Mezzetti, A. *Organometallics* **2001**, 20, 3472.
- [37] Vicente, J.; Gil-Rubio, J.; Guerrero-Leal, J.; Bautista, D. *Organometallics* **2004**, 23, 4871.

- [38] Renkema, K. B.; Werner-Zwanziger, U.; Pagel, M. D.; Caulton, K. G. *J. Mol. Catal. A* **2004**, 224, 125.
- [39] (a) Braterman, P.S.; Black, J.D. *J. Organomet. Chem.* **1972**, 39, C3–C4; (b) J.D. Black, M.J. Boylan, P.S. Braterman, *J. Chem. Soc., Dalton Trans.* **1981**, 673; (c) Anderson, F. R.; Wrighton, M. S. *Inorg. Chem.* **1986**, 25, 112; (d) Hill, R. H.; Wrighton, M. S. *Organometallics* **1987**, 6 (3), 632–638; (e) Young, K. M.; Wrighton, M. S. *Organometallics* **1989**, 8 (4), 1063–1066.
- [40] (a) Burkey, T.J. *J. Am. Chem. Soc.* **1990**, 112 (23), 8329–8333; (b) Hu, S.; Farrell, G. J.; Cook, C.; Johnston, R.; Burkey, T. J. *Organometallics* **1994**, 13 (11), 4127–4128; (c) Hester, D. M.; Sun, J.; Harper, A. W.; Yang, G. K. *J. Am. Chem. Soc.* **1994**, 114 (13), 5234–5240.
- [41] Palmer, B. J.; Hill, R. H. *Can. J. Chem.* **1996**, 74 (11), 1959–1967.
- [42] Helm, L.; Merbach, A. E. *Chem. Rev.* **2005**, 105 (6), 1923–1960;
- [43] Tanada, K.; Hashimoto, A.; Tsuji, H.; Kato, K.; Inada, Y.; Aizawa, S.; Funahashi, S. *Inorg. Chim. Acta* **2006**, 359 (2), 511–518;
- [44] Sanford, T.; Andrews, D.; Rathbone, J.; Taylor, M.; Muntean, F.; Thompson, M.; McCoy, A. B.; Parson, R.; Lineberger, W. C. *Faraday Discuss* **2004**, 127, 383–394.
- [45] Neubrand, A.; Thaler, F.; Körner, M.; Zahl, A.; Hubbard, C.D.; Eldik, R. van *J. Chem. Soc., Dalton Trans.* **2002**, 957–961.
- [46] Zalis, S.; Busby, M.; Kotrba, T.; Matousek, P.; Towrie, M.; Vlcek Jr., A. *Inorg. Chem.* **2004**, 43 (5), 1723–1734.
- [47] Ladogana, S.; Dobson, G. R.; Smit, J. P. *Inorg. Chim. Acta* **1998**, 271 (1–2), 105–111
- [48] Ladogana, S.; Dobson, G. R.; Smit, J. P. *Inorg. Chim. Acta* **1998**, 278 (2), 202–208.

- [49] Zhang, S.; Dobson, G. R.; Zang, V.; Bajaj, H. C.; Eldik, R. van *Inorg. Chem* **1990**, 29 (18), 3477–3482.
- [50] Bengali, A. A.; Stumbaugh, T. F. *Dalton Trans.* **2003**, 354.
- [51] Wells, J. R.; House, P.G.; Weitz, E. *J. Phys. Chem.* **1994**, 98 (34), 8343–8351.
- [52] Zhang, S.; Dobson, G. R. *Inorg. Chim. Acta* **1991**, 181 (1), 103–109.
- [53] Engelhardt, L. M.; Jacobsen, G. E.; White, A. H.; Raton, C. L. *Inorg. Chem.* **1991**, 30, 3980-3981.
- [54] A. L. Balch, B. J. Catalano, J. W. Lee *Inorg. Chem.* **1991**, 30, 3980-3981.
- [55] (a) T. Félix-Massa, J. E. Cortés-Figueroa *Inor. Chem. Commun.* **2009**, 12, 347–350. (b) T. Félix, J. E. Cortés-Figueroa, *J. Chem. Educ.* **2010**, 87, 426.
- [56] Schultz, R.H. *Organometallics* **2004**, 23 (19), 4349–4356;
- [57] Lugovskoy, S.; Lin, J.; Schultz, R. H. *Dalton Trans.* **2003**, 5, 3103–3110.
- [58] Biber, L.; Reuvenov, D.; Revzin, T.; Sinai, T.; Zahavi, A.; Schultz, R. H. *Dalton Trans.* **2007**, 41–51;
- [59] Dobson, G.R.; Zhang, S. *J. Coord. Chem.* **1991**, 47 (3), 409–416.
- [60] Dobson, G.R.; Smit, J.P.; Ladogana, S.; Walto, W. B. *Organometallics* **1997**, 16 (13), 2858–2861.
- [61] Ladogana, S.; Nayak, S.K.; Smit, J. P.; Dobson, J. R. *Organometallics* **1997**, 16 (13), 3051–3054.
- [62] Ladogana, S.; Nayak, S. K.; Smit, J. P.; Dobson, G. R. *Inorg. Chem.* **1997**, 36 (4), 650–655.
- [63] Zang, V.; Zhang, S.; Dobson, C.B.; Dobson, G.R.; Eldik, R. V. *Organometallics* **1992**, 11 (3), 1154–1158.

- [64] Acharyya, R.; Dutta, S.; Basuli, F.; Peng, S-M; Lee, G-H; Falvello, L. R.; Bhattacharya, S.; *Inorg. Chem.* **2006**, 45, 1252-1259.
- [65] Werner, H.; Hohn, A.; Dziallas, M. *Angew. Chem. Int. Ed. Engl.* **1986**, 25, 12, 1090-1092.
- [66] Shilov, A. E.; Shul'pin, G. B. *Chem. Rev.* **1997**, 97, 2879-2932.
- [67] Lewis, J. C.; Bergman, R. G.; Ellman, J. A. *Acc Chem Res.* **2008**, August ; 41(8): 1013–1025.
- [68] Keim, W. *J. Organomet. Chem.* **1968**, 14, 179.
- [69] Jardine, F. H. *Prog. Inorg. Chem.* **1981**, 28, 63
- [70] Bennett, M. A.; Longstaff, P.A. *Chem. Ind. (London)*, **1965**, 846.
- [71] Osborn, J. A.; Jardine, F. H.; Young, J. F.; Wilkinson, G. *J. Chem. Soc., A.* **1966**, 1711.
- [72] Grushin, V.; Marshall, W. *J. Am. Chem. Soc.* **2004**, 126, 3068-3069
- [73] Grünberg, A.; Yeping, X.; Breitzke, H.; Buntkowsky, G. *Chem. Eur. J.* **2010**, 16, 6993.
- [74] Macgregor, S. A.; Roe, D. C.; Marshall, W. J.; Bloch, K. M.; Bakhmutov, V. I.; Grushin, V. V. *J. Am. Chem. Soc.* **2005**, 127, 15304.
- [75] Macgregor, S. A.; Wondimagegn, T. *Organometallics* **2007**, 26, 1143
- [76] Macgregor, S. A. *Chem. Soc. Rev.* **2007**, 36, 67.
- [77] Rogers, J. R.; Marynick, D. S. *Chem. Phys. Lett.* **1993**, 205, 197.
- [78] Haddon, R. C. *J. Comp. Chem.* **1998**, 19, 139.
- [79] Jemmis, E. D.; Manoharan, M. *Curr. Sci.* **1999**, 76, 1122.
- [80] Babcock, A. J.; Li, J.; Lee, K.; Shapley, J. R. *Organometallics* **2002**, 21, 3940-3946.
- [81] Larsson, S. Volosov, A.; Rosen, A. *Chem. Phys. Lett.*, **1987**, 137, 501.

- [82] Rosen A.; Wastberg, B. *J. Chem. Phys.*, **1989**, *90*, 2525.
- [83] Qingshan, X.; Pérez-Cordero, E.; Echegoyen, L. *J. Am. Chem. Soc.*, **1992**, *114*, 3978.
- [84] Ohsawa, Y.; Saji, T. *J. Chem. Soc. Chem. Commun.*, **1992**, 781.
- [85] Echegoyen L.; Echegoyen, L. *E Acc. Chem. Res.*, **1998**, *31*, 593.
- [86] Dubois, D.; Jones, M. T.; Kadish, K. M. *J. Am. Chem. Soc.*, **1992**, *114*, 6446.
- [87] Zhou, F.; Jehoulet, C.; Bard, A. J. *J. Am. Chem., Soc.* **1992**, *114*, 11004.
- [88] Dubois, D.; Kadish, K. M.; Flanagan, S.; Haufiler, R. E.; Chibante, L. P. F.; Wilson, L. *J. Am. Chem. Soc.*, **1991**, *113*, 4364.
- [89] Vincent A. (2nd ed) (**2001**), *Molecular Symmetry and Group Theory*. John Wiley & Sons LTD.
- [90] Aihara, J-i. Weighted HOMO-LUMO Energy Separation as an Index of Kinetic Stability for Fullerenes. *Theor. Chem. Acc.* 1999, *102*, 134-138.
- [91] Haddon, R. C. *Acc. Chem. Res.*, **1992**, *25*, 127.
- [92] Haddon, R. C. *J. Am. Chem. Soc.*, **1997**, *119*, 1797.
- [93] Haddon, R. C. *Science*, **1993**, *261*, 1545.
- [94] Nakamura, E.; Sawamura, M. *Pure Appl. Chem.*, **2001**, *73*, 2, 355–359.
- [95] Sawamura, M.; Iikura, H.; Ohama, T.; Hacler, U. E.; Nakamura, E. *J. Organomet. Chem.*, **2000**, *599*, 32-36.
- [96] Sawamura, M.; Iikura, H.; Nakamura, E. *J. Am. Chem. Soc.*, **1996**, *118*, 12850-12851.
- [97] Ruoff, R. S.; Tse, D. S.; Malhotra, R.; Lorents, D. C. *J. Phys. Chem.* **1993**, *97*, 3379-3383.
- [98] Kramer, J.; Nçllen, Buijs, E.; Driessen, W.; Reedijk, W. L. *React. Funct. Polym.* **2003**, *1*, 57.
- [99] La Planca, S. J.; Ibers, J. A. *Inorg. Chem. Soc., A* **1966**, 1733.
- [100] Dachs, A.; Osuna, S.; Roglans, A.; Solá, M. *Organometallics* **2010**, *29*, 562–569

- [101] Hardesty, J. H.; Koerner, J. B.; Albright, T. A.; Lee, G.-Y. *J. Am. Chem. Soc.* **1999**, 121, 6055–6067.
- [102] Dachs, A.; Torrent, A.; Roglans, A.; Parella, T.; Osuna, S.; Sola, M. *Chem. Eur. J.* **2009**, 15, 5289–5300.
- [103] Yoo, K.; Jun, C.-H.; Choi, C. H.; Sim, E. *Bull. Korean Chem. Soc.* **2008**, 29, 1920–1926.
- [104] Gandon, V.; Agenet, N.; Vollhardt, K. P. C.; Malacria, M.; Aubert, C. *J. Am. Chem. Soc.* **2006**, 128, 8509–8520.
- [105] (a) Veiros, L. F.; Dazinger, G.; Kirchner, K.; Calhorda, M. J.; Schmid, R. *Chem. Eur. J.* **2004**, 10, 5860–5870. (b) Cui, Q.; Musaev, D. G.; Morokuma, K. *Organometallics* **1997**, 16, 1355–1364. (c) Cui, Q.; Musaev, D. G.; Morokuma, K. *Organometallics* **1998**, 17, 742–751. (d) Cui, Q.; Musaev, D. G.; Morokuma, K. *Organometallics* **1998**, 17, 1383–1392. (e) Zheng, W.; Ariaifard, A.; Lin, Z. *Organometallics* **2008**, 27, 246–253. (f) Abe, Y.; Kuramoto, K.; Ehara, M.; Nakatsuji, H.; Suginome, M.; Murakami, M.; Ito, Y. *Organometallics* **2008**, 27, 1736–1742.
- [106] Gaussian 03, Revision C.02, M. J. Frisch, G. W. Trucks, H. B. Schlegel, G. E. Scuseria, M. A. Robb, J. R. Cheeseman, J. A. Montgomery, Jr., T. Vreven, K. N. Kudin, J. C. Burant, J. M. Millam, S. S. Iyengar, J. Tomasi, V. Barone, B. Mennucci, M. Cossi, G. Scalmani, N. Rega, G. A. Petersson, H. Nakatsuji, M. Hada, M. Ehara, K. Toyota, R. Fukuda, J. Hasegawa, M. Ishida, T. Nakajima, Y. Honda, O. Kitao, H. Nakai, M. Klene, X. Li, J. E. Knox, H. P. Hratchian, J. B. Cross, V. Bakken, C. Adamo, J. Jaramillo, R. Gomperts, R. E. Stratmann, O. Yazyev, A. J. Austin, R. Cammi, C. Pomelli, J. W. Ochterski, P. Y. Ayala, K. Morokuma, G. A. Voth, P.

Salvador, J. J. Dannenberg, V. G. Zakrzewski, S. Dapprich, A. D. Daniels, M. C. Strain, O. Farkas, D. K. Malick, A. D. Rabuck, K. Raghavachari, J. B. Foresman, J. V. Ortiz, Q. Cui, A. G. Baboul, S. Clifford, J. Cioslowski, B. B. Stefanov, G. Liu, A. Liashenko, P. Piskorz, I. Komaromi, R. L. Martin, D. J. Fox, T. Keith, M. A. Al-Laham, C. Y. Peng, A. Nanayakkara, M. Challacombe, P. M. W. Gill, B. Johnson, W. Chen, M. W. Wong, C. Gonzalez, and J. A. Pople, Gaussian, Inc., Wallingford CT, 2004.

[107] Gaussian 09, Revision A.1, M. J. Frisch, G. W. Trucks, H. B. Schlegel, G. E. Scuseria, M. A. Robb, J. R. Cheeseman, G. Scalmani, V. Barone, B. Mennucci, G. A. Petersson, H. Nakatsuji, M. Caricato, X. Li, H. P. Hratchian, A. F. Izmaylov, J. Bloino, G. Zheng, J. L. Sonnenberg, M. Hada, M. Ehara, K. Toyota, R. Fukuda, J. Hasegawa, M. Ishida, T. Nakajima, Y. Honda, O. Kitao, H. Nakai, T. Vreven, J. A. Montgomery, Jr., J. E. Peralta, F. Ogliaro, M. Bearpark, J. J. Heyd, E. Brothers, K. N. Kudin, V. N. Staroverov, R. Kobayashi, J. Normand, K. Raghavachari, A. Rendell, J. C. Burant, S. S. Iyengar, J. Tomasi, M. Cossi, N. Rega, J. M. Millam, M. Klene, J. E. Knox, J. B. Cross, V. Bakken, C. Adamo, J. Jaramillo, R. Gomperts, R. E. Stratmann, O. Yazyev, A. J. Austin, R. Cammi, C. Pomelli, J. W. Ochterski, R. L. Martin, K. Morokuma, V. G. Zakrzewski, G. A. Voth, P. Salvador, J. J. Dannenberg, S. Dapprich, A. D. Daniels, Ö. Farkas, J. B. Foresman, J. V. Ortiz, J. Cioslowski, and D. J. Fox, Gaussian, Inc., Wallingford CT, 2009.

[108] (a) Miller, W. H. *Potential Energy Surfaces and Dynamical Calculations*, Ed. D. G. Truhlar (Plenum, New York, **1981**) 265. (a) Miller, W. H. B.; Ruf, A.; Chang, Y. T. *J. Chem. Phys.*, **1988**, 89, 6298-304.

- [109] (a) Peng, C.; Schlegel, H. B. *Israel J. of Chem.*, **1993**, 33, 449. (b) Peng, C.; Ayala, P. Y.; Schlegel, H. B.; Frisch, M. J. *J. Comp. Chem.*, **1996**, 17, 49.
- [110] (a) Espenson, J. H. *Chemical Kinetics and Reaction Mechanisms*, 2nd ed.; McGraw-Hill: New York, **1995**; pp 74-75. (b) Steinfeld, J. I.; Francisco, J. S.; Hase, W. L. *Chemical Kinetics and Dynamics*, 2nd ed.; Prentice Hall: Upper Saddle River, NJ, **1998**; pp 25-32.
- [111] (a) Giese, B. *Acc. Chem. Res.* **1984**, 17, 438; Johnson, C. D. *Chemical Reviews*, **1975**, 75, 6, 755; (b) J. Rooney, *J. Catal. Lett.*, **1998**, 50, 15-15.; (c) N. Koga, J. šesták, *J. Journal of Thermal Analysis* **1991**, 37, 1103; (d) L. Liu, Q.X. Guo, *Chem. Rev.* **2001**, 101, 673.
- [112] Matsuo, Y.; Kazukuni Tahara, K.; Nakamura, E. *J. Am. Chem. Soc.* **2006**, 128, 7154.
- [113] Goodman, J.; Grushin, V. V.; Larichev, R. B.; Macgregor, S. A.; Marshall, W. J.; Roe, D. C. *J. Am. Chem. Soc.* **2010**, 132, 12013-12026.
- [114] Bennett, M. J.; Donaldson, P. B. *Inorg. Chem.* **1977**, 16, 655
- [115] Grushin, V. V.; Marshall, W. J. *J. Am. Chem. Soc.* **2004**, 126, 3068.